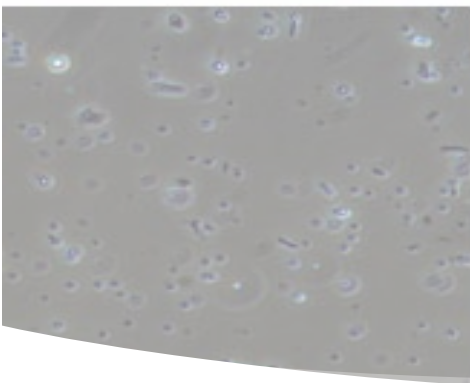


**REMOTE SENSING OF HARMFUL ALGAL  
BLOOMS IN THE INDIAN RIVER LAGOON AND  
CONNECTED WATERWAYS IN BREVARD  
COUNTY**



**Task 8.4: Indian River Lagoon HAB Remote Sensing  
Findings Memorandum**

***Final Report***

FUNDED BY:



PREPARED FOR:



PREPARED BY:



February 6, 2024

---

## CONTENTS

---

1	Executive Summary .....	1
2	Introduction .....	4
2.1	Project Objectives.....	4
2.2	Algal Remote Sensing Literature Review .....	5
2.2.1	Remote Sensing of Phytoplankton .....	5
2.3	Site Description .....	9
2.4	Surface Water Quality Monitoring .....	10
2.5	Hyperspectral Data Acquisition and Processing .....	13
2.6	Multispectral Data Acquisition and Processing .....	17
2.7	Statistical Analysis .....	18
2.7.1	Model Calibration Validation .....	18
2.7.2	Bloom Severity Index .....	19
2.7.3	Non-Parametric and Multivariate Analysis .....	20
3	Results and Data Analysis .....	22
3.1	Objective 1 .....	22
3.1.1	Sentinel Calibration Validation.....	23
3.1.2	Hyperspectral Chlorophyll Water Estimation.....	26
3.1.3	Benthic Conditions Remote Sensing.....	32
3.1.4	Cyanobacteria in the IRL.....	37
3.2	Objective 2 .....	46
3.2.1	Bloom Duration, Intensity, and Severity .....	47
3.2.2	Bloom Severity Assessment.....	66
4	Conclusions and Further Research .....	77
4.1	Conclusions.....	77
4.1.1	Remote Sensing Estimated Chlorophyll-A.....	77
4.1.2	Bloom Duration, Intensity, and Severity .....	78
4.2	Further Research .....	80
4.2.1	Phytoplankton Remote Sensing .....	80

4.2.2	HAB Pattern Analysis .....	80
5	References .....	82
6	Figure Descriptions .....	88

## LIST OF FIGURES

Figure 1. Study area boundary with the basins of the IRL within Brevard County.....	10
Figure 2. SJRWMD monthly estuary surface water sampling sites. ....	12
Figure 3. AEI UAS survey locations. ....	16
Figure 4. Sentinel 2 and Sentinel 3 data inventory from 2015 to 2023 by year and season. .....	17
Figure 5. Sentinel 2 calibration validation dataset comparison between the estimated and measured ChlA concentrations.....	24
Figure 6. Sentinel 3 calibration validation dataset comparison between the estimated and measured ChlA concentrations.....	25
Figure 7. Comparison of the ChlA estimation error of S2 and S3 for synchronous sampling days.....	26
Figure 8. Comparison of FLAME spectral signals from two SJRWMD sampling locations sampled the same day and the same location on different days. The green bar highlights the ChlA reflectance at 705 nm.....	27
Figure 9. OceanInsight FLAME Normalized Difference Chlorophyll Index (NDCI) Calibration Dataset. ....	28
Figure 10. Comparison of BaySpec spectral signals from the same location (B04) on different days. The green bar highlights the ChlA reflectance at 705 nm.....	29
Figure 11. BaySpec OCI-F Normalized Difference Chlorophyll Index (NDCI) Calibration Dataset. ....	30
Figure 12. Comparison of the ChlA estimation errors between synchronous Sentinel, FLAME, and SJRWMD measurements.....	31
Figure 13. Comparison of the ChlA estimation errors between synchronous Sentinel, BaySpec, and SJRWMD measurements.....	32
Figure 14. Comparison of Caulerpa Prolifera FLAME reflectance to open sand with and without bloom conditions, as well as muck sediment.....	33
Figure 15. Comparison of the dense Caulerpa Prolifera FLAME reflectance to water depth .....	34
Figure 16. Example IRL benthic sediments. A depicts clean sand with low organics. B depicts a mixture of sand, shell hash, and organics. C depicts the highly organic IRL muck. ....	34
Figure 17. Comparison of IRL sediment FLAME reflectance for clean sand, mucky sand, and IRL muck.....	35
Figure 18. Comparison of Caulerpa Prolifera BaySpec reflectance to open sand with and without bloom conditions, as well as muck sediment.....	36

---

Figure 19. Sykes Creek BaySpec imagery collected on October 12, 2022. The true color image is presented in panel A and the estimated ChlA concentration is presented in panel B.....	37
Figure 20. Boxplots of the cyanobacteria biomass for 2019 and 2020 by lagoon segment. The scales of the two years are not equal, 2020 is an order of magnitude larger than 2019.....	38
Figure 21. Boxplots of the cyanobacteria biomass for 2021 and 2022 by lagoon segment. ....	38
Figure 22. Comparison of the FLAME hyperspectral readings of eukaryotic and cyanobacteria phytoplankton blooms in the Indian River Lagoon. The four spectra related to Phycocyanin and Chlorophyll A are highlighted by vertical bars, from left to right, 620, 665, 705, and 755 nm. ....	40
Figure 23. Comparison of the BaySpec hyperspectral readings of eukaryotic and cyanobacteria phytoplankton blooms in the Indian River Lagoon. The four spectra related to Phycocyanin and Chlorophyll A are highlighted by vertical bars, from left to right, 620, 665, 705, and 755 nm. ....	41
Figure 24. Comparison of the measured ChlA concentrations to the percent of the sample’s biomass as cyanobacteria.....	42
Figure 25. Sentinel 3 spectral comparison of low and high cyanobacteria (CB) biomass blooms.....	43
Figure 26. Comparison of the Sentinel 3 (S3) 2BDA-PC index to the measured cyanobacteria (CB) biomass at SJRWMD sampling sites with ChlA more than 10 µg/L. ....	44
Figure 27. Comparison of the Sentinel 3 (S3) NDPCI index to the measured cyanobacteria (CB) biomass at SJRWMD sampling sites. ....	44
Figure 28. Spatial comparison of the 2022 Annual bloom intensity (BII), duration (BDI), and severity indices (BSI) for Banana River Lagoon segment 3.....	48
Figure 29. Comparison of the annual Bloom Severity Index (BSI) between 2021 and 2022 for the NIRL3 segment. ....	49
Figure 30. Comparison of the Bloom Severity Index (BSI) and the SJRWMD monthly surface water ChlA in NIRL3 segment between 2021 and 2022 .....	50
Figure 31. 2022 Bloom duration, intensity, and severity of the Southern Mosquito Lagoon (SML) and Northern-North IRL (N-NIRL).....	53
Figure 32. 2022 Bloom duration, intensity, and severity of the Northern Banana River Lagoon (NBRL).....	55
Figure 33. 2022 Bloom duration, intensity, and severity of the Southern Banana River Lagoon (SBRL).....	57

Figure 34. 2022 Bloom duration, intensity, and severity of the Central-North IRL (C-NIRL).  
..... 59

Figure 35. 2022 Bloom duration, intensity, and severity of the Southern-North IRL (S-NIRL).  
..... 61

Figure 36. 2022 Bloom duration, intensity, and severity of the Northern-Central IRL (N-CIRL).  
..... 63

Figure 37. Comparison of the cyanobacteria bloom index for a eukaryotic bloom on September 9, 2019 and a cyanobacteria bloom on August 14, 2020. .... 68

Figure 38. Sentinel 2 cumulative ChlA for 2017 and 2022 for the BRL3 segment. The SJRWMD seagrass extents for 2017 and 2021 are included..... 72

Figure 39. The weekly Bloom Severity Index (BSI) of the segment of NIRL8 proximate to the mouth of the Eau Gallie River and the entire NIRL8 segment compared to the weekly discharge from the Eau Gallie River between May to December 2016. .... 74

Figure 40. The weekly Bloom Severity Index (BSI) of the segment of NIRL8 proximate to the mouth of the Eau Gallie River and the entire NIRL8 segment compared to the weekly discharge from the Eau Gallie River between January 2017 to March 2019.  
..... 75

Figure 41. The weekly Bloom Severity Index (BSI) of the segment of NIRL8 proximate to the mouth of the Eau Gallie River and the entire NIRL8 segment compared to the weekly discharge from the Eau Gallie River between April 2019 to December 2022..... 76

## LIST OF TABLES

Table 1. Example Sentinel-2 and 3 Algae Estimation Algorithms.....	7
Table 2. Example Sentinel-2 and 3 Cyanobacteria Estimation Algorithms. Adapted from Ogashawara et al 2019.....	8
Table 3. Sentinel 2 Multi Spectral Imager (S2) and Sentinel 3 Ocean and Land Color Instrument (S3) available spectral and spatial resolution. The band number is listed in the corresponding box.....	9
Table 4. SJRWMD monthly estuary surface water sampling sites identified by basin and monitoring type.....	11
Table 5. Summary of hyperspectral data collection events from March 2022 to March 2023.....	14
Table 6. Ranges of ChIA concentrations and their corresponding Bloom Intensity Score. ....	20
Table 7. Sentinel 2 calibration validation statistics for the 2022-2023 validation dataset. ....	23
Table 8. Sentinel 3 calibration validation statistics for the 2022-2023 validation dataset. ....	25
Table 9. OceanInsight FLAME hyperspectral photometer NDCI calibration equation and performance metrics. ....	27
Table 10. BaySpec OCI-F hyperspectral photometer NDCI calibration equation and performance metrics. ....	29
Table 11. Average CB algorithm values for the three FLAME sampling events.....	39
Table 12. Average CB algorithm values for the four BaySpec sampling events.....	41
Table 13. Sentinel-3 CB for a high Cyanobacteria (CB) and a low CB bloom.....	42
Table 14. Sentinel 3 CB calibration statistics for the 2BDA-PC and NDPCI algorithms with ChIA more than 10 µg/L.....	43
Table 15. Comparison of median Bloom Severity Index (BSI) for Southern Mosquito Lagoon and Northern-North Indian River Lagoon between 2017-2019 and 2020-2022 by quarter.....	52
Table 16. Comparison of median Bloom Severity Index (BSI) for the Northern Banana River Lagoon between 2017-2019 and 2020-2022 by quarter.....	54
Table 17. Comparison of median Bloom Severity Index (BSI) for the Southern Banana River Lagoon between 2017-2019 and 2020-2022 by quarter.....	56
Table 18. Comparison of median Bloom Severity Index (BSI) for the Central-North Indian River Lagoon between 2017-2019 and 2020-2022 by quarter.....	58

Table 19. Comparison of median Bloom Severity Index (BSI) for the Southern-North Indian River Lagoon between 2017-2019 and 2020-2022 by quarter. ....	60
Table 20. Comparison of median bloom duration, intensity, and severity indices for the Northern-Central Indian River Lagoon between 2021 and 2022.....	62
Table 21. Summary of significant differences in the median Bloom Severity Index (BSI) between 2017-2019 and 2020-2022 by Indian River Lagoon segment. ....	64
Table 22. Percent of each segment identified to have an increasing, decreasing, or no trend in monthly BSI between 2016 and 2022 as determined by the Seasonal Mann-Kendall trend test per Sentinel-3 pixel.....	66
Table 23. Cyanobacteria (CB) biomass percentage and Chlorophyll A (ChlA) concentration ( $\mu\text{g/L}$ ) for the Southern Mosquito Lagoon (SML) and Northern-North IRL in 2019 and 2020.....	67
Table 24. Differences in the median BSI, salinity, and temperature by percent of monthly total flow as baseflow for the NIRL5 to NIRL8 segments from 2016 to 2022.....	69
Table 25. Differences in the OSTDS density, average annual flow, TN, and TP loading per acre, and median BSI for the NIRL5 to NIRL8 segments from 2016 to 2022. ....	70
Table 26. Differences in the average monthly flow, TN, and TP loading per acre, and median and average BSI for the NIRL5 to NIRL8 segments. ....	70
Table 27. Binned percent of weeks in 2017 and 2022 of BRL3 and SML2 by their Bloom Duration Index (BDI).....	73
Table 28. Binned percent of weeks in 2017 and 2022 of BRL3 and SML2 by their Bloom Intensity Index (BII). ....	73
Table 29. Binned percent of weeks in 2017 and 2022 of BRL3 and SML2 by their Bloom Severity Index (BSI). ....	73

## List of Acronyms

---

2BDA-PC	2 Band Algorithm for Phycocyanin
3BDA-PC	3 Band Algorithm for Phycocyanin
BRL	Banana River Lagoon
BDI	Bloom Duration Index
BII	Bloom Intensity Index
BSI	Bloom Severity Index
CB	Cyanobacteria
ChIA	Chlorophyll A
CI	Cyanobacteria Index
CIRL	Central Indian River Lagoon
CM	St Johns River Water Management District Continuous Monitoring Station
EOS	Earth Observing Satellites
ESA	European Space Agency
FDEP	Florida Department of Environmental Protection
FLH	Fluorescence Line Height
HAB	Harmful Algal Bloom
IRL	Indian River Lagoon
MCI	Maximum Chlorophyll Index
ML	Mosquito Lagoon
MODIS	MODerate Resolution Imaging Spectroradiometer
MSI	Sentinel-2 Multi Spectral Imager
NDCI	Normalized Difference Chlorophyll Index
NDPCI	Normalized Difference Phycocyanin Index
NIR	Near InfraRed
NIRL	North Indian River Lagoon
NTU	Nephelometric Turbidity Units
OLCI	Sentinel-3 Ocean and Land Color Instrument
POR	Period of Record
Q1	First Quarter of a Year; January, February, and March
Q2	Second Quarter of a Year; April, May, June
Q3	Third Quarter of a Year; July, August, September
Q4	Fourth Quarter of a Year; October, November, December
RMSE	Root Mean Square Error
PC	Phycocyanin
SAV	Submerged Aquatic Vegetation
SeaWiFS	Sea-viewing Wide Field-of-view Sensor
SJRWMD	St Johns River Water Management District

SLH	Scattering Line Height
SML	Southern Mosquito Lagoon
TSM	Total Suspended Matter
TSS	Total Suspended Solids
UAS	Unmanned Aircraft Systems

# 1 EXECUTIVE SUMMARY

---

Applied Ecology, Inc. (AEI) was contracted by Brevard County under Task Order No. 19-4477-012-EC SOIRL to develop and implement a framework for rapid detection of Harmful Algal Bloom (HAB) activity in the Indian River Lagoon (IRL) as part of a Florida Department of Environmental Protection (FDEP) Innovation Grant INV14. The methods developed in this report were utilized in the creation of a rapid HAB identification and characterization process. This effort included a brief review of relevant literature on phytoplankton remote sensing, a summary of multispectral and hyperspectral data collection analysis methods, and results that include bloom patterns and relationships with IRL watershed variables that contribute to algal blooms.

This report's first research objective was the determination of the continued efficiency of the European Space Agency's Sentinel-2 (S2) and Sentinel-3 (S3) satellites to estimate HAB conditions in the IRL. The first objective was evaluated by hypotheses which focused on verifying the ability to estimate HAB density using remote sensing and then confirming that the satellite estimates matched locally collected hyperspectral data. The first objective was then further evaluated by another pair of hypotheses which sought to identify the influence of benthic conditions on the HAB estimates and assess the ability to differentiate cyanobacteria dominated HABs with satellite and hyperspectral data.

Previous AEI research identified the Normalized Difference Chlorophyll Index (NDCI) as an effective means to estimate Chlorophyll A (ChIA) concentrations in the IRL with the S2 and S3 satellites. The NDCI's continued performance was confirmed using 2022 ground-truthed data collected by the St. Johns River Water Management District (SJRWMD). The S2 NDCI algorithm regressed against measured Chl-a concentrations had an  $R^2$  of 0.87 and RMSE of 4.54  $\mu\text{g/L}$  and the S3 NDCI algorithm had an  $R^2$  of 0.93 and RMSE of 4.70  $\mu\text{g/L}$  in 2022. The RMSE values can be interpreted as the algorithms margin of error or ability to estimate ChIA concentrations within 4.54  $\mu\text{g/L}$  for S2 and 4.70  $\mu\text{g/L}$  for S3. Both  $R^2$  values demonstrate a strong fit between the estimated ChIA concentrations using satellite algorithms and measured field data.

The NDCI algorithm was then applied to hyperspectral data collected by a handheld and Unmanned Aircraft System (UAS) mounted sensor to further validate the algorithm. The performance of the hyperspectral sensors was lower compared to S2 and S3, but the majority of the 27 synchronous satellite and hyperspectral ChIA estimations were within 5  $\mu\text{g/L}$ . The handheld OceanInsight FLAME NDCI algorithm had an  $R^2$  of 0.66 and RMSE of 4.96  $\mu\text{g/L}$  and the BaySpec OCI-F NDCI algorithm had an  $R^2$  of 0.53 and RMSE of 3.98  $\mu\text{g/L}$  in 2022. As the majority of the ChIA measurements available to compare with the hyperspectral data were below 10  $\mu\text{g/L}$ , this highlighted a limitation with the sensor to estimate low concentrations of ChIA in the water column.

The comparison of reflectance between Submerged Aquatic Vegetation (SAV) and phytoplankton identified very similar reflectance patterns with substantial overlap in the spectral bands that the NDCI utilizes to estimate ChlA concentrations. The FLAME and BaySpec hyperspectral reflectance did not appear to confirm any unique features of the SAV *Caulerpa Prolifera* to aid in the differentiation of the two sources of ChlA. S2 and S3 estimated ChlA was also heavily influenced by the presence of SAV and under no-bloom conditions could be used to accurately estimate SAV coverage. The evaluation of SAV coverage estimation for the Banana River Lagoon (BRL) segment between Cape Canaveral and Cocoa Beach from 2017 and 2022 identified a 78% loss in coverage which largely mirrored the reported seagrass loss by the SJRWMD for that segment.

HAB phytoplankton includes eukaryotic and cyanobacteria taxa, which both contain ChlA and the NDCI alone is unable to differentiate between them. However, cyanobacteria have a unique photosynthetic pigment called phycocyanin which has unique spectral features separate from ChlA. Both hyperspectral sensors were able to confirm these features from a bloom of the IRL *Picocyanobacteria spp.* A pair of Sentinel cyanobacteria estimation algorithms were then ground-truthed using algal enumerated samples. The two algorithms had similar performance, with the Normalized Difference Phycocyanin Index (NDPCI) having an  $R^2$  of 0.66 and RMSE of 11.5% and 2 Band Algorithm for Phycocyanin (2BDA-PC) with an  $R^2$  of 0.65 and RMSE of 11.7%.

This report's second research objective was to evaluate the Sentinel derived data to determine the spatiotemporal variability of HABs in the IRL. The first hypothesis of this objective was to determine if HABs in the IRL were increasing in intensity, duration, and severity. To address this hypothesis, a trio of novel HAB metrics was created for use with Sentinel estimated ChlA. The Bloom Duration Index (BDI) is a standard measure of the length of time a bloom lasts while the Bloom Intensity Index (BII) is a standard measure of bloom concentration. The BDI and BII together create the Bloom Severity Index (BSI) which estimates the potential harm caused by long lasting, high concentration blooms on a given location.

These indices were used to determine if HAB duration, intensity, and severity was increasing throughout the IRL. Between 2017-2019 and 2020-2022, there appeared to be a decreasing trend in severity for the Northern-North IRL (N-NIRL) and BRL. The NIRL1 segment was the only IRL segment to have significant decreases in severity across all months between 2017-2019 and 2020-2022. The largest decreases in the BRL BSI was observed during January-March and July-September. However, there also appeared to be an increasing trend in BSI for the Central-NIRL, Southern-NIRL, and North-Central IRL (N-CIRL). For these areas, the largest BSI increases from 2017-2019 to 2020-2022 were observed during January-March.

Additional analysis was performed using the indices to identify the relationship between blooms and their potential drivers. The influence of rainfall and density of Onsite Sewage Treatment and Disposal Systems (OSTDS) or septic systems was examined for the segments of the NIRL between the cities of

Cocoa and Melbourne. These segments were identified to have significantly higher BSI during months with very low rainfall, while there was no significant difference in BSI during wet months. Of these segments, a significantly higher BSI was identified in the northernmost NIRL5 both overall and during low rainfall periods. As the southern NIRL8 had a higher density of OSTDS and modeled nutrient inputs from its drainage area, this may suggest that the elevated BSI in the north segment may be due to other factors than OSTDS.

The relationship between bloom activity and the presence of SAV was explored by comparing the BDI, BII, and BSI between Southern Mosquito Lagoon (SML) and the BRL. The BRL3 segment was estimated to have had a 78% decline in SAV coverage between 2017 and 2022. It was compared against SML2 which was estimated to not have lost SAV between 2017 and 2022. The BRL3 segment was observed to have lower BDI, BII, and BSI after its SAV loss whereas the SML2 had higher BDI, BII, and BSI. This suggests a more complex relationship between SAV coverage and bloom activity than can be simply explained by the presence of SAV and HABs. Additionally, the persistence of the SML2 SAV despite bloom activity also suggests that the segment's characteristics may help mitigate bloom impacts.

To assess the impact of muck sediments and their removal on bloom activity, the BSI of the area near the mouth of the Eau Gallie River was compared to the overall BSI of the NIRL8 segment. Both prior to and during the dredging project, the BSI around the mouth of the Eau Gallie River was significantly higher than the overall segment. This suggests that for the Eau Gallie River, the presence of muck may have been leading to elevated BSI. Following the completion of the muck dredging in March 2019, the portion of the segment next to the mouth of the river had significantly lower BSI than the entire segment suggesting that the removal of the muck in the Eau Gallie River helped reduce bloom activity.

Overall, this project was able to validate a suite of remote sensing tools that can be applied to the IRL for rapid and detailed assessments of bloom activity. The Sentinel satellites can provide a regular assessment of bloom concentrations, extents, and even identify cyanobacteria. Then when paired with the use of UAS mounted sensors the lack of data due to persistent cloud cover can be avoided and has the potential to provide additional bloom speciation. Continued collection of bloom spectral data needs to be performed, as only a portion of the bloom-causing phytoplankton in the IRL were observed in this study. Beyond identifying bloom patterns and their potential causes, imagery can also be used to supplement the ongoing SAV monitoring efforts within the IRL. Future assessment of bloom and SAV patterns could integrate other remotely sensed data such as sea surface temperature and precipitation. Additionally, the BSI should be compared against known HAB related events such as fish kills to refine the accuracy of the scale.

## 2 INTRODUCTION

---

The Indian River Lagoon has experienced catastrophic losses of seagrass habitat over the past decade, due primarily to nutrient-driven Harmful Algal Blooms (HABs). Brevard County has been actively providing grants and implementing projects through the Save our Indian River Lagoon Project Plan to reduce nutrient loads to the Indian River Lagoon to improve conditions for seagrass growth. Ultimately, reducing nutrient loads will reduce the frequency and severity of algal blooms that increase turbidity and reduce seagrass viability.

With an increasing frequency of HAB occurrences in the IRL over the last decade, the identification of potential HAB triggers and hotspots of activity is vital to Brevard County's efforts to manage watershed sources of nutrients to the IRL. The use of remote sensing technologies is a cost-effective and encompassing approach for providing rapid identification of HAB formation, the lifecycle of the HAB, and identification of hotspots of HAB occurrences. The European Space Agency (ESA) Sentinel-2 (S2) and Sentinel-3 (S3) satellites provide high spatial, spectral, and temporal resolution as well as having a proven record in published literature for the evaluation of HABs (Caballero et al 2020, Kravitz et al 2020). The Sentinel satellites when paired with the monthly water quality monitoring data collected by the St. Johns River Water Management District (SJRWMD) can accurately estimate the variability of IRL HABs in space and time. These identified patterns can then be further examined to determine their potential causes and effects on the aquatic ecosystems of the IRL. The increased availability and accessibility of Unmanned Aircraft Systems (UAS) and advanced remote sensing methods such as hyperspectral sensors provide additional means for the assessment of HAB activity.

Applied Ecology, Inc. (AEI) was contracted by Brevard County under Task Order No. 19-4477-012-EC SOIRL to develop and implement a framework for rapid detection of HAB activity in the IRL for the Florida Department of Environmental Protection (FDEP) Innovation Grant INV14. The findings from this memo provide the stakeholders and management of the IRL additional tools in tracking Harmful Algal Blooms (HAB) and an assessment of potential factors which influence the spatiotemporal distribution of HAB activity.

This annual report provides a brief review of relevant literature on phytoplankton remote sensing, a summary of hyperspectral data collection analysis methods, and results that include bloom patterns and relationships with IRL watershed variables.

### 2.1 PROJECT OBJECTIVES

The hyperspectral remote sensing data collected during this project were used to test the most robust set of HAB identification algorithms from the literature to be used with S2 and S3 satellites. These selected algorithms were then used to perform a spatiotemporal interpretation of the available IRL

Sentinel imagery from 2015-2022. The following research objectives and hypotheses of the overall study are evaluated in this report:

- Objective 1: Determine the most efficient algorithms for the Sentinel-2 and 3 sensors to estimate conditions in the IRL
  - Hypothesis 1A: Within the IRL, the 705 nm fluorescence peak can explain the majority of variation in Chlorophyll A (ChlA) concentrations.
  - Hypothesis 1B: Variations in the ChlA fluorescence, reflectance, and absorbance peaks are not significantly different between Sentinel Top of Atmosphere Reflectance and the drone and handheld sensor Remote Sensing Reflectance.
  - Hypothesis 1C: Variation in the water column ChlA concentrations is significantly different from benthic conditions
  - Hypothesis 1D: HAB causing cyanobacteria have a significantly different spectral profile from HAB causing eukaryotic algae.
- Objective 2: Determine the spatiotemporal variability of HABs in the IRL
  - Hypothesis 2A: HAB intensity, scale, and duration has been increasing throughout the IRL.
  - Hypothesis 2B: HABs occur more frequently and in proximity to locations with household Onsite Sewage Treatment & Disposal Systems (OSTDS).
  - Hypothesis 2C: HABs occur more frequently in proximity to large stormwater outfalls.
  - Hypothesis 2D: HABs occur less frequently in areas with Submerged Aquatic Vegetation (SAV).
  - Hypothesis 2E: HAB duration is greatest in areas with a muck type benthic characteristic.
  - Hypothesis 2F: Muck removal projects have resulted in a decrease in proximate HAB activity.

## 2.2 ALGAL REMOTE SENSING LITERATURE REVIEW

---

### 2.2.1 REMOTE SENSING OF PHYTOPLANKTON

While multispectral imagers (e.g., Landsat, SPOT) have been used regularly since the 1970's, the widespread use of hyperspectral imaging is a relatively recent trend. The major difference between multispectral and hyperspectral images is that hyperspectral sensors collect a greater number of spectral bands than multispectral sensors, providing enough information to identify and distinguish differences between similar, but different, materials. In application, the hyperspectral sensor collects narrow, contiguous wavelength bands across the entire spectrum. Multispectral sensors in turn have

fewer bands centered over wavelengths selected for their unique features, allowing for less expensive data collection from a larger distance like the Earth's orbit. For example, the unique wavelength spectral signature for chlorophyll-a (ChlA) was used to establish the multispectral bands of several past and present Earth Observing Satellites (EOS).

Different proxy measurements have been used for detection of HABs, the most common being ChlA and phycocyanin (PC) (Khan et al., 2021). Of the pigments active in photosynthesis, ChlA has the strongest influence on the reflected spectral signal of water and can be easily detected by satellite sensors (Maxwell & Johnson 2000). Cyanobacteria have, in addition to ChlA, the pigment phycocyanin (PC) (Ogashawara et al., 2013). This makes it possible to assess ChlA by examining the variation in Photosynthetically Active Radiation (PAR; 400-700 nm) reflectances. ChlA preferentially absorbs energy in the blue and red spectra, resulting in the relatively high reflectance in the green spectrum (Morel & Prieur 1977; Tedetti et al., 2011). The ChlA pigment also reflects strongly in a narrow portion of the the NearInfraRed (NIR) range, specifically at 705 nm (Gitelson et al., 1996; Gower et al. 2008).

ChlA has frequently been used as a surrogate to estimate cyanobacteria (CB) density because analytical and spectral measurement of PC is difficult (Matthews and Bernard 2015). PC is considered an accessory pigment of chlorophyll, along with allophycocyanin and phycoerythrin, and it is blue in color, capable of absorbing orange and red light at a wavelength of about 620 nm and reflecting between 550 nm and 650 nm. Allophycocyanin absorbs and emits a longer wavelength around 650 nm and 660 nm (El-Ahem et al., 2021; Wang et al., 2016). Cyanobacteria also have a unique biophysical behavior of forming surface scums that strongly reflect in the NIR range, easily distinguishing it from open water, which will absorb NIR (Duan, Ma, & Hu 2012).

The remote sensing of harmful algae in Florida was initially driven by the need to track *K. brevis* "Red Tide" blooms along the Gulf Coast of the state (Tyler et al., 2009). Due to the coarse spatial resolution and limited spectral bands of the satellite sensors such as Sea-viewing Wide Field-of-view Sensor (SeaWiFS) and MODerate Resolution Imaging Spectroradiometer (MODIS), analysis was limited to the coastal ocean and large inland lakes such as Okeechobee (Hu 2005). The Medium Resolution Imaging Spectrometer (MERIS) improved both the spatial resolution (300m compared to MODIS 1km) and spectral bands centered on reflectance peaks suited to evaluating more optically complex waters (Kalogirou et al., 2013).

The estimation of ChlA is commonly performed using band ratios, which examine differences in the ChlA reflectance and absorption features, are resistant to confounding factors in the water column, and allow comparison between different scenes of data (Cabellero et al., 2021, Ogashawara 2013, Rodriguez et al., 2020). One of the more widespread ratios is the Normalized Difference Chlorophyll Index (NDCI) which was developed for MERIS and is the ratio of the difference between the 705 nm and 665 nm bands (**Table 1**). To distinguish cyanobacteria from eukaryotic algae, one approach has been to use the Cyanobacteria Index (CI), which incorporates the shape of the spectrum between the

665 nm, 680 nm, and 709 nm bands (Slonecker et al., 2021). Mishra et al. (2021) demonstrated that the existing CI algorithm, which uses Sentinel-3 Ocean and Land Color Instrument (OLCI) and MERIS data, is 84% accurate for determining cyanotoxin-producing cyanobacteria in freshwater lakes across the United States.

**Table 1. Example Sentinel-2 and 3 Algae Estimation Algorithms**

Ratio Name	Ratio Equation
Normalized Difference Chlorophyll Index (NDCI) (Mishra & Mishra 2012)	$\frac{(R_{705\text{ nm}} - R_{665\text{ nm}})}{(R_{705\text{ nm}} + R_{665\text{ nm}})}$
Cyanobacteria Index (CI) (Wynne et al., 2018)	$(R_{665\text{ nm}} - R_{680\text{ nm}}) + (R_{705\text{ nm}} - R_{665\text{ nm}}) * \frac{(R_{705\text{ nm}} - R_{665\text{ nm}})}{(R_{705\text{ nm}} + R_{665\text{ nm}})}$
Maximum Chlorophyll Index (MCI) (Gower et al 1999)	$R_{705\text{ nm}} - 1.005 (R_{665\text{ nm}} + (R_{740\text{ nm}} - R_{665\text{ nm}}) * \frac{(705\text{ nm} - 665\text{ nm})}{(740\text{ nm} - 665\text{ nm})})$
Fluorescence Line Height (FLH) (Hu & Feng 2016)	$R_{680\text{ nm}} - (R_{665\text{ nm}} + (R_{755\text{ nm}} - R_{665\text{ nm}}) * \frac{680\text{ nm} - 665\text{ nm}}{755\text{ nm} - 665\text{ nm}})$
Scattering Line Height (SLH) (Kudela et al., 2015)	$R_{715\text{ nm}} - [R_{655\text{ nm}} + \frac{R_{755\text{ nm}} - R_{655\text{ nm}}}{755\text{ nm} - 655\text{ nm}} (715\text{ nm} - 655\text{ nm})]$

The IRL’s phytoplankton population has a diverse mixture of both cyanobacteria and eukaryotic cells. As both phytoplankton utilize the ChlA pigment for photosynthesis, the cyanobacteria’s use of phycocyanin provides a unique reflectance signal with maximum absorption between 615 and 620 nm with strongest reflectance around 650 nm, (Cai et al, 2001). Three algorithms were evaluated for their ability to differentiate between the two pigments (Ogashawara et al 2019) **(Table 2)**.

The 2 Band Algorithm for Phycocyanin (2BDA-PC) is an inverse relationship between the ChlA reflectance peak around 705 nm and the phycocyanin absorption trough at 620 nm. As more of the biomass of the bloom is comprised of CB, we would expect the PC (620 nm reflectance) to be lower than the ChlA reflectance (705 nm), resulting in a larger 2BDA-PC index value. The opposite is true for the 3 Band Algorithm for Phycocyanin (3BDA-PC) which subtracts the 705 nm ChlA reflectance peak from the 620 nm PC absorption trough and multiplies the difference by the 755 nm pure water absorption peak. Unlike the 2BDA-PC algorithm, the 3BDA-PC algorithm describes a direct relationship in ChlA and PC spectral signatures such that the more PC that is present, the lower the index. Like the 2BDA-PC index, the Normalized Difference Phycocyanin Index (NDPCI), calculates the difference between the CB absorption trough at 620 nm and the ChlA 705 nm reflectance peak and divides it by the sum of the two spectra. The normalized difference has the benefit of being resistant

to atmospheric interference and is more accurate for comparison of imagery collected on different days. With the NDPCI index, as more of the bloom biomass is comprised of CB, we would expect the PC (620 nm reflectance) to be lower than the ChIA reflectance (705 nm), resulting in a more positive index value.

**Table 2. Example Sentinel-2 and 3 Cyanobacteria Estimation Algorithms. Adapted from Ogashawara et al 2019.**

Ratio Name	Ratio Equation
<b>NDPCI</b>	$\frac{(R_{705\text{ nm}} - R_{620\text{ nm}})}{(R_{705\text{ nm}} + R_{620\text{ nm}})}$
<b>2BDA-PC</b>	$\frac{(R_{705\text{ nm}})}{(R_{620})}$
<b>3BDA-PC</b>	$(R_{620\text{ nm}} - R_{705\text{ nm}}) \times R_{755\text{ nm}}$

HABs generally occur with eutrophic conditions; however, the trigger for HAB initiation can vary by a water body’s chemistry, species present, or climatic factors (Huisman et al., 2018). Remote sensing of HABs in the IRL began with the 2011 “Superbloom”, utilizing the MERIS sensor to track the progression of the bloom throughout the lagoon and identified the potential impact of salinity and weather on the bloom lifecycle (Kamerosky et al., 2015). However the loss of the MERIS sensor in 2012 limited the evaluation of further blooms. The European Space Agency (ESA) continued the legacy of MERIS with the Sentinel-2 Multi Spectral Imager (MSI) launched in 2015 and 2017, along with the Sentinel-3 Ocean and Land Color Instrument (OLCI) launched in 2016 and 2018.

The MSI has 10 bands in the visible to NIR spectrum and a revisit time of approximately 2.5 days over Florida with the pair of satellites (**Table 3**). The OLCI has 21 bands in the visible to NIR spectrum and has a revisit time of approximately 1 day over Florida with the pair of satellites. The spatial resolution is another key difference between the two sensors, with the OLCI at 300 m compared to the 10-60 m of the MSI. As the spatial distribution and density of HABs can vary widely in the IRL (AEI 2022a), the difference in the spatial resolution of the two satellites can complicate direct comparison between collected environmental samples and the sensor data and between the two sensors.

Judice et al., (2020) successfully applied a principal component spectral decomposition approach to the OLCI to identify *Aureoumbra lagunesis* blooms occurring in the Banana River segment of the IRL. Previous assessments of these algorithms for use in the IRL identified the NDCl as the best performing for both the MSI and OLCI across the entire IRL from 2015 to 2021 (AEI 2022a).

**Table 3. Sentinel 2 Multi Spectral Imager (S2) and Sentinel 3 Ocean and Land Color Instrument (S3) available spectral and spatial resolution. The band number is listed in the corresponding box.**

	S2	S2	S2	S3
Wavelength (nm)	10 m	20 m	60 m	300 m
400				B1
412.5				B2
443			B1	B3
490	B2			B4
510				B5
560	B3			B6
620				B7
665	B4			B8
673.7				B9
680.2				B10
705		B5		B11
740		B6		
753.7				B12
761.2				B13
764.3				B14
767.5				B15
783		B7		B16
842	B8			
865		B8a		B17
885				B18
900				B19
945			B10	B20
1020				B21

*S2 and S3 band numbers are provided. The S2 bands are colored in yellow and S3 bands colored in green.*

## 2.3 SITE DESCRIPTION

The Indian River Lagoon (IRL) is an Estuary of National Significance within the US EPA National Estuary Program with more than 1 million residents in its increasingly developed watershed (US Census 2021). The IRL is located along 250 km (155 miles) of the Florida east coast with over 750 square km (290 square miles) of surface water, between multiple jurisdictions with a range of surrounding land cover types and benthic environments. The project is focused on the watershed basins of the IRL within

Brevard County (**Figure 1**), which includes the north and south Mosquito Lagoon, North IRL, Banana River, and Central IRL.

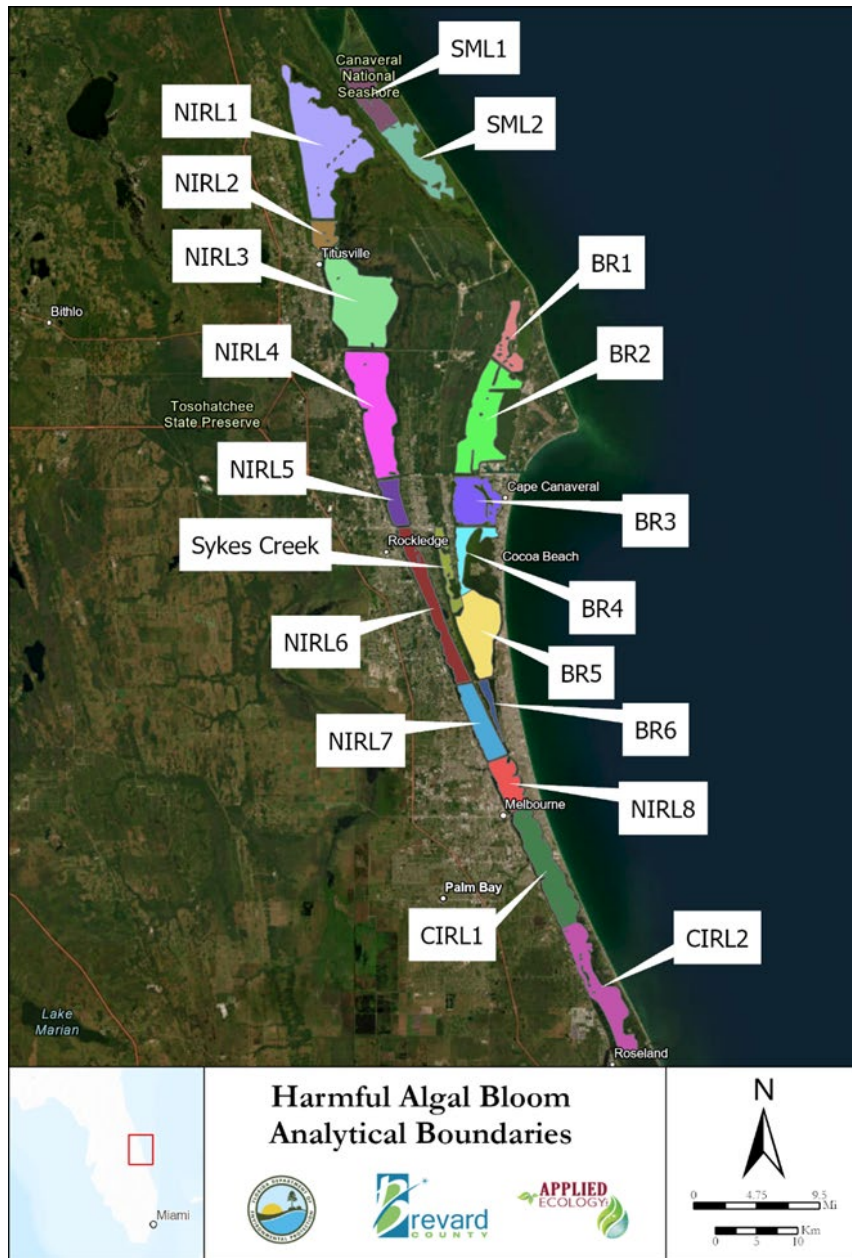


Figure 1. Study area boundary with the basins of the IRL within Brevard County. [Long Description of Figure 1.](#)

## 2.4 SURFACE WATER QUALITY MONITORING

To calibrate and compare remotely captured spectral signatures, AEI obtained water quality data from the SJRWMD monthly surface water quality grab sites and in-situ monitoring data (**Figure 2, Table 4**). Available corrected ChlA, turbidity, total suspended solids (TSS), and color was obtained for the stations from January 2015 to March 2023 using the SJRWMD Environmental Data Retrieval Tool. The other water quality constituents represent

parameters likely to interfere with the spectral properties of water. They were used to identify samples which had the least number of confounding factors to enable a clear spectral signature.

Additionally, Dr. Ed Philips of the University of Florida performed algae enumeration on the monthly SJRWMD samples from select sites between 2019 and 2023. These data were obtained through the IRL National Estuary Program.

**Table 4. SJRWMD monthly estuary surface water sampling sites identified by basin and monitoring type.**

Site Name	Basin	Monitoring Type
B02	Banana River	Grab
B04	Banana River	Grab and CM
B05	Banana River	Grab
B06	Banana River	Grab
B09	Banana River	Grab
NFH01S	Banana River	Grab
I23	Central IRL	Grab
I24	Central IRL	Grab
I26	Central IRL	Grab
I27	Central IRL	Grab
I28	Central IRL	Grab
SUS	Central IRL	Grab
ML02	Mosquito Lagoon	Grab and CM
BFRR	North IRL	Grab
I02	North IRL	Grab
I06	North IRL	Grab
I07	North IRL	Grab
I09E	North IRL	Grab
I10	North IRL	Grab
I13	North IRL	Grab and CM
I15	North IRL	Grab
I16	North IRL	Grab
I18	North IRL	Grab
I21	North IRL	Grab
IRCMTITUS01	North IRL	Grab and CM

*At B04, ML02, I13, and IRCMTITUS01 there is a continuous monitoring (CM) station present.*



Figure 2. SJRWMD monthly estuary surface water sampling sites. [Long Description of Figure 2.](#)

## 2.5 HYPERSPECTRAL DATA ACQUISITION AND PROCESSING

Two sets of hyperspectral data were collected using an OceanInsight FLAME hyperspectrometer (FLAME) and a BaySpec OCI-F hyperspectral camera (BaySpec) mounted on a small Unmanned Aircraft System (sUAS). The FLAME is a handheld Visible to Near InfraRed (VIS-NIR) sensor with 480 spectral bands between 350 to 1000 nm, averaging a 1.34 nm spectral resolution per band. The first set of data was collected by boat using the FLAME at locations along the UAS flight path. Remote sensing reflectance was calculated by measuring the percentage of ambient sunlight being reflected by the water's surface for each spectral band. The collected data were processed using the OceanInsight OceanView application and the reflectance data were exported to Microsoft Excel for further analysis.

The second set of data was collected using the BaySpec mounted on a Harris Aerial Hx8 UAS. The BaySpec OCI-F is also a VIS-NIR sensor which collects 120 spectral bands between 400 to 1000 nm via a push-broom method of imagery collection. Relative reflectance was calculated by measuring the percent of ambient sunlight, as determined by a 95% white Spectralon reference sheet, being reflected by the water's surface for each spectral band. The OCI-F was flown at an altitude of 400 feet (122 meters) by an FAA certified Part 107 pilot. The collected data was processed by the BaySpec CubeCreator program and the hyperspectral rasters were exported to ESRI ArcPro 3.0 for further analysis.

There was a total of 40 hyperspectral data collection events performed across the IRL between March 2022 and March 2023 (**Table 5**). Eighteen (18) of these events were performed in conjunction with the SJRWMD surface water data collection to compare actual surface water quality measurements with estimated concentrations. All 18 of these sampling events included data collection with BaySpec and 10 of these events included data collection by both the FLAME and BaySpec.

AEI performed twenty-two (22) additional hyperspectral sampling events to better understand and identify benthic conditions using both FLAME and BaySpec data (**Figure 3**). During the sampling events, field data were collected that included temperature, depth to bottom (DTB), pH, conductivity, dissolved oxygen, and turbidity. Simultaneously, AEI collected surficial benthic sediment samples with a petite ponar to evaluate sediment type, color, and presence of Submerged Aquatic Vegetation (SAV).

**Table 5. Summary of hyperspectral data collection events from March 2022 to March 2023.**

Date	Type	Location	Data Collected
3/10/2022	SJRWMD	C-BRL, S-BRL	UAS and FLAME
4/4/2022	AEI	N-CIRL	UAS and FLAME
4/6/2022	SJRWMD	N-CIRL	UAS and FLAME
4/28/2022	AEI	S-BRL	UAS and FLAME
5/3/2022	SJRWMD	N-NIRL	UAS and FLAME
5/4/2022	SJRWMD	C-NIRL, S-NIRL	UAS and FLAME
5/24/2022	SJRWMD	NBRL, CIRL	UAS Only
5/26/2022	AEI	S-NIRL	UAS and FLAME
5/27/2022	AEI	N-CIRL	UAS and FLAME
6/1/2022	SJRWMD	S-BRL	UAS Only
6/6/2022	SJRWMD	NIRL	Rain
6/7/2022	SJRWMD	N-CIRL	UAS
6/13/2022	SJRWMD	N-CIRL	UAS Only
7/7/2022	SJRWMD	C-NIRL, S-NIRL	FLAME Only
8/3/2022	SJRWMD	N-NIRL, S-BRL	UAS and FLAME
8/4/2022	SJRWMD	S-NIRL, N-CIRL	UAS and FLAME
8/30/2022	AEI	N-CIRL	UAS and FLAME
8/30/2022	AEI	N-CIRL	UAS and FLAME
9/1/2022	AEI	N-CIRL	UAS and FLAME
9/1/2022	AEI	N-CIRL	UAS and FLAME
9/7/2022	AEI	S-BRL	Rain
9/7/2022	SJRWMD	N-CIRL	UAS Only
9/22/2022	AEI	C-NIRL	UAS, FLAME, Phyto
10/5/2022	SJRWMD	N-NIRL	UAS and FLAME
10/6/2022	SJRWMD	C-BRL, S-BRL	UAS and FLAME
10/12/2022	AEI	S-BRL	UAS and FLAME
10/12/2022	AEI	C-NIRL	UAS and FLAME
10/13/2022	SJRWMD	S-BRL, C-CIRL	UAS and FLAME
10/27/2022	AEI	N-BRL	UAS and FLAME
11/1/2022	SJRWMD	N-BRL, S-BRL	UAS
11/2/2022	SJRWMD	C-NIRL, S-NIRL	UAS
11/29/2022	AEI	S-NIRL	UAS and FLAME

Date	Type	Location	Data Collected
11/29/2022	AEI	N-CIRL	UAS and FLAME
12/7/2022	AEI	C-BRL	UAS, FLAME, Phyto
12/7/2022	AEI	C-BRL	UAS, FLAME, Phyto
1/6/2023	AEI	S-NIRL	UAS, FLAME, Phyto
1/6/2023	AEI	N-CIRL	UAS, FLAME, Phyto
1/12/2023	AEI	N-NIRL	UAS and FLAME
1/19/2023	AEI	C-BRL	UAS and FLAME
1/19/2023	AEI	C-NIRL	UAS and FLAME
3/3/2023	SJRWMD	C-BRL, S-BRL	UAS, FLAME, Phyto

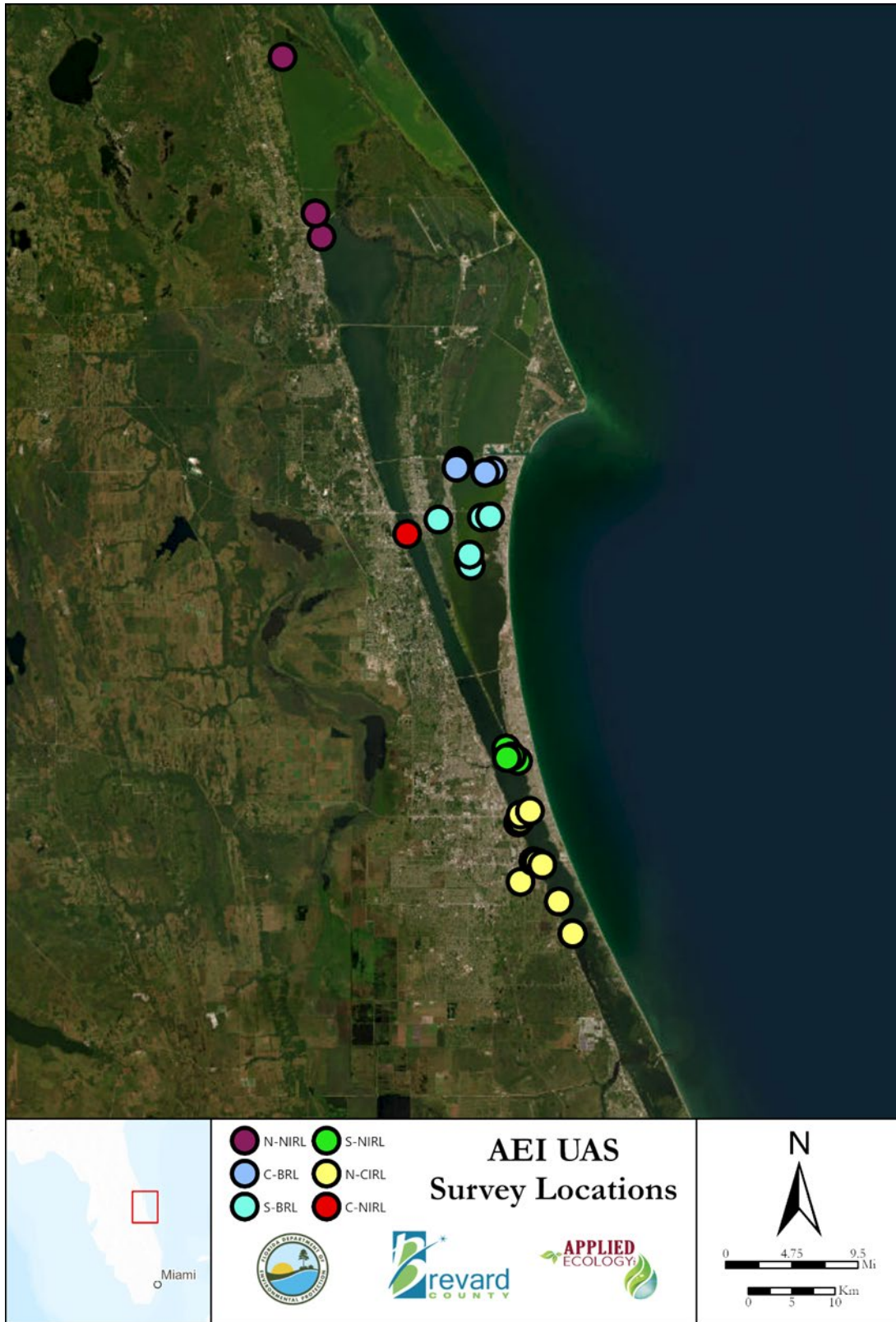
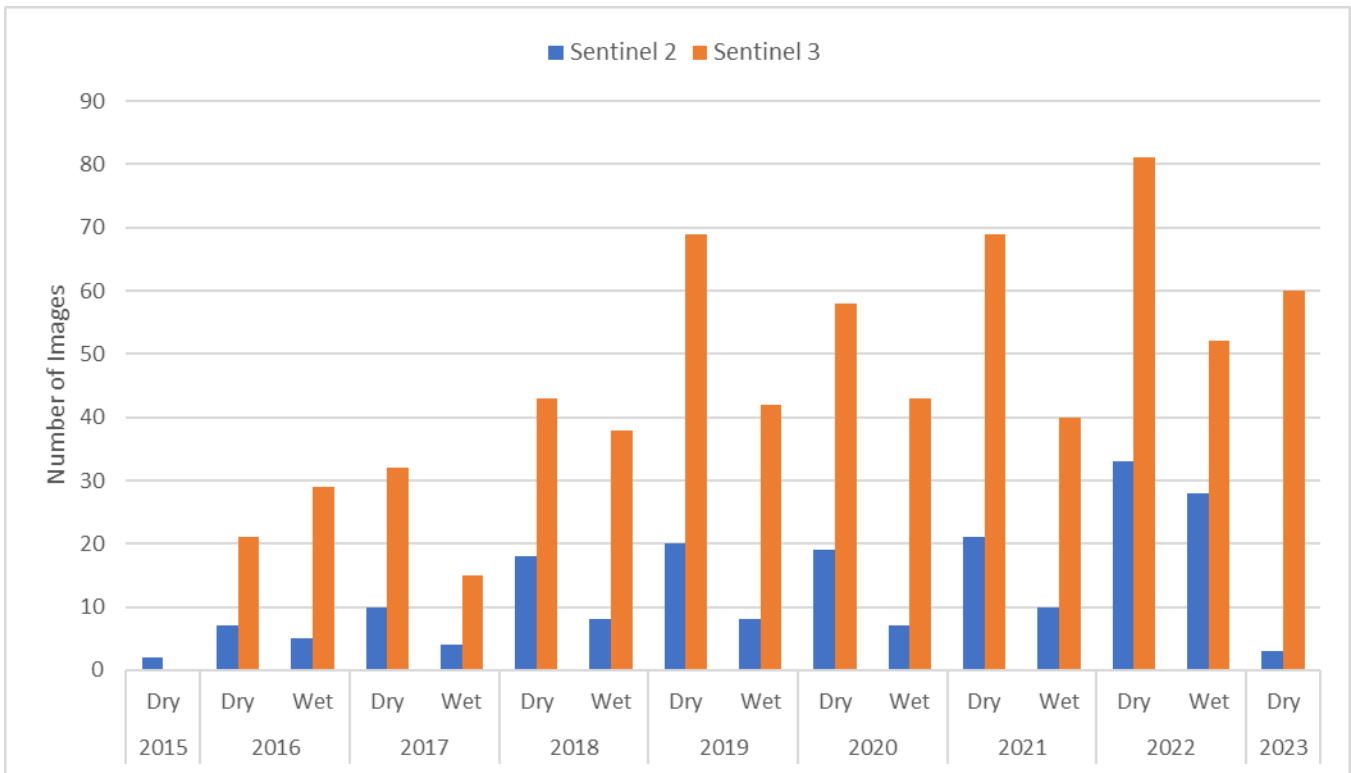


Figure 3. AEI UAS survey locations. [Long Description of Figure 3.](#)

## 2.6 MULTISPECTRAL DATA ACQUISITION AND PROCESSING

Satellite remote sensing data from S2 and S3 satellites were acquired for their period of record starting in 2015 to 2023. S2 and S3 imagery was downloaded through the European Space Agency’s Copernicus Open Access Hub and processed to L1C Top of Atmosphere (ToA) Reflectance and a cloud mask generated using the SentiNel Application Platform (SNAP). A total of 203 S2 and 692 S3 images were obtained from 2015 to 2023 (**Figure 4**). No atmospheric correction was applied to the imagery as these methods are likely to disrupt the red edge bands of the selected band indices. The downloaded imagery was processed and stored as a multidimensional raster dataset in ESRI ArcPro 3.0. The spectral values of pixels that were within 24 hours of the SJRWMD surface water collection were extracted through the ArcPro Multidimensional Sampling tool and stored in a Microsoft Office Excel Workbook. The extracted spectra were then converted to estimated ChIA using the NDCI and then estimated CB percentages using the indices listed in **Table 2**.



**Figure 4. Sentinel 2 and Sentinel 3 data inventory from 2015 to 2023 by year and season. [Long Description of Figure 4.](#)**

Following the conversion of S2 imagery to ChIA estimates, a likely SAV mask was generated to reduce the impact of ChIA overestimations by flagging the pixel for removal from analysis. The S2 scenes for use in the creation of the SAV mask were selected based on having full coverage of the IRL in Brevard County, SJRWMD surface sampling with ChIA below 10 µg/L for a given basin, and then manual comparison of the image to the previous S2 and S3 scene to confirm a lack of bloom activity. The

selected S2 images were then aggregated by year by determining the median ChIA estimate for a pixel across all the images in the year. This was to both estimate SAV coverage change and tailor the mask to each year. A threshold of 30 µg/L of yearly median estimated ChIA was selected based on 2022 field observations, with values above the threshold being categorized as likely SAV and used to create the mask.

## 2.7 STATISTICAL ANALYSIS

### 2.7.1 MODEL CALIBRATION VALIDATION

A total of 142 S2 and 536 S3 scenes of clear or low cloud cover were obtained from 2015 to 2021 for the purpose of calibrating the NDCI for each sensor using the SJRWMD surface water ChIA data (AEI 2022a, Kamerosky et al 2023). The reflectance data from the two satellites was then calibrated against the ChIA determined by the SJRWMD surface water sampling to create the conversion equations (**Equation 1, Equation 2**)

$$\text{Equation 1. } S2 \text{ Estimated ChIA} = 297.36 (NDCI)^2 + 313.98(NDCI) + 36.152$$

$$\text{Equation 2. } S3 \text{ Estimated ChIA} = 437.07(NDCI)^2 + 348.98(NDCI) + 33.928$$

The estimated ChIA concentrations from the NDCI was then evaluated on its internal strength of correlation, Root Mean Square Error (RMSE), Bias, and the Nash–Sutcliffe model efficiency coefficient (Nash). For these equations,  $n$  is the dataset size,  $M$  is measured concentrations,  $\bar{M}$  is the mean of all measured concentrations, and Est is the model estimated concentrations.

The RMSE is a measure of the overall variation of the measured data from the model. The Bias measure determines if the estimation model tends to underestimate (values closer to -1), overestimate (values closer to 1), or neither (values at 0). The Nash value qualifies how accurate the estimation model is by determining how well the estimated values relate to the mean of the measured concentrations. A Nash value of 0 would mean that the estimated values are not representative of the measured values while a value of 1 would mean that there is no difference in the overall estimated and measured datasets. The calibrated S2 equation had an  $R^2$  of 0.81, RMSE of 14.14 µg/L of ChIA, Bias of 0.00 µg/L, and Nash value of 0.81. The S3 equation had an  $R^2$  of 0.92, RMSE of 9.92 µg/L ChIA, Bias of -0.03 µg/L, and a Nash value of 0.92.

**Equation 3.**  $RMSE = \sqrt{\frac{1}{n} \sum_{i=1}^n (Est_i - M_i)^2}$

**Equation 4.**  $Bias = \frac{1}{n} \sum_{i=1}^n (Est_i - M_i)$

**Equation 5.**  $Nash = 1 - \frac{\sum_{i=1}^n (M_i - Est_i)^2}{\sum_{i=1}^n (M_i - \bar{M})^2}$

As part of this study, a re-evaluation of the previously calibrated algorithms was performed to confirm the accuracy and performance of the equations. For the validation of these two NDCI equations, an additional 61 S2 and 156 S3 images were selected from January 2022 to March 2023. The same image pre-processing was performed, with 9 pixels around the SJRWMD sampling point extracted and averaged. For S3 the pixel that aligned with the SJRWMD sampling location was selected. Additionally, this subset of imagery was used in the evaluation of the NDCI for the OceanInsight FLAME hyperspectrometer and BaySpec OCI-F hyperspectral camera. The RMSE, Bias, and Nash criteria were used in the assessment of the NDCI accuracy and performance.

### 2.7.2 BLOOM SEVERITY INDEX

The duration and intensity of HABs in the IRL can impact the survivability of a range of aquatic flora and fauna. A long lasting and intense bloom is more likely to stress SAV due to decreased light availability for photosynthesis. Then prolonged bloom activity increases the likelihood of anoxic conditions as organic decomposition of phytoplankton depletes dissolved oxygen, which in turn could result in fish kills. Lastly, intense blooms also increase the potential for harmful concentrations of ecological toxins from the HAB phytoplankton, such as saxitoxins released by *Pyrodinium bahamense*.

In this research, we define a Bloom Severity Index (BSI) which is based on the compounding relationship between the intensity and duration of a bloom and is estimated by the Bloom Intensity Index (BII) and the Bloom Duration Index (BDI). The intensity, duration, and severity were calculated for each day of S3 imagery at a 300 m spatial resolution using ESRI ArcPro and Microsoft Excel. Because of the S3's faster repeat times, there are more images available for analysis and higher spectral resolution to reduce interference from SAV or shallow water.

The Bloom Intensity Index (BII) describes the potential harm of an algal bloom on any single day in terms of the estimated ChlA concentration. The BII provides a scale for defining ChlA concentrations from 0 to 81 µg/L, and then normalized to 0.0625 to 1.0 (**Table 6**). A value of 0.0625 is assigned to a bloom with ChlA concentrations from 0-20 µg/L, while a value of 1 is assigned to a bloom with ChlA concentrations 81 µg/L and above. The assumption of this scale is that for a given location there is potentially 16 times more harm caused by ChlA concentration above 81 µg/L than if it was less than

20 µg/L. This assumption is based on the compounding harm of extreme concentrations of ChIA which includes the impacts on light availability for SAV, but also oxygen depletion and toxin releases.

**Table 6. Ranges of ChIA concentrations and their corresponding Bloom Intensity Score.**

ChIA Concentration (µg/L)	Bloom Intensity Score (Unitless)
0-20	0.0625
21-40	0.125
41-60	0.25
61-80	0.5
81 <	1

The Bloom Duration Index (BDI) describes the potential cumulative harm caused by bloom activity over time. The phytoplankton of the IRL typically have short bloom and bust cycles which can range from 3-5 days (Phlips et al 2021). The BDI examines bloom activity over the previous 21 days of available imagery to assess the persistence of the algal bloom and distinguish between short or long blooms. A BDI score of 1 for a given location would mean that over the previous 21 days, the ChIA concentration was always above 81 µg/L. The 21-day interval was selected to account for the normal phytoplankton lifecycles in the IRL as well as reducing the chance of BDI over or under estimation due to the irregular availability of data caused by cloud cover.

The BDI and BII are multiplied to create the Bloom Severity Index (BSI). The maximum BSI value for a given location is 1, which would mean that over the last 21 days 100% of the available S3 images had an estimated ChIA concentration above 81 µg/L. This would represent the maximum possible harm caused by an intense, long-lasting bloom. If there was no S3 data for a given pixel for 21 days, the BSI was not calculated for that day. The potential harm determined by BII, BDI, and BSI are also considered to be additive, meaning that the annual potential harm caused by bloom activity can be determined by summing all the calculated values in a year.

### 2.7.3 NON-PARAMETRIC AND MULTIVARIATE ANALYSIS

The BII, BDI, and BSI values were determined by the Shapiro-Wilk test to have non-normal distributions across all IRL segments.

To determine if HAB activity in the IRL was increasing in intensity, scale, and duration the non-parametric paired sample Sign and Wilcoxon Signed-Rank tests were applied. For all cells in a given lagoon segment the BII, BDI, and BSI of a given cell was compared between the median values by quarter for the years 2017-2019 and then 2020-2022. To assist in the analysis of HAB trends over time as they relate to muck dredging activity, a Mann-Kendall trend test was conducted on the BSI values of the cells around the mouth of the Eau Gallie River. Then to assist in the analysis of trends in the BSI

over the study period, a Seasonal Mann-Kendall Trend test was conducted with the seasonal blocks divided into January to March, April to June, July to September, and October to December.

Due to the high density of stormwater outfalls throughout the IRL and the observed impact of wind on daily bloom movement, stormwater runoff and OSTDS analysis was performed at the segment scale. To determine the relationship between stormwater runoff and BSI, a non-parametric Kruskal-Wallis comparison of independent samples and Steel-Dwass-Critchlow-Fligner (SDCF) multiple pairwise comparison test was applied. Then to determine the relationship between OSTDS and BSI, a non-parametric Friedmans comparison of paired samples and Nemenyi's multiple paired method was applied. From 2016 to 2022 there were a total of 78 months of S3 estimated BSI.

These were then compared to the estimated percentage of total monthly flow as baseflow from the Spatial Watershed Iterative Loading (SWIL) for the IRL from 2016 to 2022 (AEI 2022b) as well as field measured temperature and salinity by the SJRWMD. The SWIL model estimates the volume of water, total nitrogen (TN), and total phosphorus (TP) discharged by segmenting the hydrological and nutrient contributions of subsurface flow and direct rainfall runoff.

The contributions of portions of a basin are determined by land use, soil type, precipitation, evapotranspiration, peer-reviewed event mean concentrations, and runoff coefficients. Subsurface flow is the water that moves from the ground and into the surface water bodies and is estimated using monthly evapotranspiration, rainfall, and existing groundwater storage. The direct rainfall runoff is in turn estimated by using the monthly rainfall, specific runoff factors for land use types, and then interception by stormwater treatment systems. The monthly rainfall estimate was acquired from the SJRWMD NEXRAD rainfall estimates.

## 3 RESULTS AND DATA ANALYSIS

---

### 3.1 OBJECTIVE 1

The goals of the Objective 1 hypotheses were to confirm the continued performance of the NDCI algorithm with the Sentinel satellites, to examine the cross compatibility of the hyperspectral and satellite sensors, and to test whether it was possible to differentiate phytoplankton types and benthic conditions using both sensor types. The following sections provide detailed descriptions of the hypothesis testing, and a general summary of hypotheses outcomes.

**Hypothesis 1A:** Within the IRL, the 705 nm fluorescence peak can explain the majority of variation in ChIA concentrations.

The calibration validation of the S2 and S3 sensors to estimate ChIA through the NDCI was confirmed to continue to be highly accurate in 2022. While the FLAME and BaySpec generally had lower performance than the Sentinel satellites, the majority of ChIA variation was explained by the variation in the 705 nm peak. Therefore hypothesis 1A was supported by this research.

**Hypothesis 1B:** Variations in the ChIA fluorescence, reflectance, and absorbance peaks are not significantly different between Sentinel Top of Atmosphere Reflectance and the UAS and handheld sensor Remote Sensing Reflectance.

The comparison of simultaneous hyperspectral, Sentinel, and SJRWMD surface water samples identified a general agreement in ChIA estimation. The FLAME readings in general had more agreement with both Sentinel and the SJRWMD samples than the BaySpec. Hypothesis 1B appears to be supported but additional samples should be collected to generate a more robust dataset.

**Hypothesis 1C:** Variation in the water column ChIA concentrations is significantly different from benthic conditions

This study identified two general types of benthic conditions, open substrate and Submerged Aquatic Vegetation (SAV). FLAME, BaySpec, and Sentinel estimations of ChIA were not impacted by the open substrate type. The presence of SAV was identified to contribute to the 705 nm peak and in general matched the spectral signal of phytoplankton. Hypothesis 1C is supported for open substrate benthic conditions, but not for SAV due to the overlap along the 705 nm ChIA peak.

**Hypothesis 1D:** HAB causing cyanobacteria have a significantly different spectral profile from HAB causing eukaryotic algae.

Three (3) Cyanobacteria (CB) estimation algorithms were evaluated for FLAME, BaySpec, and Sentinel 3 using algal enumerated field samples collected by AEI and SJRWMD. Despite a limited dataset of four (4) samples, there appeared to be observable spectral differences between the CB and eukaryotic

phytoplankton. The CB estimation algorithms were effective when applied to S3 imagery, although only when estimated ChlA concentrations were above 10 µg/L. Hypothesis 1D appears to be supported by this research, however additional samples should be collected for greater confidence.

### 3.1.1 SENTINEL CALIBRATION VALIDATION

Based on the results of the hypotheses testing under Objective 1, AEI selected the NDCI as the most accurate ChlA estimation algorithm for both S2 and S3 datasets and more details of this process and results are outlined in AEI 2022a. To measure the accuracy of the calibrated NDCI, the S2 and S3 estimated ChlA for the year 2022 were compared against the available SJRWMD surface water sampling data.

#### 3.1.1.1 Sentinel 2 Chlorophyll Water Estimation

The S2 calibration validation dataset included measured ChlA concentrations in the IRL that ranged from 1.70 to 67.90 µg/L and had a median value 10.20 µg/L. The dataset included 113 sampling locations with 7 points in the Mosquito Lagoon, 59 in the NIRL, 28 in the Banana River Lagoon, and 19 in the CIRL. The NDCI algorithm validation dataset had an R<sup>2</sup> of 0.87, RMSE of 4.54 µg/L, Bias of -1.20 µg/L, and a Nash criterion of 0.98 (**Table 7**). There did not appear to be any notable outliers in the validation dataset (**Figure 5**).

**Table 7. Sentinel 2 calibration validation statistics for the 2022-2023 validation dataset.**

R <sup>2</sup>	RMSE	Bias	Nash
0.87	4.54	-1.20	0.98

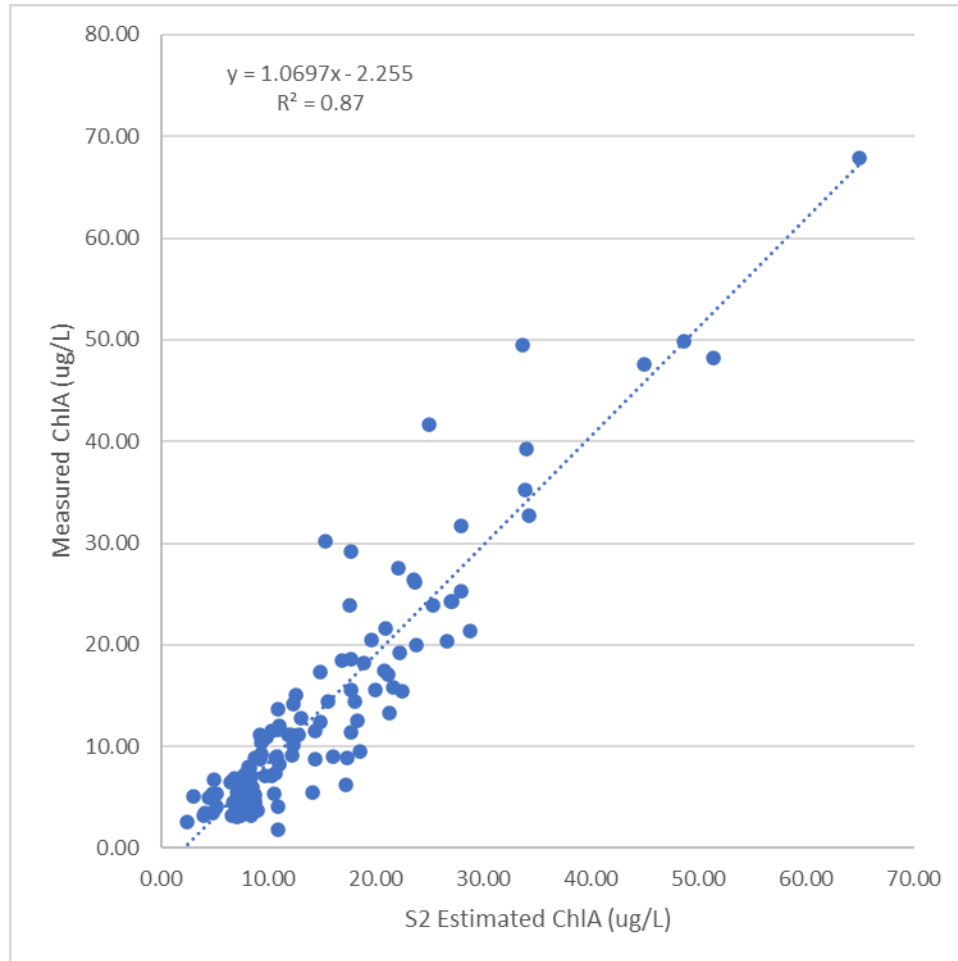


Figure 5. Sentinel 2 calibration validation dataset comparison between the estimated and measured ChIA concentrations. [Long Description of Figure 5.](#)

### 3.1.1.2 Sentinel 3 Chlorophyll Water Estimation

The S3 calibration validation dataset was also found to be representative of the measured ChIA in the IRL with the highest ChIA value at 67.9  $\mu\text{g/L}$ , lowest at 1.10  $\mu\text{g/L}$ , and a median value of 7.10  $\mu\text{g/L}$ . This calibration dataset contained a total of 180 sampling locations with 15 in the Mosquito Lagoon (ML), 83 in the NIRL, 49 in the Banana River Lagoon (BRL), and 27 in the CIRL. The S3 NDCI algorithm had a  $R^2$  of 0.93, RMSE of 4.70  $\mu\text{g/L}$ , a Bias of 2.20  $\mu\text{g/L}$ , and a Nash criterion of 0.95 (**Table 8**). The NDCI algorithm did not have any clear outliers ChIA (**Figure 6**). However, for 37 points where the measured ChIA was below 10  $\mu\text{g/L}$ , the NDCI estimated ChIA was negative.

The quantification of low concentrations of ChIA is a known challenge for satellite-based estimation of ChIA in complex coastal waters (Kamerosky et al 2015) and S3 appears to have more of a challenge than S2 with ChIA concentrations below 10  $\mu\text{g/L}$ . This may be due to the S3's 300 m pixel size, compared to the 60 m kernel applied to the S2.

**Table 8. Sentinel 3 calibration validation statistics for the 2022-2023 validation dataset.**

$R^2$	RMSE	Bias	Nash
0.93	4.70	2.20	0.95

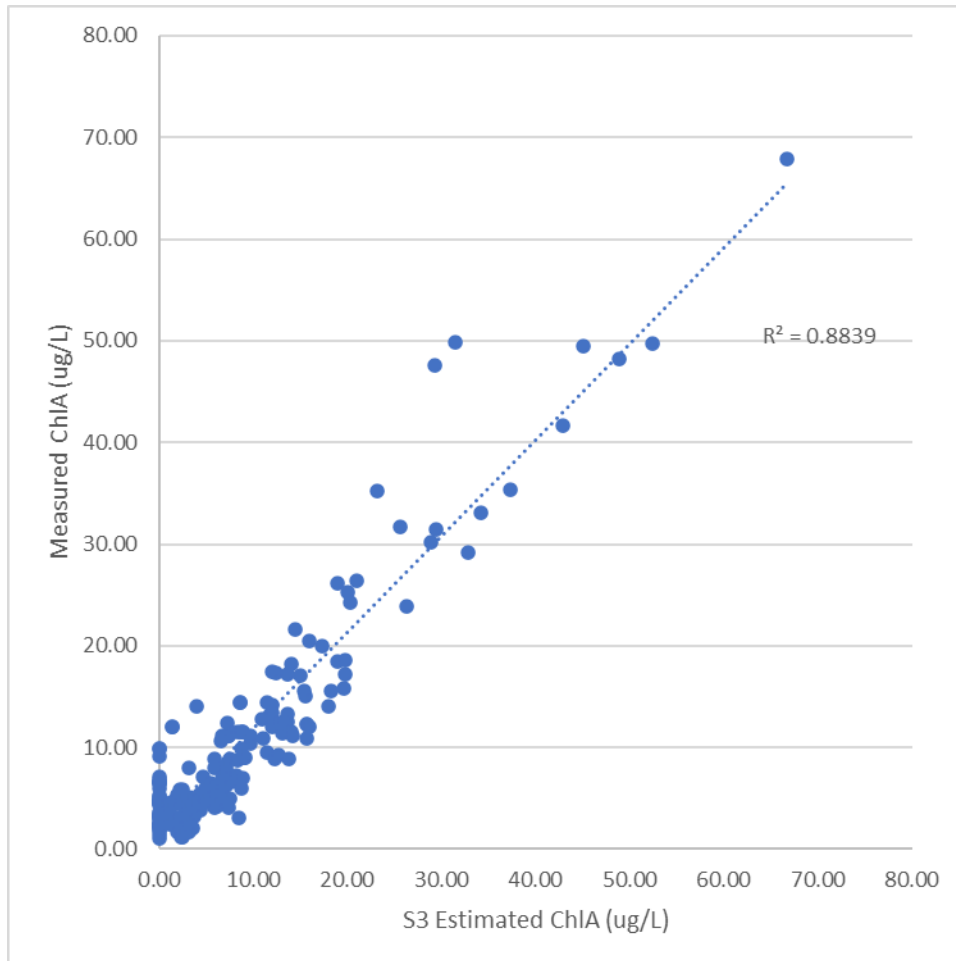


**Figure 6. Sentinel 3 calibration validation dataset comparison between the estimated and measured ChIA concentrations. [Long Description of Figure 6.](#)**

### 3.1.1.3 Sentinel 2 and 3 Cross Validation

To further confirm the validity of S2 and S3 ChIA estimates, a subset of 2022 imagery was identified where both the S2 and S3 overpass were within 24 hours of the SJRWMD surface water grab. The error of ChIA estimation for S2 and S3 for a given sample site on a given day was plotted to determine if there was a systematic pattern of over or underestimation by either sensor (**Figure 7**).

A total of 34 samples in 2022 were used in the analysis, including 4 in SML, 21 in NIRL, 3 in BRL, and 6 in the CIRL. The highest measured ChIA in this dataset was 67.9  $\mu\text{g/L}$ , lowest was 10.45  $\mu\text{g/L}$ , and the median was 15.7  $\mu\text{g/L}$ . For 28 of the 34 (82%), the estimated ChIA from both S2 and S3 sites were within 5  $\mu\text{g/L}$  of the measured ChIA. There was at least one clear outlier for both S2 and S3, which is likely the result of spatial variation between the sample collection location and sensor’s pixel. This low

level of ChIA error between the S2 and S3 sensors supports the interchangeability of their ChIA estimates in the IRL.

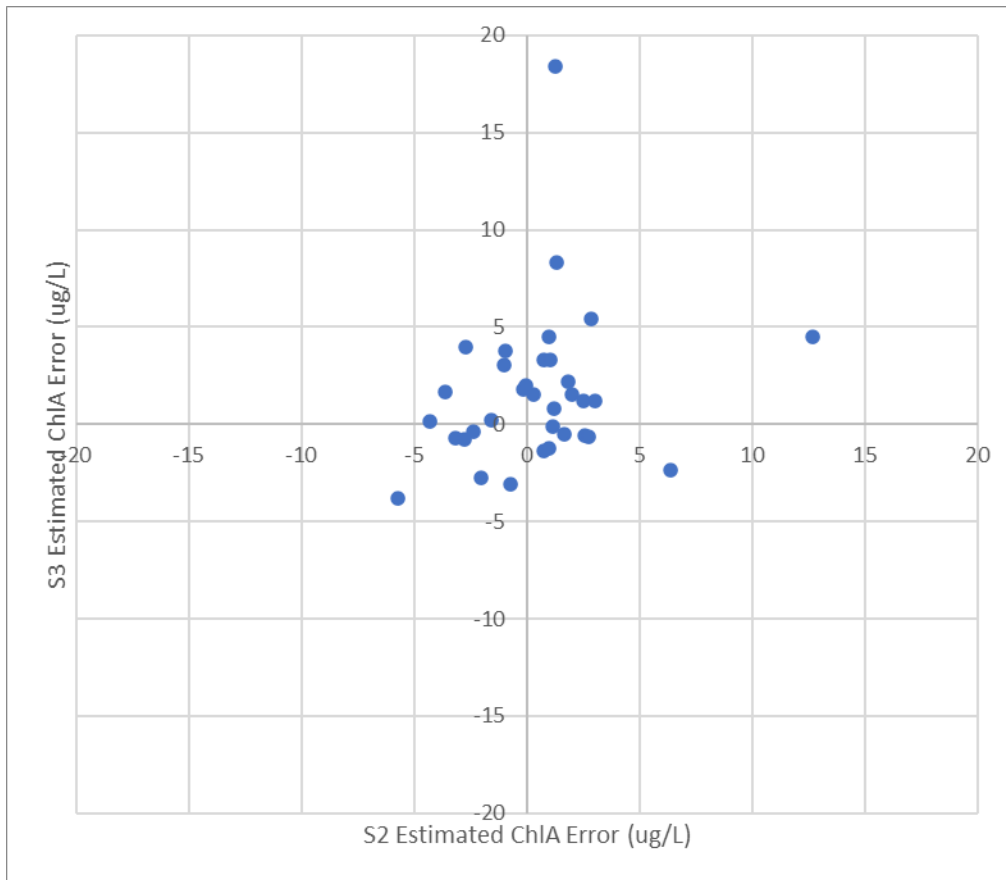


Figure 7. Comparison of the ChIA estimation error of S2 and S3 for synchronous sampling days. [Long Description of Figure 7.](#)

### 3.1.2 HYPERSPECTRAL CHLOROPHYLL WATER ESTIMATION

During this research, AEI performed 40 sampling events using the OceanInsight FLAME handheld hyperspectral photometer and the BaySpec OCI-F hyperspectral camera. Ten (10) of the FLAME sampling events and eighteen (18) of the BaySpec sampling events were collected at the same time as the SJRWMD surface water sampling events.

#### 3.1.2.1 FLAME

From the ten (10) SJRWMD FLAME sampling events, there were twenty-five (25) hyperspectral readings successfully collected fourteen (14) in the NIRL, eight (8) in the BRL, and three (3) in the CIRL. The highest ChIA concentration was 36.26  $\mu\text{g/L}$ , the lowest was 3.16  $\mu\text{g/L}$ , and the median 11.38  $\mu\text{g/L}$ . As expected, there was a strong peak reflectance around the 705 nm spectrum from the sample collected on July 7, 2022, at the SJRWMD sampling site I18 (**Figure 8**). For comparison, the reflectance collected on the same day at another location (I10) with minimal ChIA lacked this 705 nm peak as did a sample collected at the I18 site two months prior. This supports the conclusion that the NDCI can be applied to the FLAME data to create an estimate of ChIA.

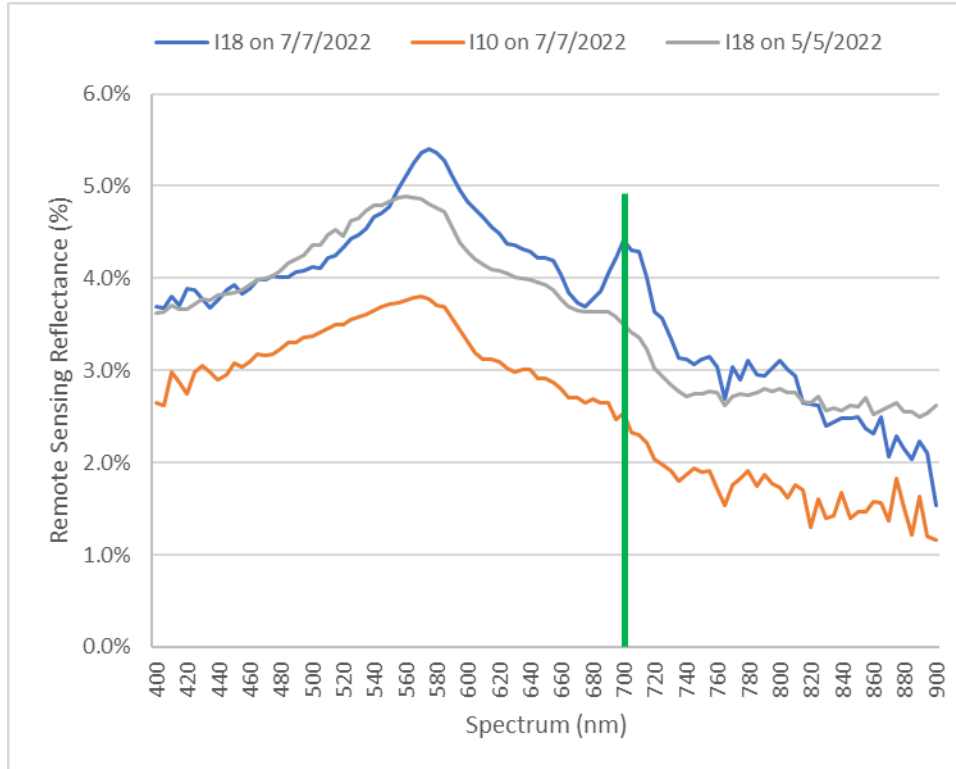


**Figure 8. Comparison of FLAME spectral signals from two SJRWMD sampling locations sampled the same day and the same location on different days. The green bar highlights the ChlA reflectance at 705 nm. [Long Description of Figure 8.](#)**

The FLAME NDCI algorithm regressed against the measured ChlA had a  $R^2$  of 0.66, RMSE of 4.96  $\mu\text{g/L}$ , Bias of 0.00  $\mu\text{g/L}$ , and a Nash criterion of 0.90 (**Table 9**). There did not appear to be any clear outlier points or trends within the dataset (**Figure 9**). Due to the lower range of ChlA concentrations in the calibration dataset, estimations of ChlA around the range of 60-80  $\mu\text{g/L}$  have a higher chance of error. While there was a low RMSE, little to no bias in the estimation of ChlA, and a high Nash criterion, because the FLAME had a lower  $R^2$  than the S2 and S3 NDCI estimations compared to actual measurement, further refinement of the FLAME method is recommended to improve its accuracy and validity. Potential sources of error could be from local variations in the ChlA concentration around the sampling site, as the spectral reading was taken from the bow of the boat and the SJRWMD grab sample from the stern. Additionally, as the SJRWMD water sampling was performed primarily in the mornings there was often insufficient ambient light to collect a hyperspectral measurement.

**Table 9. OceanInsight FLAME hyperspectral photometer NDCI calibration equation and performance metrics.**

Equation	$R^2$	RMSE	Bias	Nash
$\text{ChlA} = 1759.1(\text{NDCI})^2 + 247.92(\text{NDCI}) + 12.117$	0.66	4.96	0.00	0.90

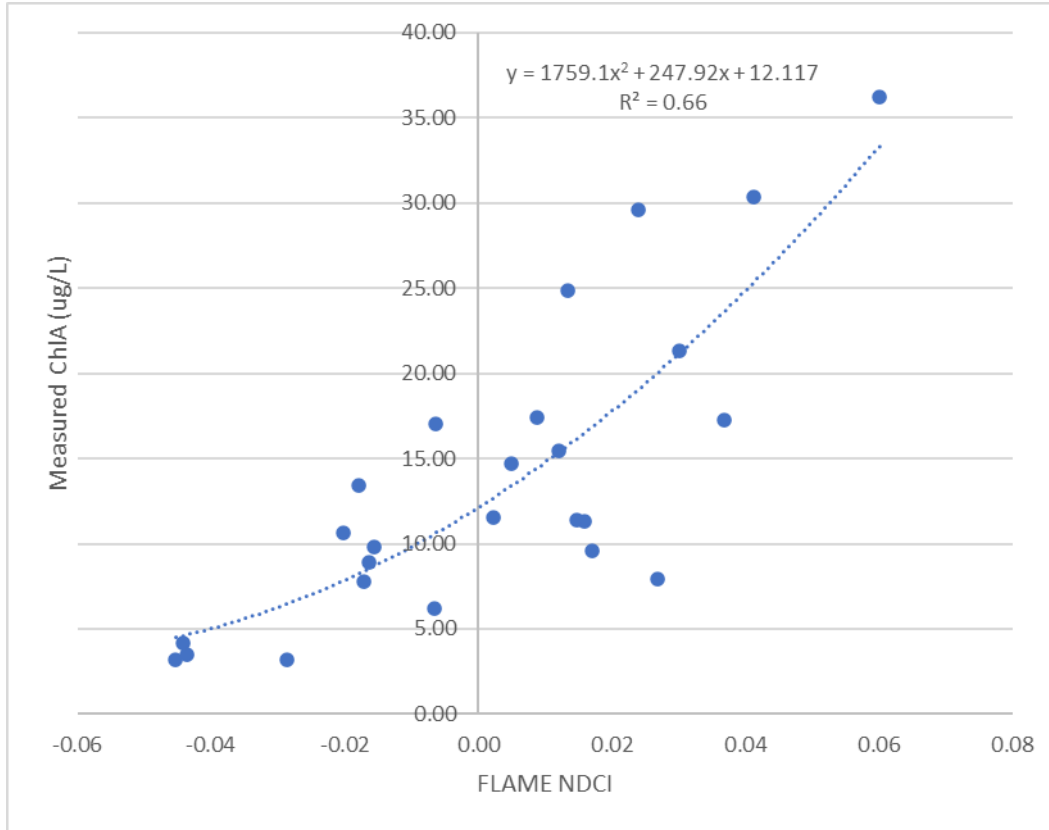


Figure 9. OceanInsight FLAME Normalized Difference Chlorophyll Index (NDCI) Calibration Dataset. [Long Description of Figure 9.](#)

### 3.1.2.2 BaySpec

There were thirty-one (31) hyperspectral readings successfully collected with the UAV mounted, BaySpec spectrometer in conjunction with SJRWMD water quality sampling events, including 14 in the NIRL, 5 in the BRL, and 12 in the CIRL. The highest ChIA concentration was 29.58  $\mu\text{g/L}$ , the lowest was 1.99  $\mu\text{g/L}$ , and the median was 6.11  $\mu\text{g/L}$ . As with the FLAME measurements, there was a strong peak reflectance around the 705 nm spectrum collected on November 1, 2022, at SJRWMD sampling site B04 where a bloom was occurring (**Figure 10**). For comparison, the reflectance collected almost 6 months prior during low ChIA conditions lacks the 705 nm peak. This supports the conclusion that the NDCI can be applied to the BaySpec data to create an estimate of ChIA.

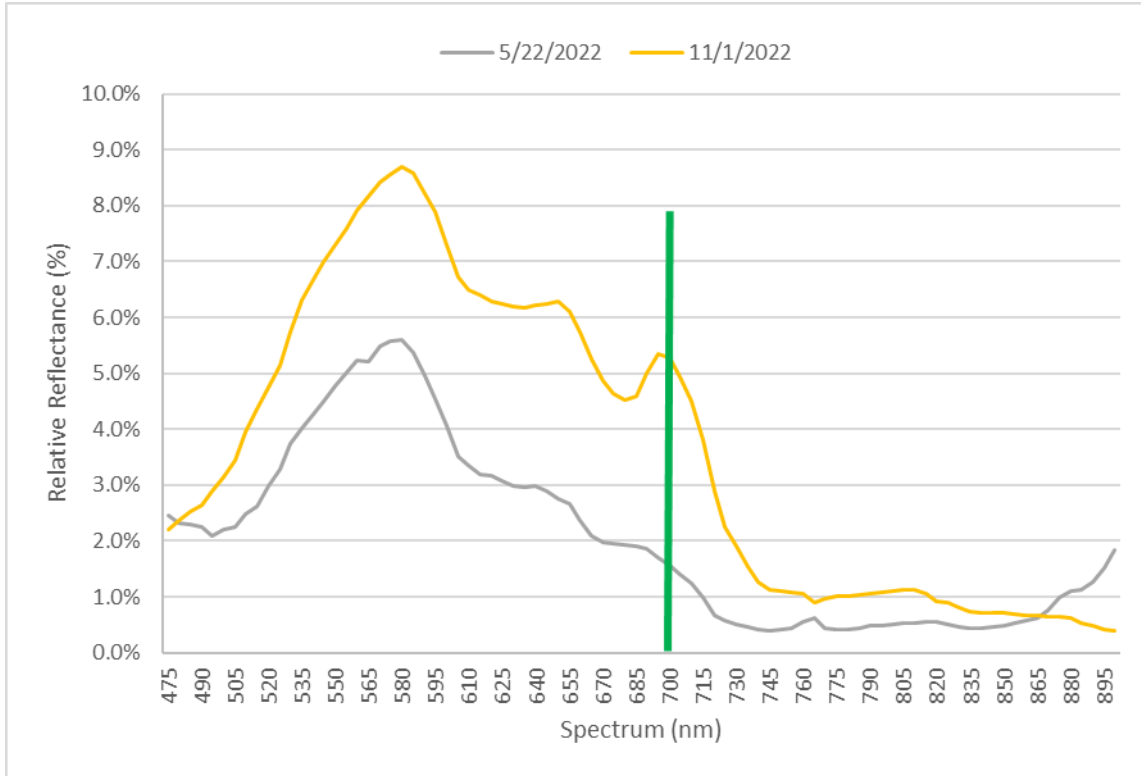


Figure 10. Comparison of BaySpec spectral signals from the same location (B04) on different days. The green bar highlights the ChlA reflectance at 705 nm. [Long Description of Figure 10.](#)

The BaySpec NDCI algorithm regressed against measured ChlA concentrations had a R2 of 0.53, RMSE of 3.98 µg/L, Bias of 0.00 µg/L, and a Nash criterion of 0.84 (Table 10). There did not appear to be any clear outlier points or trends within the dataset (Figure 11). Due to the lower range of ChlA concentrations in the calibration dataset, estimations of ChlA around the range of 60-80 µg/L are likely to have greater error.

Table 10. BaySpec OCI-F hyperspectral photometer NDCI calibration equation and performance metrics.

Equation	R <sup>2</sup>	RMSE	Bias	Nash
ChlA = 470.14(NDCI) <sup>2</sup> + 112.42(NDCI) + 10.546	0.53	3.98	0.00	0.84

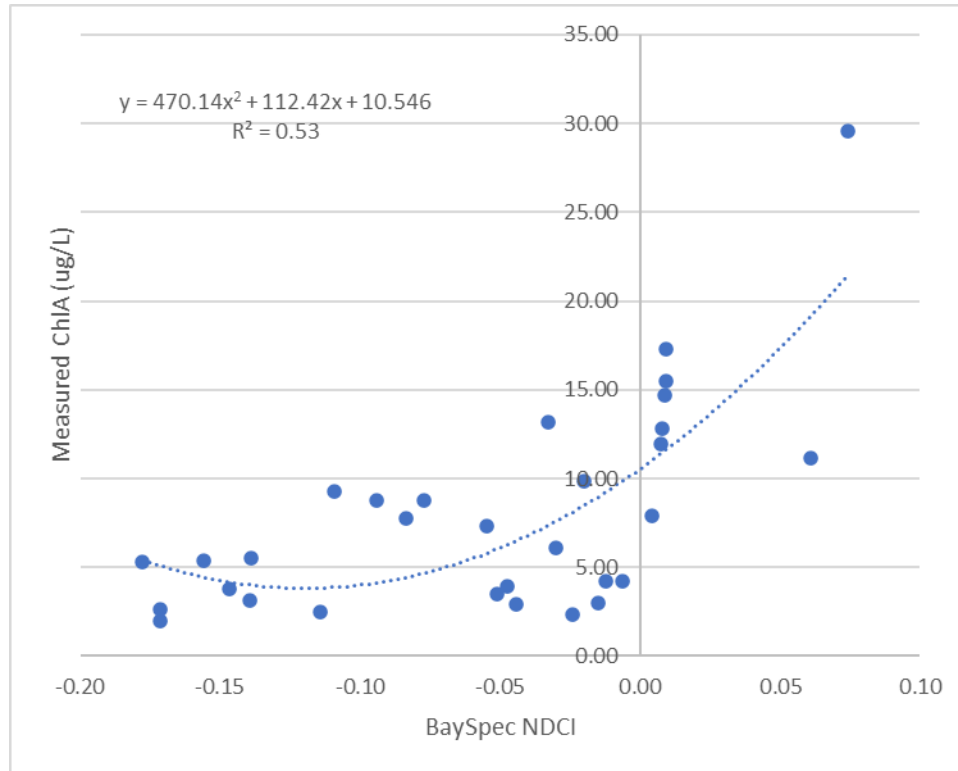


Figure 11. BaySpec OCI-F Normalized Difference Chlorophyll Index (NDCI) Calibration Dataset. [Long Description of Figure 11.](#)

While there was also a low RMSE, little to no bias in the estimation of ChlA, and a high Nash criterion in the comparison of BaySpec estimates and actual concentrations, the lower  $R^2$  suggests that further refinement of the use of the BaySpec for ChlA estimation is required to ensure valid and reproducible results. Potential sources of error could be due to local variations in the ChlA concentration around the sampling sites, differences between the time of the flyover and sample collection. Due to logistical constraints, every effort was made to ensure no more than 1 hour between sample collection and the UAV flyover. Additionally, as the SJRWMD water sampling was performed primarily in the mornings there was often insufficient ambient light to collect a hyperspectral measurement.

### 3.1.2.3 Hyperspectral and Sentinel NDCI Comparison

The compatibility of the NDCI estimated ChlA concentrations between the hyperspectral and Sentinel was evaluated by comparing their respective estimation errors to a SJRWMD surface water sample. In 2022 there were a total of fourteen (14) events where a FLAME measurement was collected within 24 hours of either a S2 or S3 overpass and a SJRWMD sample. For BaySpec there were a total of thirteen (13) events that were within 24 hours of either a S2 or S3 overpass and a SJRWMD surface water sample. There were no events when both FLAME and BaySpec measurements were within 24 hours of Sentinel overpasses and a SJRWMD surface water sample.

There were four (4) events when the FLAME and S2 measurements and ten (10) events when the FLAME and S3 measurements aligned with SJRWMD surface water samples (**Figure 12**). The SJRWMD

observed ChIA for these events ranged from 2.51 to 15.47  $\mu\text{g/L}$ . Thirteen (13) of the fourteen (14) events were collected within the NIRL, with one (1) in the BRL. Three (3) of the FLAME and S2 measurements and three (3) of the FLAME and S3 measurements were within 5  $\mu\text{g/L}$  of the SJRWMD measured ChIA concentration. There was a notable outlier with an S3 measurement having a -10.6  $\mu\text{g/L}$  error.

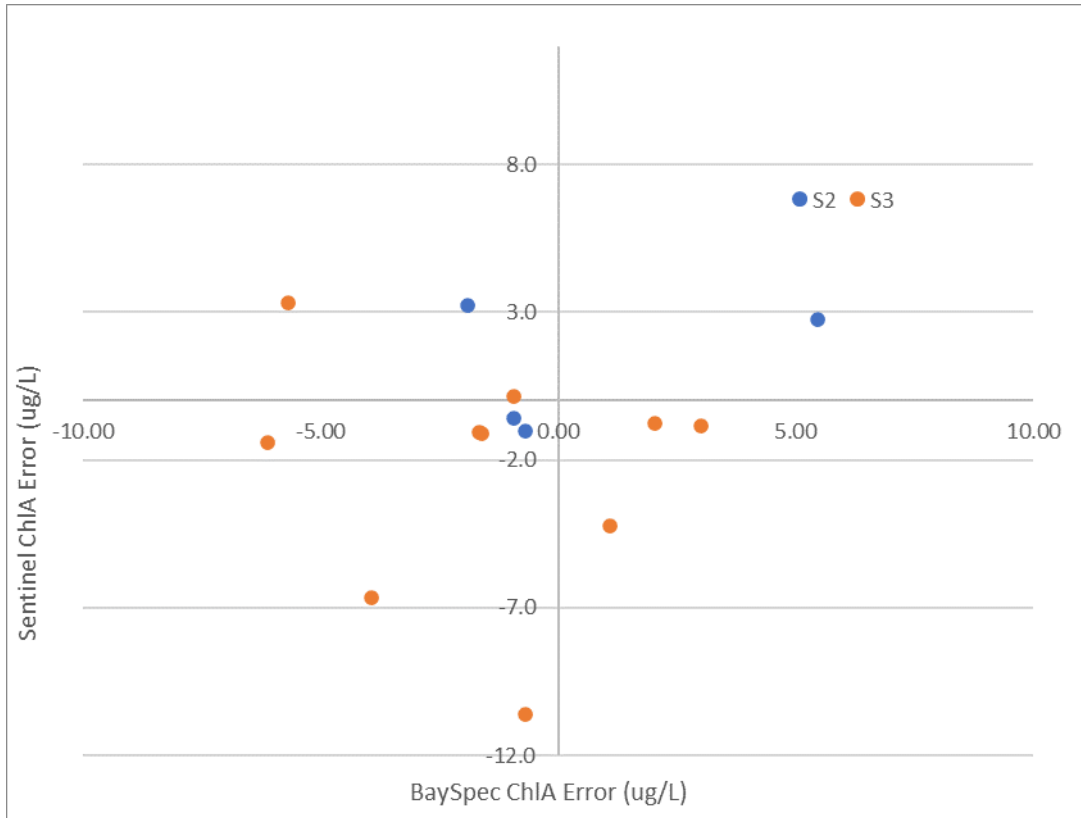


**Figure 12. Comparison of the ChIA estimation errors between synchronous Sentinel, FLAME, and SJRWMD measurements. [Long Description of Figure 12.](#)**

There were three (3) events when the BaySpec and S2 measurements aligned and ten (10) events when the BaySpec and S3 measurements aligned with SJRWMD surface water samples (**Figure 13**). Six (6) measurements were collected within the NIRL, one (1) in the SML, and five (5) in the BRL. The SJRWMD measured ChIA for these events ranged from 6.22 to 17.02  $\mu\text{g/L}$ .

None of the BaySpec and S2 measurements were within the 5  $\mu\text{g/L}$  marginal error of the SJRWMD ChIA. However, five (5) of the BaySpec and S3 measurements were within an error of 5  $\mu\text{g/L}$  of the SJRWMD ChIA. There does not appear to be a clear pattern between error of ChIA estimation.

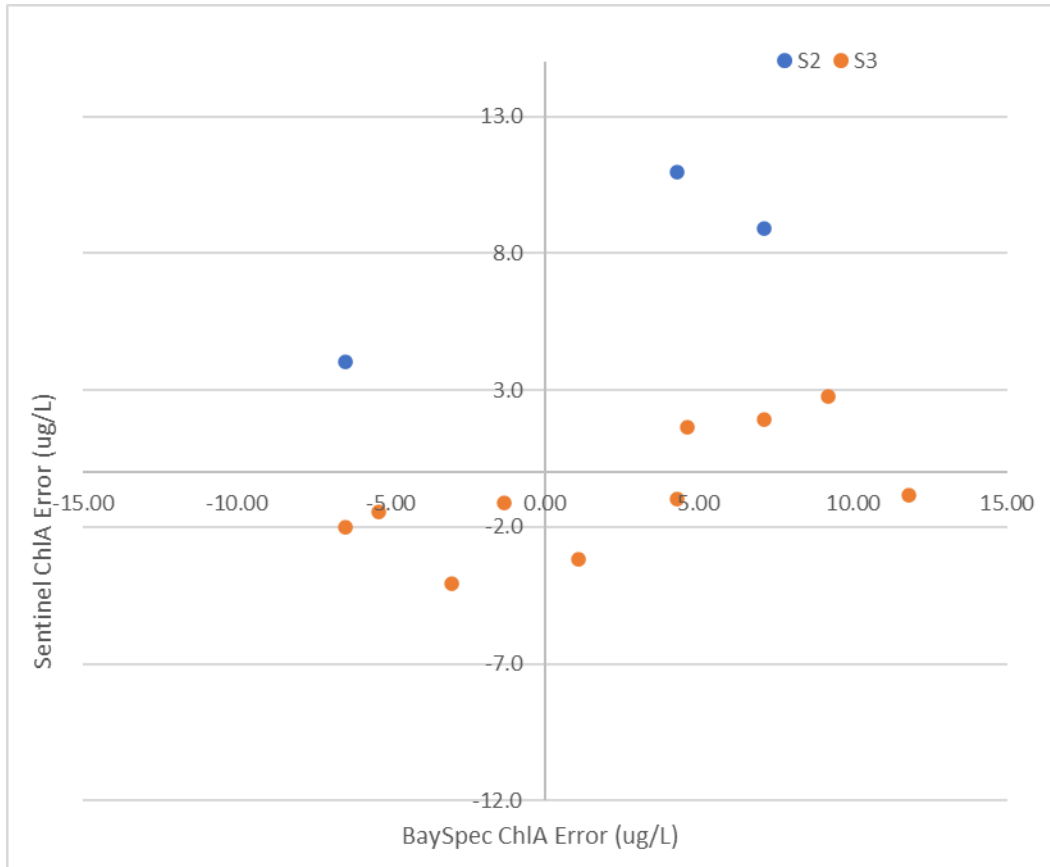


Figure 13. Comparison of the ChlA estimation errors between synchronous Sentinel, BaySpec, and SJRWMD measurements. [Long Description of Figure 13.](#)

Overall, there is general agreement between the FLAME and Sentinel satellites and between the BaySpec and Sentinel satellites regarding ChlA spectral features. It appeared that the FLAME measurements had better agreement, but due to both the small sample size and low ChlA concentrations, more measurements should be collected of higher ChlA concentrations to improve this analysis.

### 3.1.3 BENTHIC CONDITIONS REMOTE SENSING

#### 3.1.3.1 Hyperspectral

##### 3.1.3.1.1 FLAME

Of the 22 benthic sampling events, *Caulerpa Prolifera* was the only Submerged Aquatic Vegetation (SAV) found in abundance. There was a total of 9 FLAME readings collected over dense *Caulerpa* beds when the water had low turbidity (<5 NTU). As *Caulerpa* contains ChlA, it has a similar reflectance and absorption as phytoplankton (650 - 705 nm). This overlap could lead to overestimations of water column ChlA concentration by Sentinel remote sensing. As the *Caulerpa* is distinct from open sand and muck benthic types, it can be identified by the NDCI during low phytoplankton conditions (**Figure 14**). There were 3 FLAME readings over IRL muck, all from the mouth of Turkey Creek.

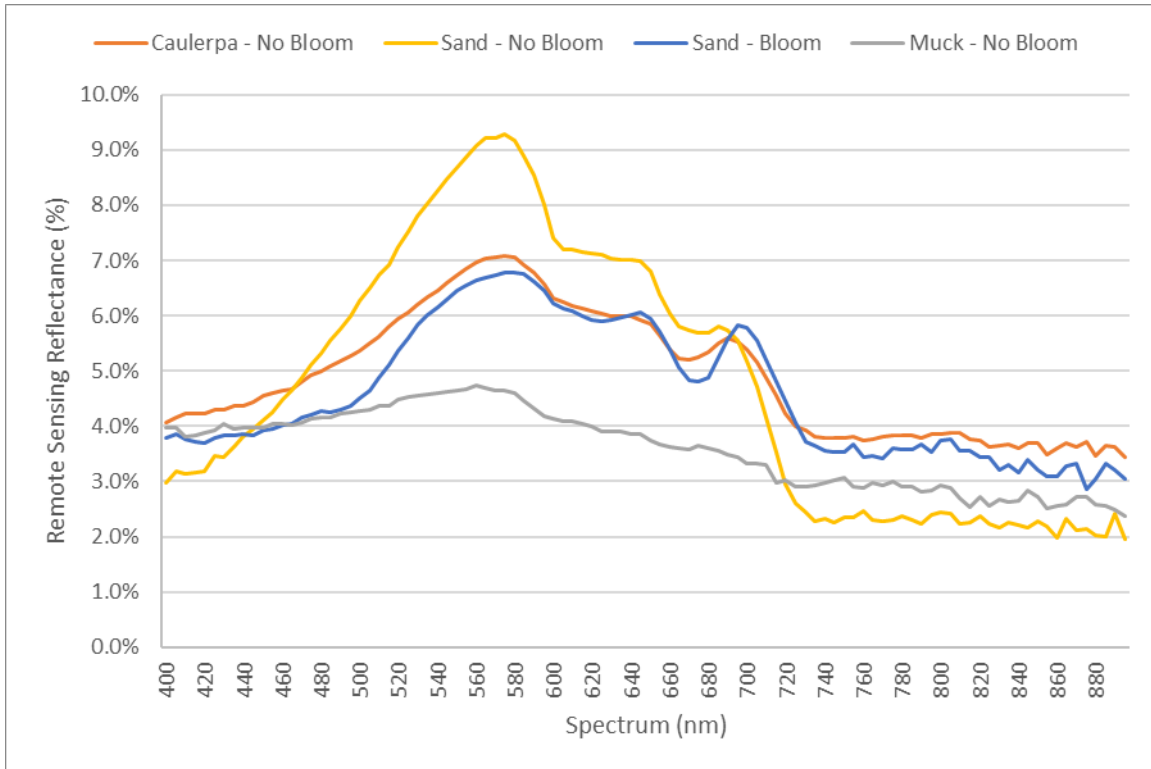


Figure 14. Comparison of *Caulerpa Prolifera* FLAME reflectance to open sand with and without bloom conditions, as well as muck sediment.  
[Long Description of Figure 14.](#)

A subset of these signatures is highlighted in **Figure 15** to demonstrate the impact of water depth on the reflectance of the *Caulerpa*. At shallower depths, there appears to be a small reflectance peak around 640 nm. Additionally, the 705 peak appears to shift towards 650 with increasing depths. Based on the FLAME readings, there does not appear to be a significant difference between the reflectance of phytoplankton and *Caulerpa* ChlA.

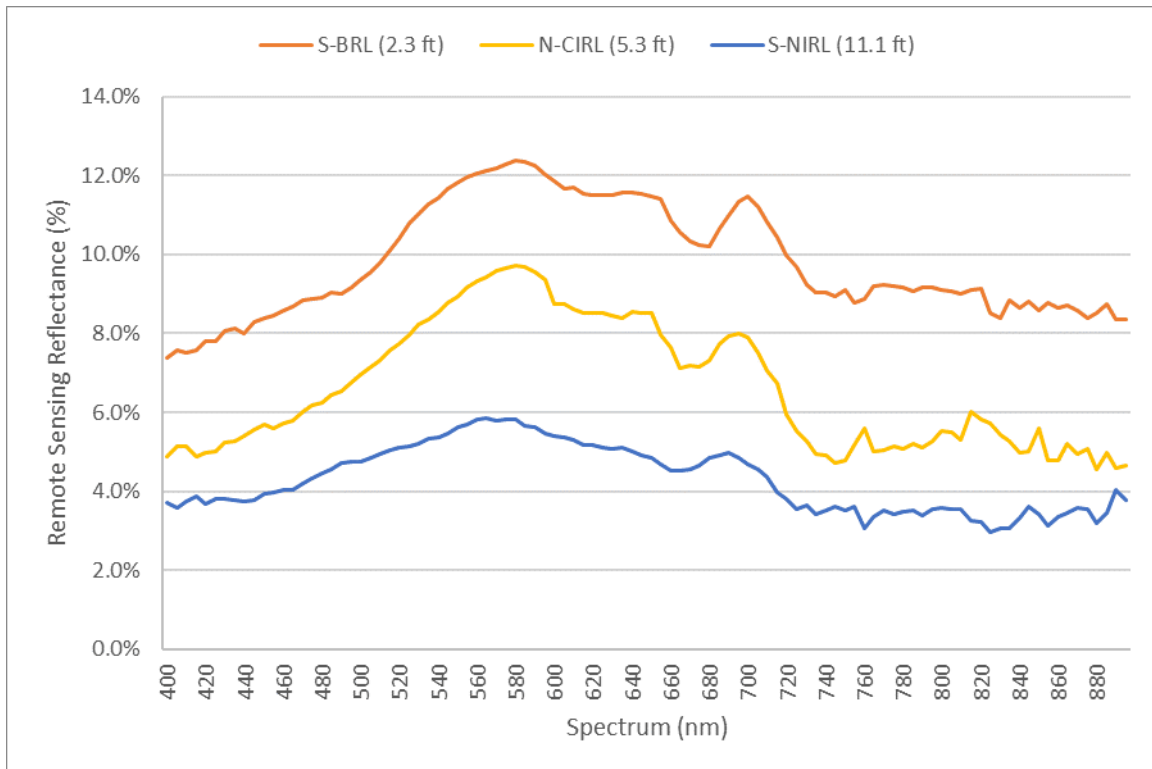


Figure 15. Comparison of the dense *Caulerpa Prolifera* FLAME reflectance to water depth. [Long Description of Figure 15.](#)

There were three types of benthic sediments encountered during the study: clean sand, mucky sand, and the IRL muck (**Figure 16**). Of these three sediment types, the clean sand had the strongest reflectance with well-defined peaks across the spectrum (**Figure 17**). The difference in mucky sand and IRL muck reflectance were minor, with the mucky sand having more pronounced reflectance peaks between 600 and 705 nm. The lack of a strong difference between these two benthic types suggests that classification at higher spectral and spatial resolutions may not be viable.



Figure 16. Example IRL benthic sediments. A depicts clean sand with low organics. B depicts a mixture of sand, shell hash, and organics. C depicts the highly organic IRL muck. [Long Description of Figure 16.](#)

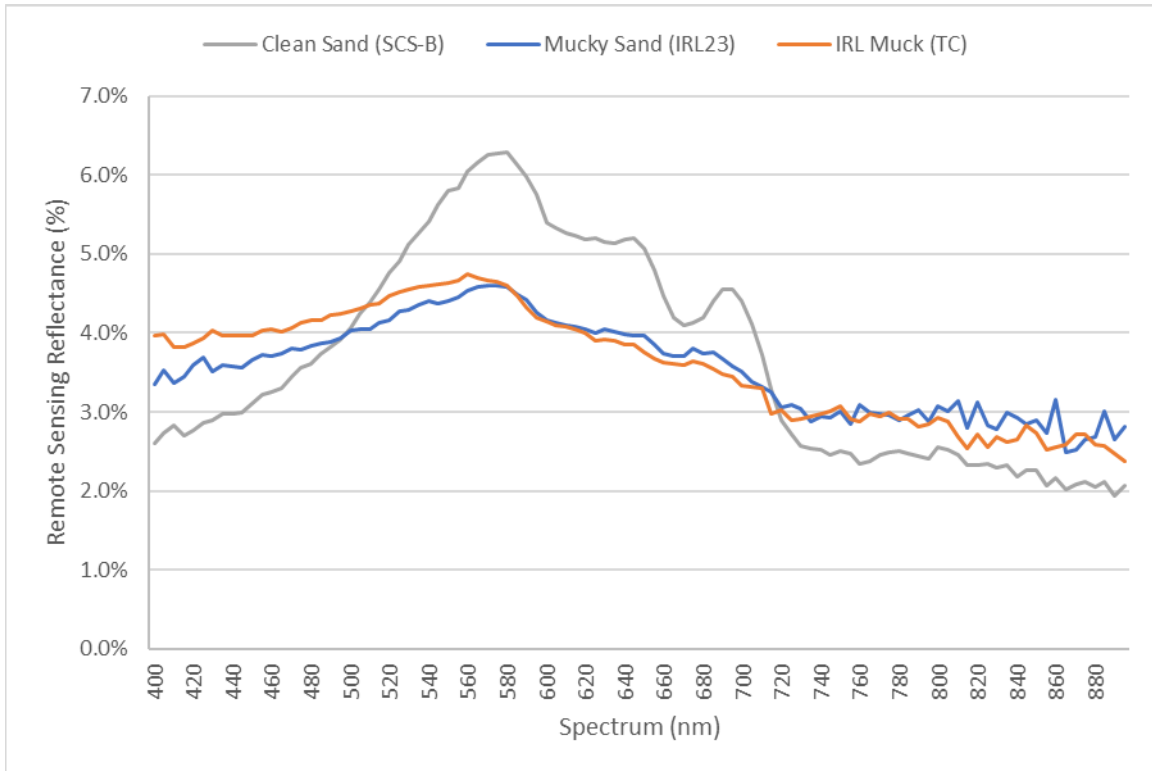


Figure 17. Comparison of IRL sediment FLAME reflectance for clean sand, mucky sand, and IRL muck. [Long Description of Figure 17.](#)

### 3.1.3.1.2 BaySpec

From the 22 benthic sampling events, a total of 50 field confirmed *Caulerpa* beds were extracted from the BaySpec imagery with low turbidity (<5 NTU). Similar to the FLAME measurements, the *Caulerpa* 705 nm reflectance peak overlaps with the phytoplankton peak and no significant difference was found between the reflectance of phytoplankton and *Caulerpa* Ch1A.

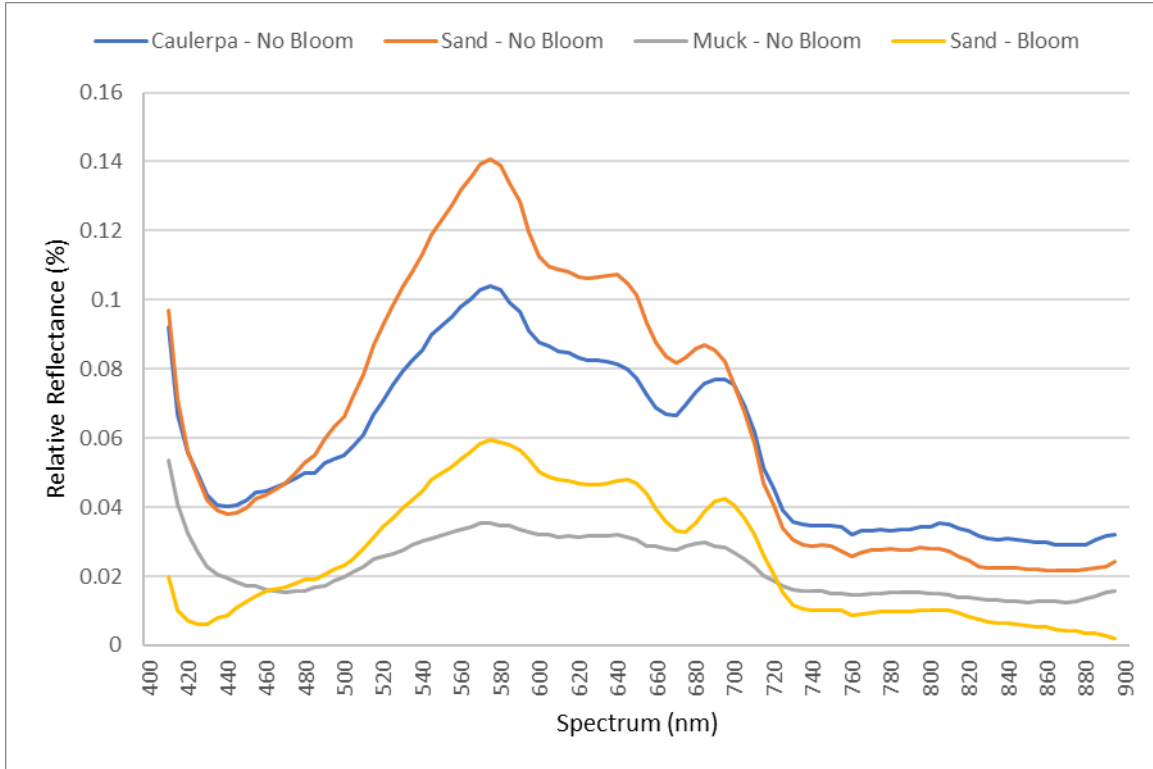


Figure 18. Comparison of *Caulerpa Prolifera* BaySpec reflectance to open sand with and without bloom conditions, as well as muck sediment.  
[Long Description of Figure 18.](#)

**Figure 19** is an example flight of the BaySpec over Sykes Creek on October 12, 2022. This example highlights the impact of the *Caulerpa* beds on the estimation of water column ChlA. The western portion of the flight path includes the shallowest point that *Caulerpa* was observed (2.3 ft), and here the NDCI estimated ChlA was 30 µg/L. Following the path from west to east, the depth increases to 5.4 ft and the *Caulerpa* influence on the NDCI decreases. This mirrors the findings of the FLAME observation of *Caulerpa* beds at increasing depths. Additionally, the change in depth demonstrates the impact of water depth where there are sandy bottoms, showing higher estimated ChlA in shallow water than the deeper water to the east. While the presence of *Caulerpa* complicates the estimation of water column ChlA, under low phytoplankton conditions the NDCI could be used to map the SAV coverage in the IRL.

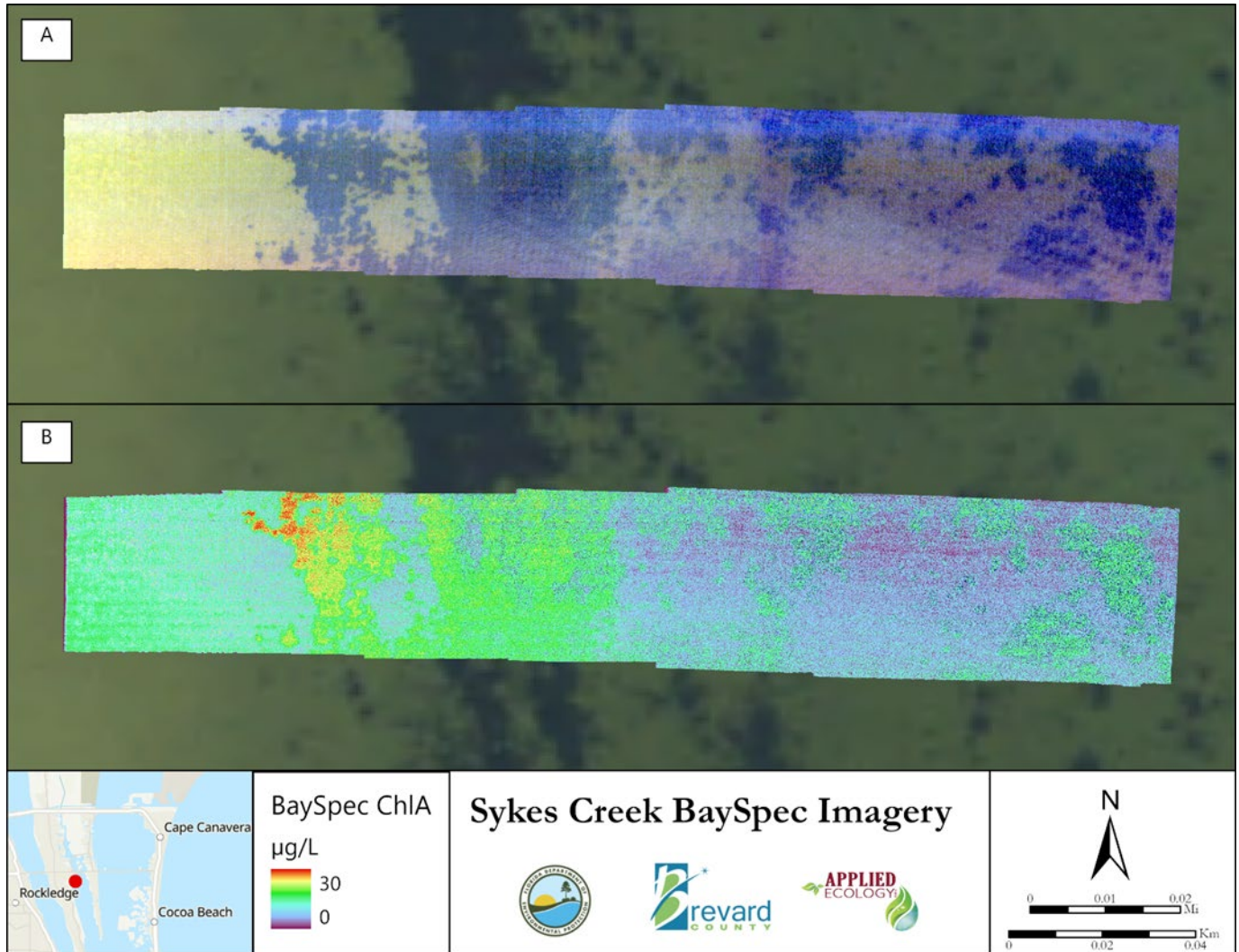


Figure 19. Sykes Creek BaySpec imagery collected on October 12, 2022. The true color image is presented in panel A and the estimated ChlA concentration is presented in panel B. [Long Description of Figure 19.](#)

### 3.1.4 CYANOBACTERIA IN THE IRL

Between 2019 and 2023, *picrocyanobacteria* and *synechococcus* were the most observed cyanobacteria (CB) in the IRL. Of the 150 sampling days, *Picrocyanobacteria* was observed 150 times, *synechococcus* was observed 149 times, and followed by *cyanobium* with 33 observations.

The abundance of CB has varied across time and space within the IRL (**Figure 20, Figure 21**). A prolonged CB bloom in 2020 was focused in the BRL whereas in 2019 and 2020 CB blooms were more frequent in the SML and NIRL. The North CIRL was the only segment to have consistently low CB dominated blooms. The blooms of 2020 included the longest period that *cyanobium* was observed in the lagoon with 26 consecutive events from August 2020 to March 2021.

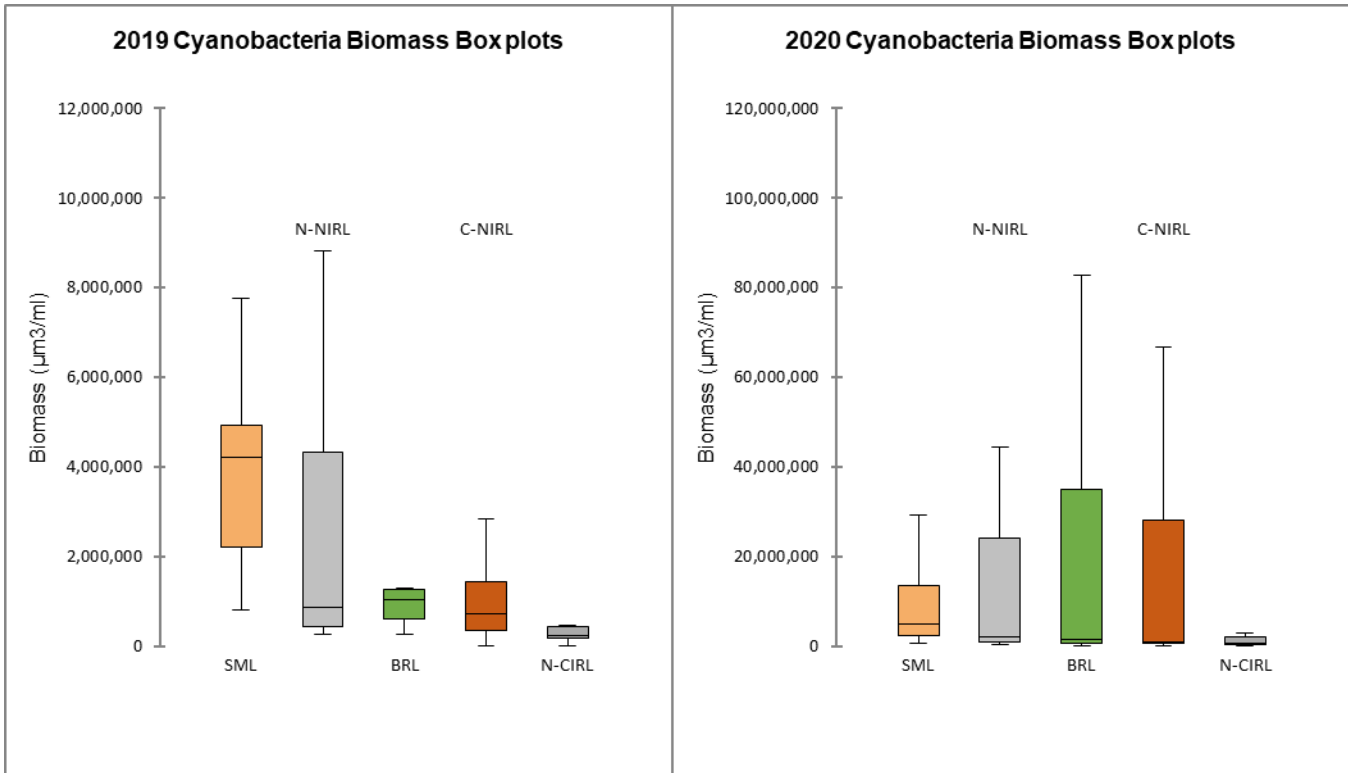


Figure 20. Boxplots of the cyanobacteria biomass for 2019 and 2020 by lagoon segment. The scales of the two years are not equal, 2020 is an order of magnitude larger than 2019. [Long Description of Figure 20.](#)

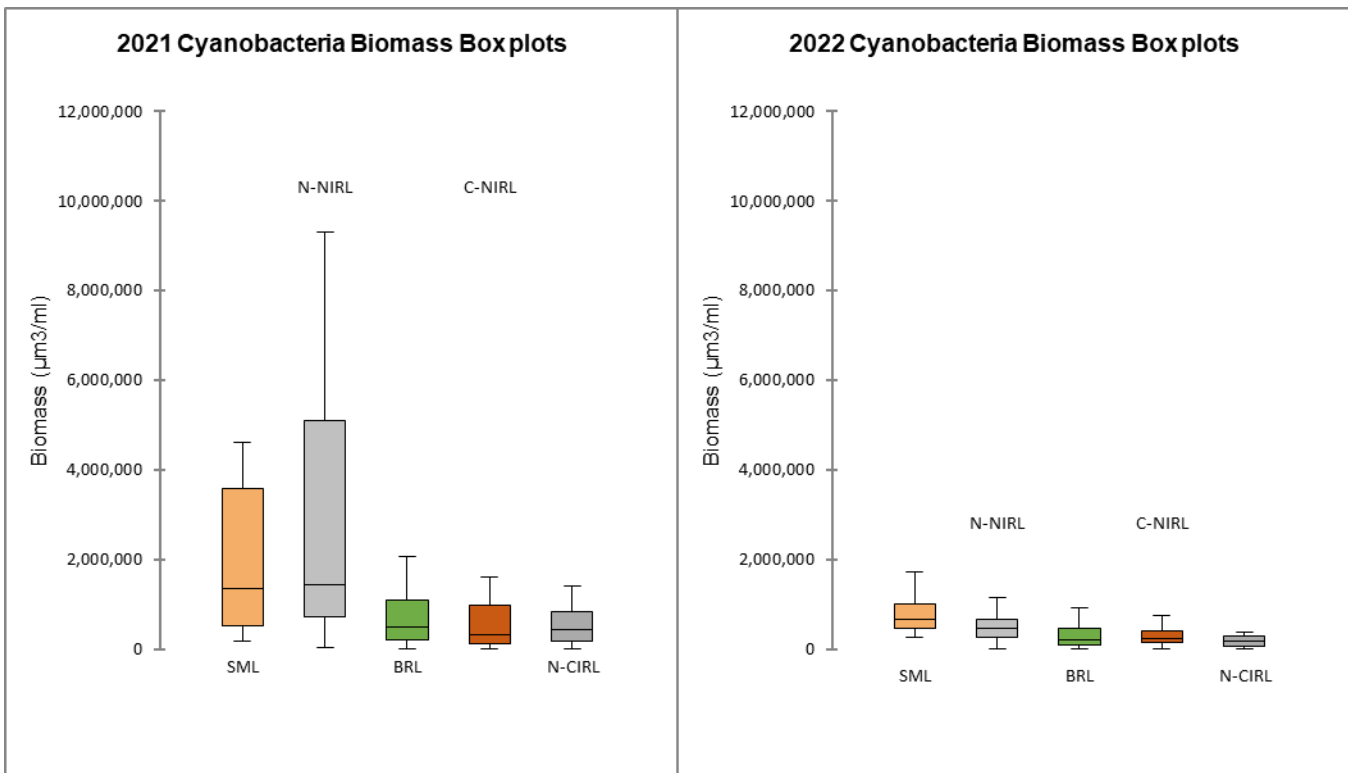


Figure 21. Boxplots of the cyanobacteria biomass for 2021 and 2022 by lagoon segment. [Long Description of Figure 21.](#)

### 3.1.4.1 Distinguishing HAB species with Hyperspectral Imagery

#### 3.1.4.1.1 FLAME

A total of 3 FLAME sampling events were completed in areas with similar benthic conditions when there was measurable phytoplankton (>10 µg/L) in the water column and an algal enumeration sampling event was occurring. Two of the samples were dominated by eukaryotic phytoplankton, *Pyrodinium bahamense* on 9/26/2022 in the NIRL3 segment and *Akashiwo sanguinea* on 1/6/2023 in the NIRL8 segment. One sample was dominated by the CB *Picocyanobacteria spp.* in the BRL4 on 12/7/2022, The three CB algorithms were applied to the averaged spectral data to generate representative index values (**Table 11, Figure 22**). As there were insufficient samples to perform statistical analysis, a qualitative assessment was performed.

The two key characteristics of these indices are to differentiate PC and ChlA dominated blooms, while resisting the cross-correlation with ChlA concentration. In the eukaryotic *P. bahamense* and *A. sanguinea* blooms, there was less than 10% CB biomass in the samples. The 3BDA-PC values for those two samples should have been similar as they would have had less PC present, however the *A. sanguinea* sample was closer to that of the CB. Both the 2BDA-PC and NDPCI algorithms appeared to have an increased index value in comparison to increased ChlA. There may also be a measurable PC reflectance peak around 650 nm, however no publicly available satellite sensor currently covers that spectrum. Due to the lack of additional samples, a strong conclusion cannot be reached regarding the best performing algorithm.

**Table 11. Average CB algorithm values for the three FLAME sampling events.**

Algorithm	Picocyanobacteria spp.	Pyrodinium bahamense	Akashiwo sanguinea
2BDA-PC	1.27	1.15	1.12
3BDA-PC	-0.0014	-0.0005	-0.0010
NDPCI	0.12	0.07	0.05
ChlA (NDCI)	33.7	22.4	19.1
Biomass CB	5,051,153	353,724	428,306
Biomass Total	5,629,705	6,176,660	34,066,435

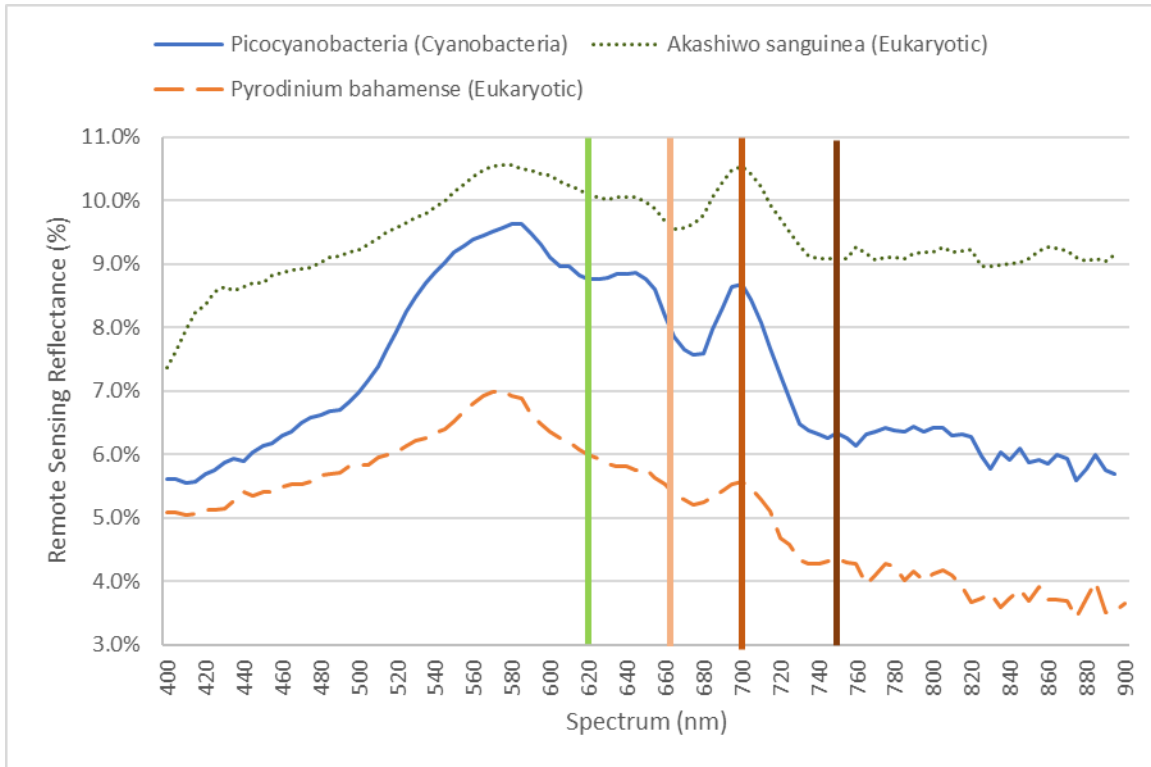


**Figure 22. Comparison of the FLAME hyperspectral readings of eukaryotic and cyanobacteria phytoplankton blooms in the Indian River Lagoon. The four spectra related to Phycocyanin and Chlorophyll A are highlighted by vertical bars, from left to right, 620, 665, 705, and 755 nm. [Long Description of Figure 22.](#)**

### BaySpec

There was a total of 4 sampling events using the UAV mounted BaySpec spectrometer that coincided with measurable phytoplankton ( $>10 \mu\text{g/L}$ ), an algal enumeration sample, and consistent benthic conditions. The dominant phytoplankton in these samples was the eukaryotic *Pyrodinium bahamense* on 9/26/2022 in the NIRL3 segment, the CB *Picocyanobacteria spp.* in BRL4 on 12/7/2022, eukaryotic *Akashiwo sanguinea* on 1/6/2023 in the NIRL8, and eukaryotic *Ceratium furca* in BRL6 on 3/7/2023. The three CB algorithms were applied to the averaged spectral data to generate representative index values (**Table 12, Figure 23**). As there were insufficient samples to perform statistical analysis, a qualitative assessment was performed.

In comparison to the FLAME indices, the 2BDA-PC and NDPCI had similar behavior with the CB dominated sample having the largest index value of all the samples. Also, the BaySpec 3BDA-PC index appeared to differentiate between CB dominated samples than the FLAME. Due to the lack of additional samples, a strong conclusion cannot be reached regarding the best performing algorithm.

Table 12. Average CB algorithm values for the four BaySpec sampling events.

Algorithm	Picocyano bacteria spp.	Pyrodinium bahamense	Akashiwo sanguinea	Ceratium furca
2BDA-PC	1.07	0.89	0.93	0.73
3BDA-PC	-0.00003	0.00020	0.00046	0.00007
NDPCI	0.04	-0.06	-0.04	-0.15
ChIA (NDCI)	42.4	32.7	19.8	6.3
Biomass CB	5,051,153	353,724	428,306	985,591
Biomass Total	5,629,705	6,176,660	34,066,435	3,008,806

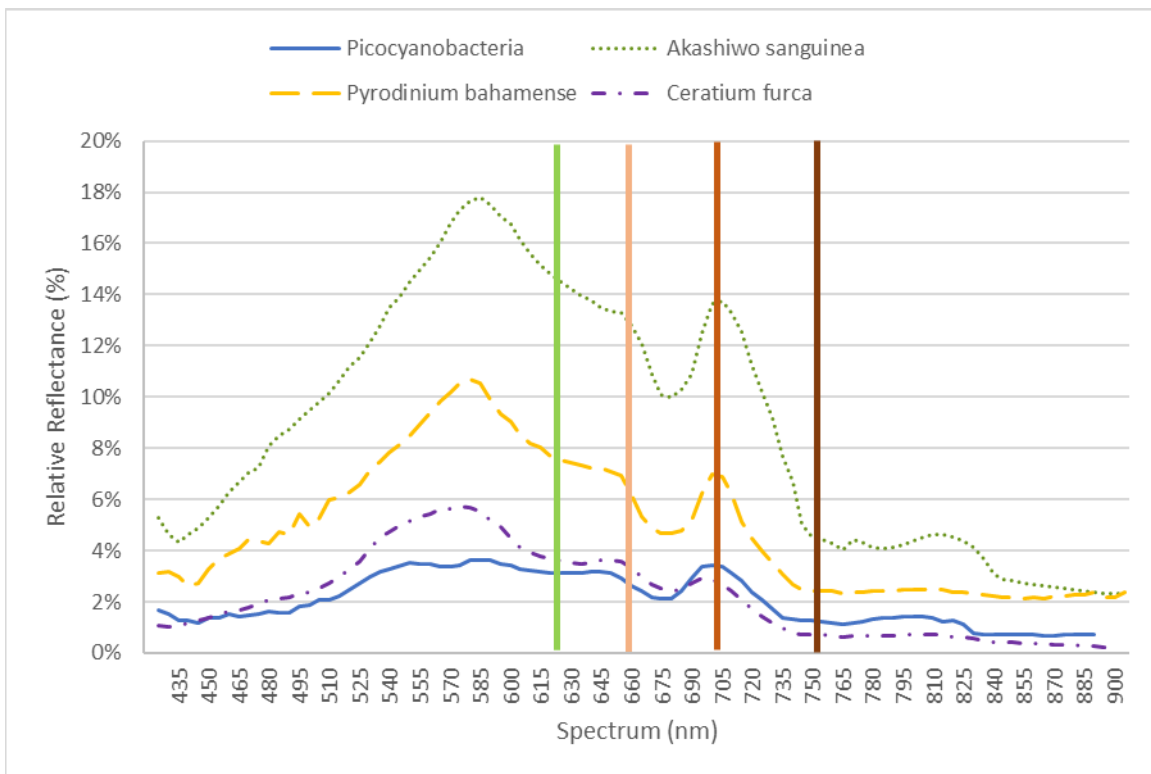
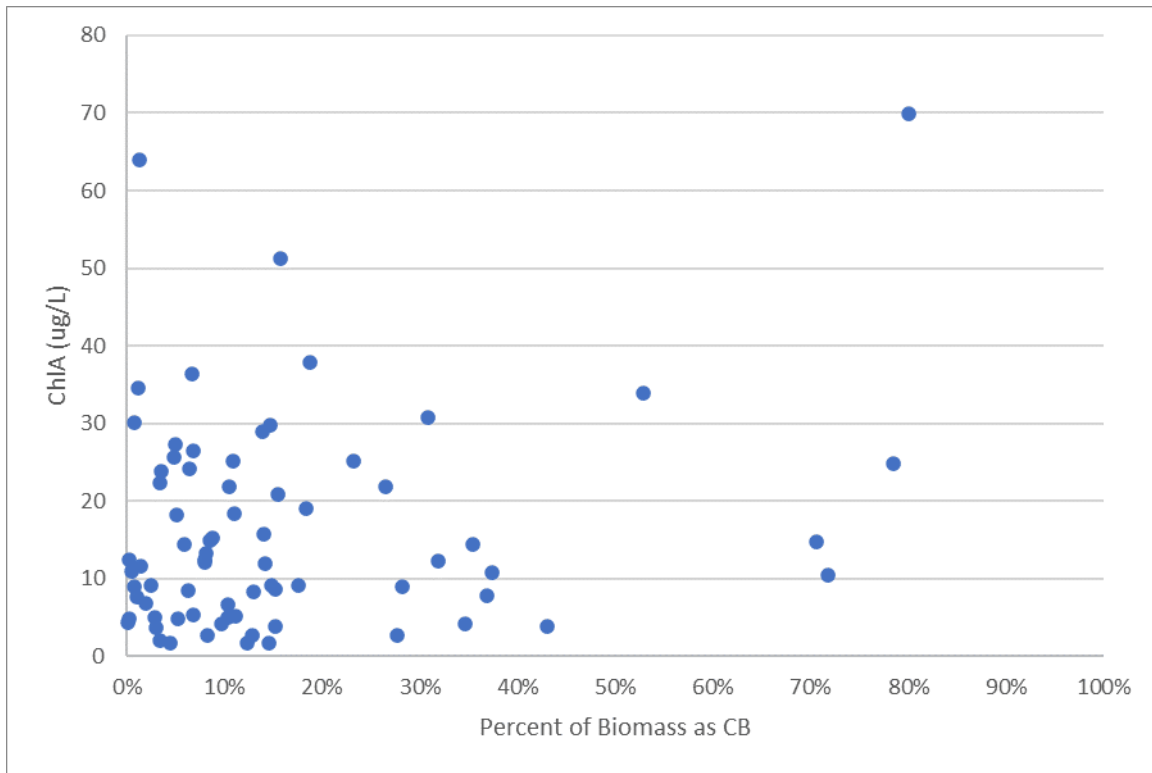


Figure 23. Comparison of the BaySpec hyperspectral readings of eukaryotic and cyanobacteria phytoplankton blooms in the Indian River Lagoon. The four spectra related to Phycocyanin and Chlorophyll A are highlighted by vertical bars, from left to right, 620, 665, 705, and 755 nm. [Long Description of Figure 23.](#)

### 3.1.4.2 Distinguishing HAB species with Multispectral

The assessment of the CB estimation algorithms was performed on S3 data due to the higher spectral resolution of its bands as well as specific bands targeted to CB spectral features. The dataset contained a total of 86 points including 17 points in Mosquito Lagoon, 24 in NIRL, 32 in Banana River, and 13 in CIRL with ChIA concentrations that ranged from 1.7 to 69.9  $\mu\text{g/L}$  and a median value of 12.1  $\mu\text{g/L}$ . The percentage of the phytoplankton biomass as CB ranged from 80.1% at the highest, 0.1% at the lowest, and a median of 10.4%, demonstrating that this subset represents the full range of

measurements in the measured dataset. There does not appear to be a relationship between the ChlA concentration and the percent CB biomass (**Figure 24**).



**Figure 24. Comparison of the measured ChlA concentrations to the percent of the sample’s biomass as cyanobacteria. [Long Description of Figure 24.](#)**

A comparison of a single high CB biomass bloom (ML02) and a low CB biomass bloom (NFH01S) was performed to evaluate the CB estimation algorithms in various conditions (**Table 13, Figure 25**). ML02 had a ChlA concentration of 69.9 µg/L and a CB biomass percentage of 80.1%, which was dominated by a mixture of *Cyanobium* and *Synechococcus* as determined by the UF Philips lab. NFH01S had a similarly high ChlA of 63.9 µg/L but a CB biomass percentage of 1.3%, which was dominated by the eukaryote *Cerataulina pelagica*. All three of the algorithms had larger index values for the CB dominated sample having higher values. The 3BDA-PC algorithm was the inverse of what was expected, as a CB dominated sample would have more PC absorption which should result in a lower 620 nm reflectance relative to the ChlA 705 nm reflectance. The 3BDA-PC algorithm was not evaluated for the full calibration dataset.

**Table 13. Sentinel-3 CB for a high Cyanobacteria (CB) and a low CB bloom.**

Site	Date	ChlA (µg/L)	% CB	2BDA PC	3BDA PC	NDPCI
ML02	12/02/2020	69.9	80.1%	0.92	11.00	-0.04
NFH01S	01/04/2021	63.9	1.3%	0.78	8.08	-0.12

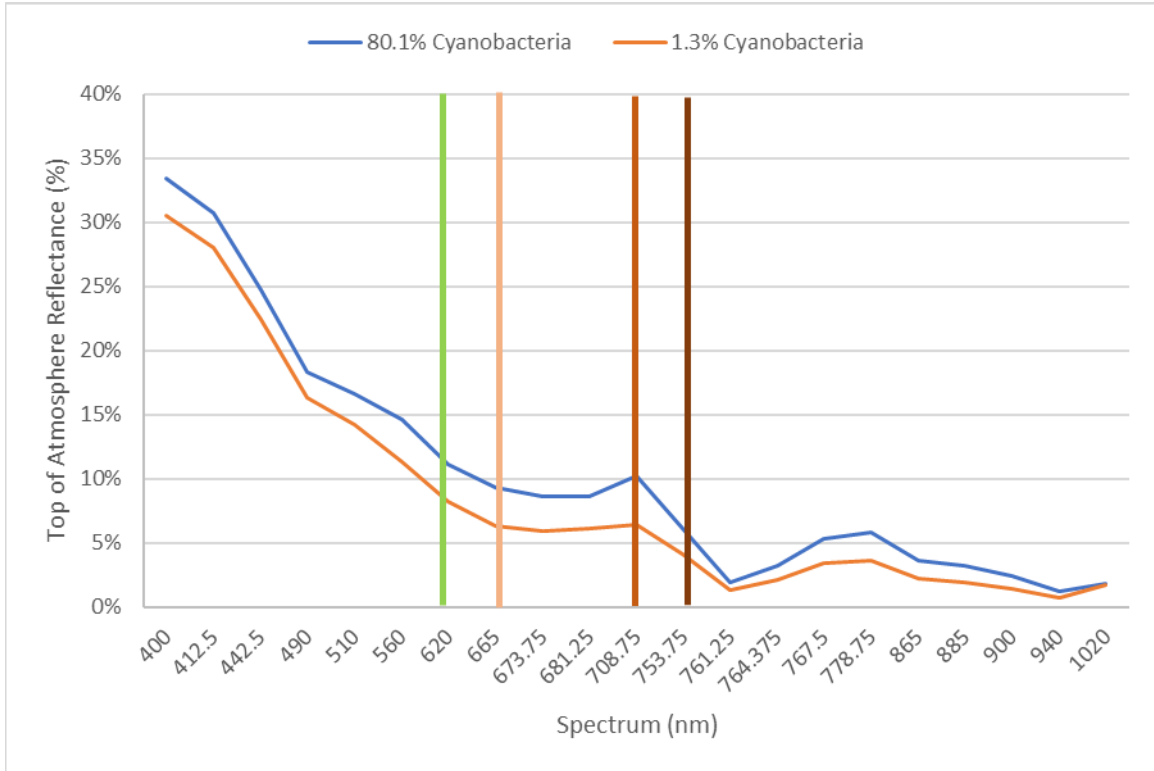


Figure 25. Sentinel 3 spectral comparison of low and high cyanobacteria (CB) biomass blooms. [Long Description of Figure 25.](#)

For the calibration dataset, both the 2BDA-PC and NDPCI algorithms had a low but significant ( $p < 0.0001$ )  $R^2$  of 0.23 and 0.22, respectively. However, after the application of a ChIA filter, removing concentrations below 10  $\mu\text{g/L}$ , a stronger correlation was identified. This filter reduced the calibration dataset from 86 to 17 points, which resulted in an increased median ChIA of 25.22  $\mu\text{g/L}$  and a moderately strong  $R^2$  of 0.66 and 0.65 ( $p < 0.0001$ ) and no obvious outliers (**Figure 26, Figure 27**). The RMSE, Bias, and Nash criterion between the two algorithms was practically the same. With 2BDA-PC and NDPCI RMSE's of 11.5% and 11.7% then Bias of -2% and -1%, respectively. Both algorithms had a Nash criterion of 0.99. For this calibration dataset, either of the equations could be used with S3 and have similar estimates of CB concentrations.

Table 14. Sentinel 3 CB calibration statistics for the 2BDA-PC and NDPCI algorithms with ChIA more than 10  $\mu\text{g/L}$ .

Algorithm	Algorithm	$R^2$	RMSE	Bias	NSE
2BDA-PC	$y = 22.189x^2 - 32.932x + 12.304$	0.66	11.5%	-2%	0.99
NDPCI	$y = 62.256x^2 + 18.353x + 1.4321$	0.65	11.7%	-1%	0.99

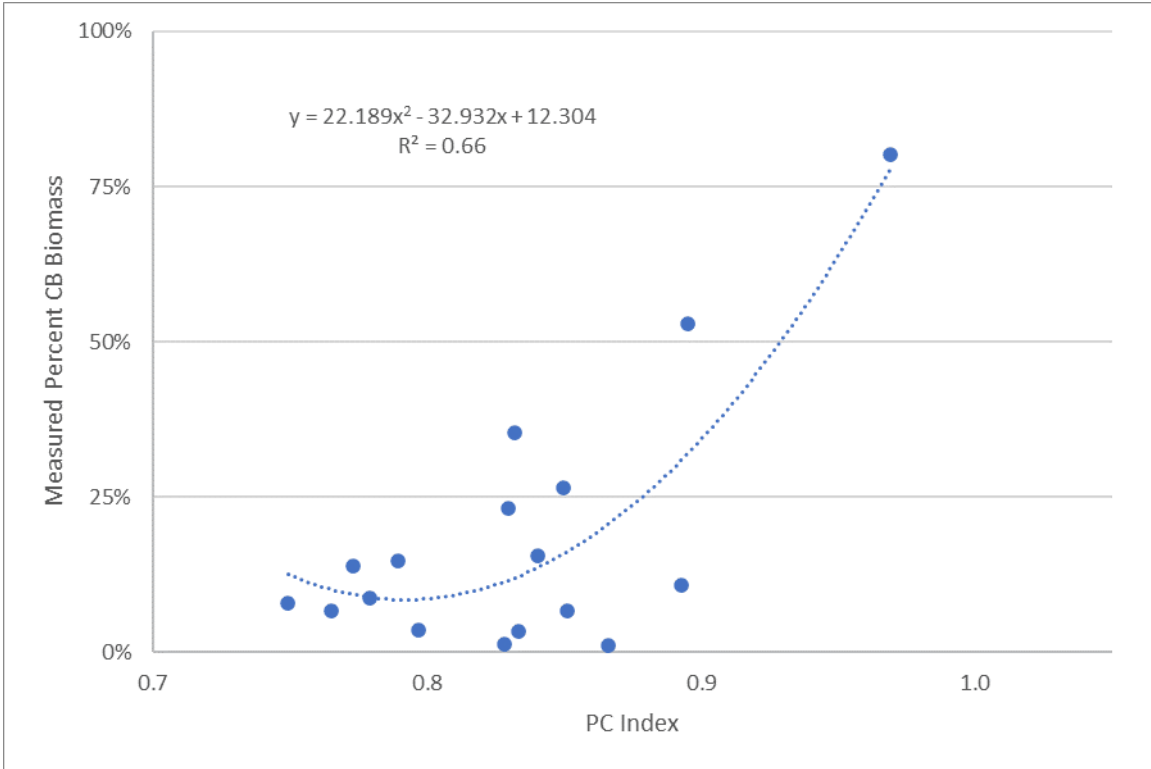


Figure 26. Comparison of the Sentinel 3 (S3) 2BDA-PC index to the measured cyanobacteria (CB) biomass at SJRWMD sampling sites with ChlA more than 10 µg/L. [Long Description of Figure 26.](#)

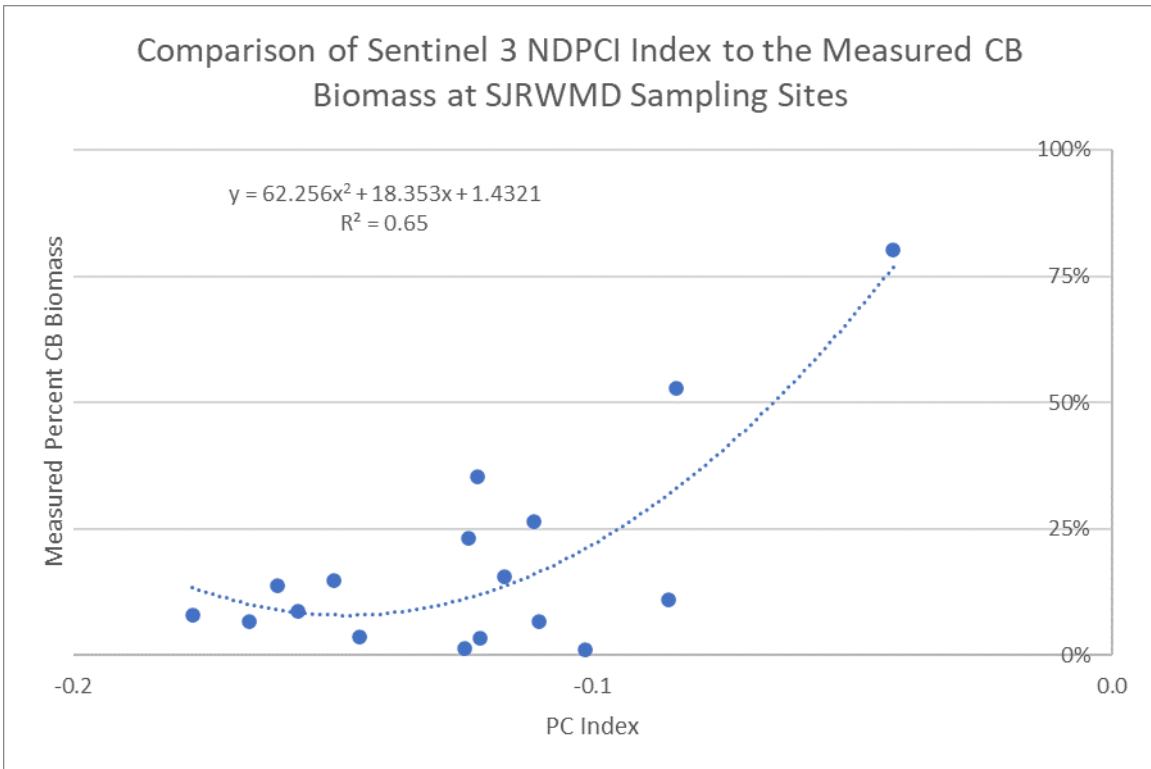


Figure 27. Comparison of the Sentinel 3 (S3) NDPCI index to the measured cyanobacteria (CB) biomass at SJRWMD sampling sites. [Long Description of Figure 27.](#)

Due to the identical performance by the two CB estimation algorithms with the reduced dataset, it is unclear which is the better performing algorithm. However, as the normalized difference of the NDPCI was intended to improve performance over a range of days and atmospheric conditions, this could mean that these influences impact CB indicator reflectance equally. Since the initial dataset had to be filtered for low ChIA concentrations, it is recommended that either of the indices are only applied to higher S3 NDCI estimated ChIA concentrations with a minimum of at least 10 µg/L.

## 3.2 OBJECTIVE 2

The intent of the Objective 2 hypotheses was to analyze the available S3 imagery of the IRL to identify any patterns in bloom activity and determine if the patterns relate to potential drivers of bloom activity. The following sections provide detailed descriptions of the hypothesis testing, and a general summary of hypotheses outcomes is provided below.

**Hypothesis 2A:** HAB intensity, scale, and duration has been increasing throughout the IRL.

Between 2017-2019 and 2020-2022, there appeared to be a decreasing trend in the BSI for the N-NIRL and BRL. The NIRL1 segment was the only to have significant decreases in BSI across all quarters between 2017-2019 and 2020-2022. The majority of the decreases in BSI observed in the BRL occurred during Q1 (January-March) and Q3 (July-September). However, there also appeared to be an increasing trend in BSI for the C-NIRL, S-NIRL, and N-CIRL. For these areas, the largest increases in BSI between 2017-2019 to 2020-2022 was observed during Q1. The hypothesis appears to have been correct for the segments of the IRL from NIRL5 to NIRL8 and then the N-CIRL.

**Hypothesis 2B:** HABs occur more frequently in proximity to large stormwater outfalls.

This hypothesis was tested by examining the relationship between the percent of total water inflow into the NIRL-5, NIRL-6, NIRL-7, and NIRL-8 basins coming from subsurface flow. AEI was unable to identify locations within the IRL which were within the same region that did not have similar numbers of stormwater outfalls. There was a significant relationship identified between the lack of stormwater runoff and the increased median BSI. When the monthly total flow into these basins was over 90% subsurface flow the median BSI was 0.021, as opposed to the 0.010 median BSI when subsurface flow was less than 60%. This suggests that for these segments of the IRL, that increased bloom activity may occur during dry periods when there is little to no flow from stormwater outfalls.

**Hypothesis 2C:** HABs occur more frequently in proximity to locations with household Onsite Sewage Treatment & Disposal Systems (OSTDS).

This hypothesis was tested by also examining the relationship between the percent of total water inflow into the NIRL-5, NIRL-6, NIRL-7, and NIRL-8. The NIRL-5 and NIRL-8 segments had the highest density of OSTDS systems at 0.26 and 0.33 OSTDS/Acre, respectively. They also had similar average annual water inflows, TN, and TP loadings per acre. However, a significantly higher median BSI was identified in the NIRL-5 (0.012) and NIRL-6 (0.009) basins compared to NIRL-7 (0.005) and NIRL-8 (0.004). When considering the subsurface flow, NIRL-5 had the significantly highest median BSI at 0.014 when subsurface flow comprised over 80% of the total flow into the segment, along with the lowest average water inflow under those conditions. No clear conclusion can be made regarding hypothesis 2C for these basins, however it may be the flushing of a segment during drier periods may suppress bloom activity.

**Hypothesis 2D:** HABs occur less frequently in areas with Submerged Aquatic Vegetation (SAV).

This hypothesis tested if the abundance of SAV in a segment suppresses bloom duration and intensity. The BDI was compared between the SAV abundant SML2 and the SAV depleted BRL-2 segments. No significant relationship was found between either the abundance or absence of SAV and BDI. However, the stability of SAV coverage in the SML1 over several years of bloom activity highlights a potential resistance to blooms in the segment.

**Hypothesis 2E:** HAB duration is greatest in areas with a muck type benthic characteristic.

It appears that hypothesis 2E is accurate for the Eau Gallie River, as the BSI of the area around the river's mouth was consistently lower following dredge operations. However, with only 24 weeks of pre-dredge observations, there may be other impacts such as climatic conditions that should be explored.

**Hypothesis 2F:** Muck removal projects have resulted in a decrease in proximate HAB activity.

This assessment of the pre, during, and post muck dredging of the Eau Gallie River appears to identify that the removal of muck from the mouth of the river has reduced the BSI in the immediate area. Hypothesis 2F appears to be accurate for the Eau Gallie muck removal, in that the BSI of blooms near the river's mouth decreased in the years following the muck removal. As there was no significant difference in BSI before and during the muck removal, it appears that the method of muck removal may not have increased bloom activity.

---

### 3.2.1 BLOOM DURATION, INTENSITY, AND SEVERITY

#### 3.2.1.1 Spatial and Temporal Bloom Severity

As previously mentioned in Section 2.7, the Bloom Severity Index (BSI) is a measure of both bloom concentration as measured by the Bloom Intensity Index (BII) and bloom timeframe as measured by the Bloom Duration Index (BDI). The three indices are additive, allowing comparisons of monthly or annual estimates of severity over time. AEI used the S3 imagery to calculate a standard BSI score for each of the S3 images 300-meter resolution cells to facilitate comparisons over time and space. A cell was assigned a BSI score of 1 if on the imaging date, the cell had an estimated ChlA concentration above 80 µg/L for the preceding 21 days of the available S3 imagery.

**Figure 28** provides an example of the spatial variation in the BII, BDI, and BSI for the BRL3 segment in 2022. Over the course of the year, there was more intense and longer lasting bloom activity in the north portion of the segment along the SR 528 causeway. However, there also appeared to be long lasting, low intensity blooms occurring on the west of the segment and then short lived, high intensity blooms in the eastern half. With the BII and BDI combined to calculate the BSI, the most severe bloom activity appears to be in the northwest corner of the segment, followed by the northeast corner, and then the entire west border. The identification of these locations can then lead to a more focused

analysis of the bloom patterns in this segment. As the indices are calculated for each day of imagery, the annual sums of the BII and BDI combined will not equal the BSI.

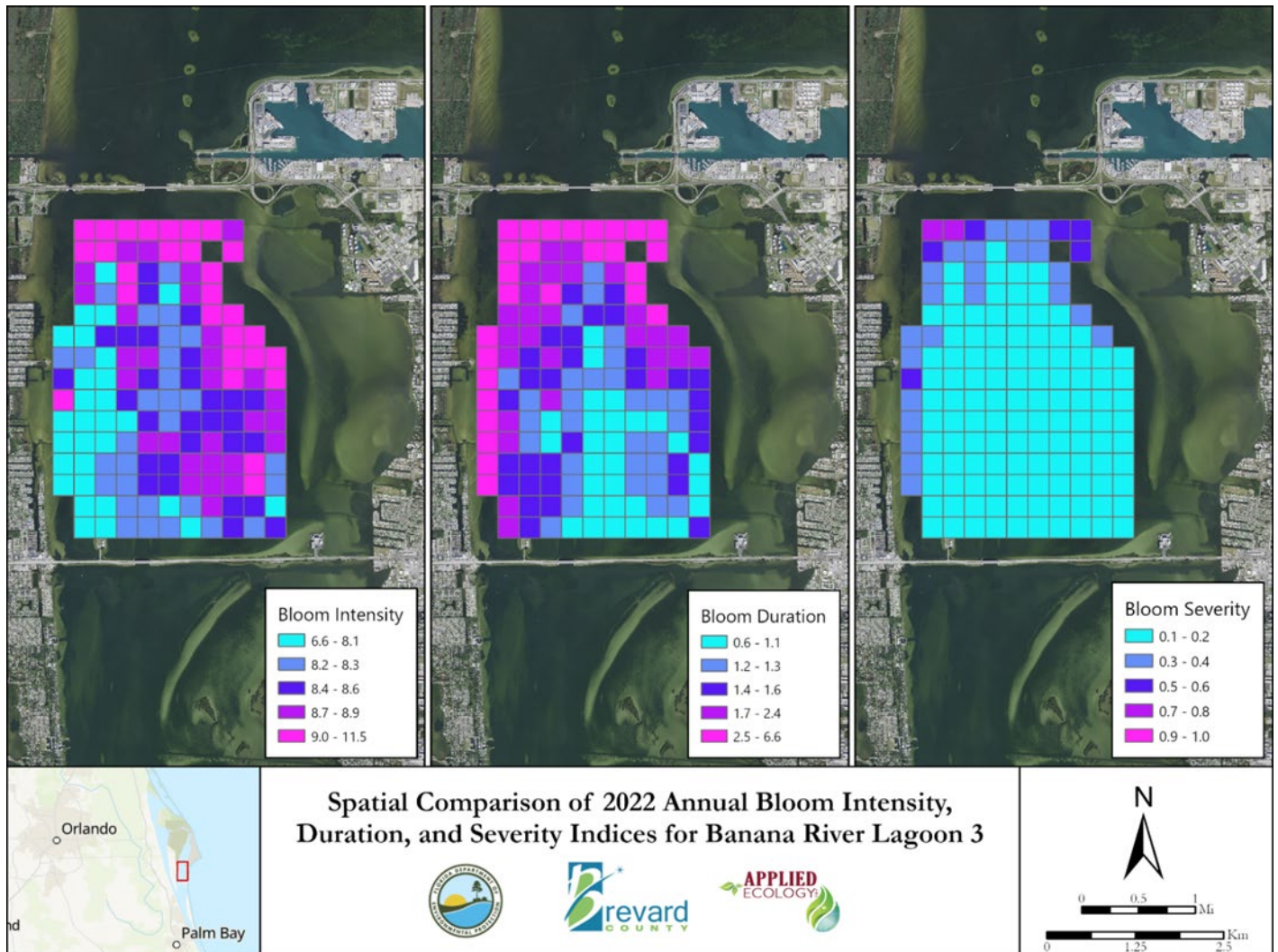


Figure 28. Spatial comparison of the 2022 Annual bloom intensity (BII), duration (BDI), and severity indices (BSI) for Banana River Lagoon segment 3. [Long Description of Figure 28.](#)

Another value of the S3 BSI is in its spatially contiguous assessment of bloom activity, providing additional information to fill the data gaps between field collected sampling locations. **Figure 29** shows the spatial distribution of bloom severity (BSI) in the years 2021 and 2022 and three SJRWMD monthly surface water monitoring sites located in the NIRL-3 segment. The two SJRWMD sampling sites missed the elevated bloom levels along the southwest edge of the segment in 2022. This is likely the reason there are such large differences in the estimated monthly BSI scores and the SJRWMD ChIA measurements for the basin (**Figure 30**). Additionally, in 2021 there was an annual sum of 0.22 BSI compared to 0.12 for 2022. The 2021 bloom activity was segment wide, whereas in 2022 the bloom activity was concentrated in the southwest of the segment. This highlights the challenge of calculating segment wide statistics due to the highly spatial nature of blooms in the IRL.

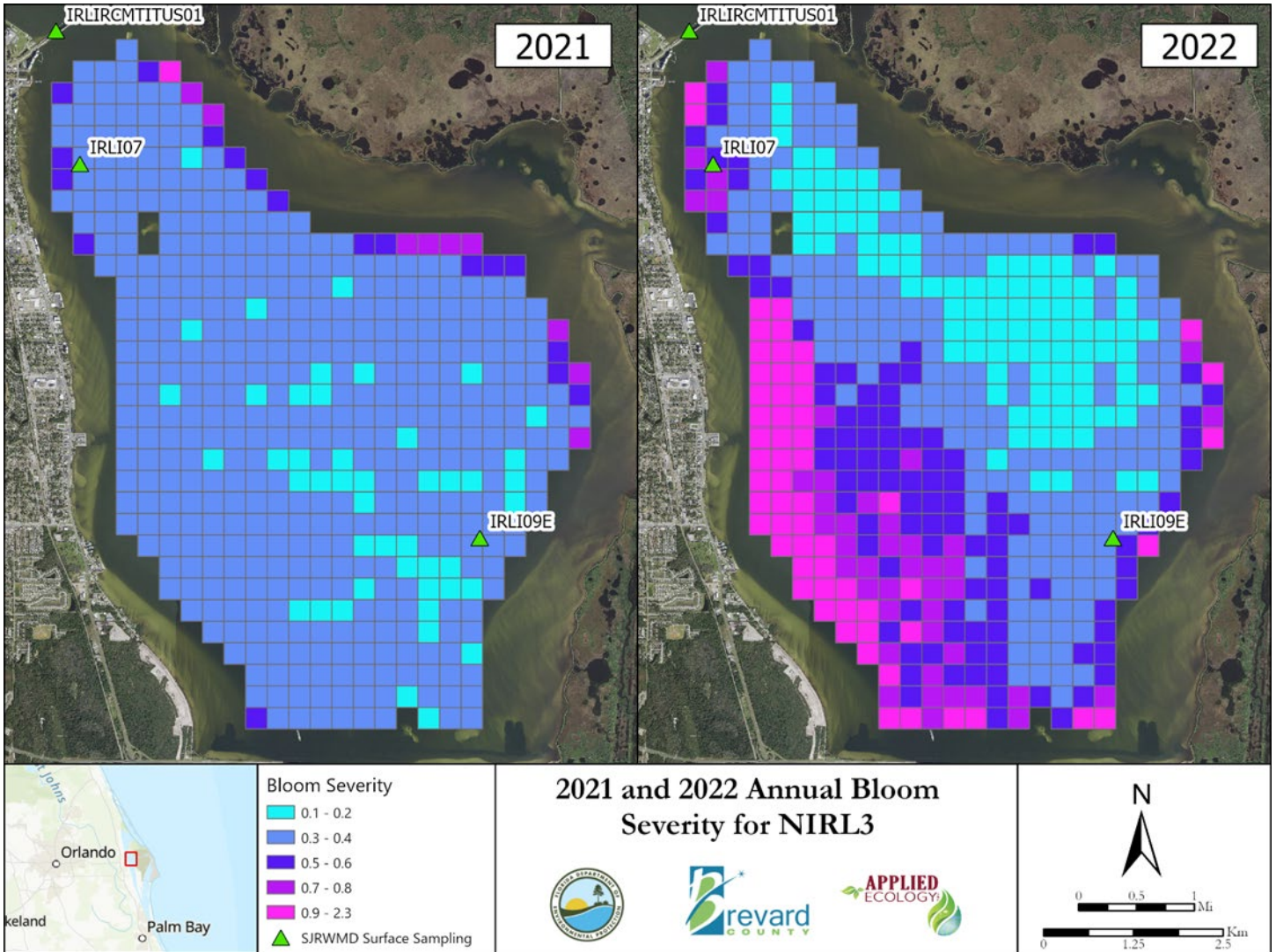


Figure 29. Comparison of the annual Bloom Severity Index (BSI) between 2021 and 2022 for the NIRL3 segment. [Long Description of Figure 29.](#)

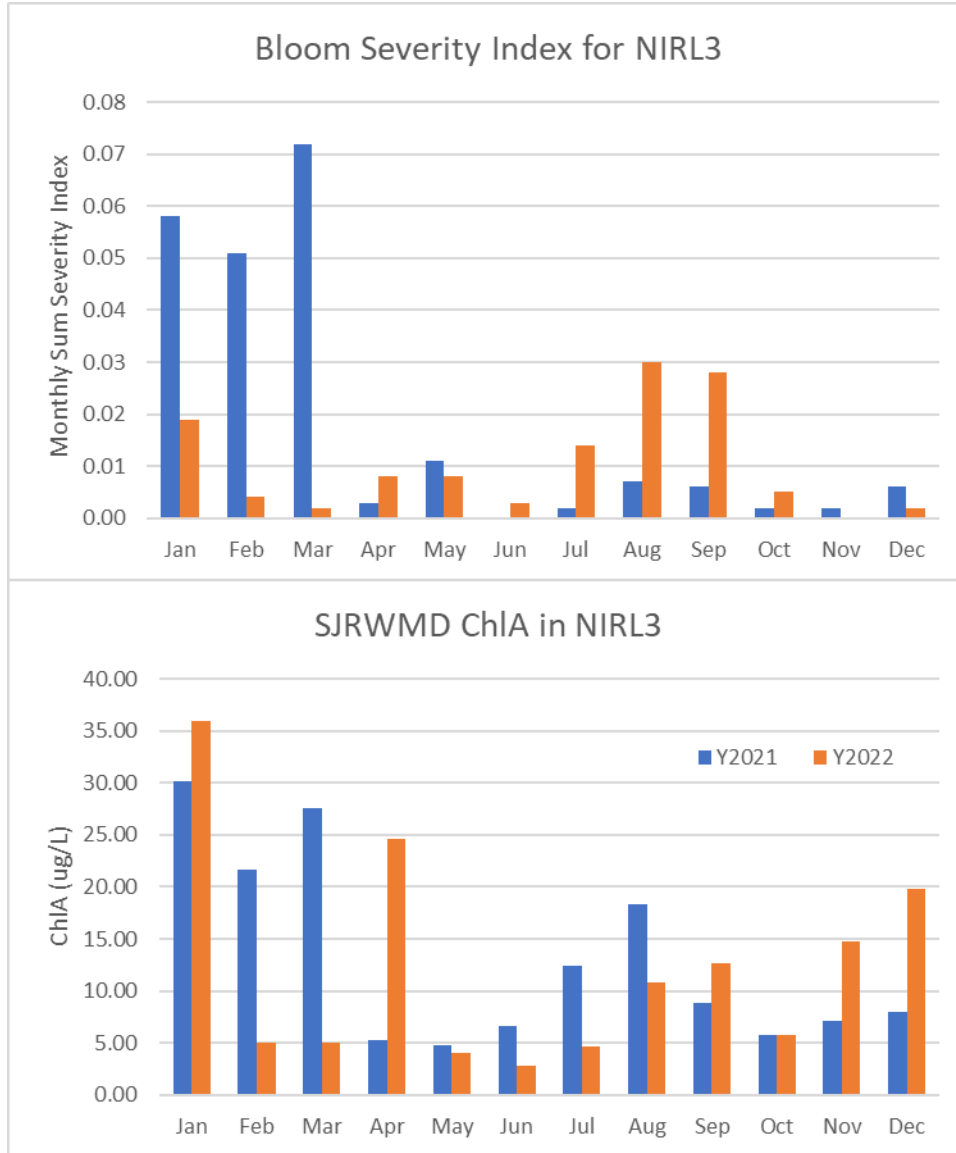


Figure 30. Comparison of the Bloom Severity Index (BSI) and the SJRWMD monthly surface water ChlA in NIRL3 segment between 2021 and 2022. [Long Description of Figure 30.](#)

### 3.2.1.2 2022 Bloom Summary

This section summarizes the 2022 year for the 6 analytical regions of the IRL in Brevard County and describes differences in bloom duration, intensity, and severity over the year 2022. Looking more closely at the regions allows a greater understanding of the complexity of bloom dynamics in terms of intensity and duration as they relate to severity. Additionally, a comparison was performed on the median BSI between the years 2017-2019 and 2020-2022. This analysis divided the year into four (4) quarters; Q1 (January-March), Q2 (April-June), Q3 (July-September), and Q4 (October-December).

As the BII and BDI are all calculated daily, the annual sum of the BSI will not be the same as the annual sum of BII and BDI multiplied. For example, if for the first half of a year there was a long lasting but moderate bloom, this would increase both the annual BII and BDI. Then if in the second half of the year there were a series of short-lived blooms above 80 µg/L, the annual BII would be increased substantially more than the BDI. Additionally, as the BII and BDI are values between 0 and 1 the value of the BSI will be a tenth smaller.

#### 3.2.1.2.1 Southern Mosquito Lagoon and Northern-North Indian River Lagoon

For the SML and N-NIRL segments in general, there were larger areas of elevated BSI during the 2020-2022 period for the first two (2) quarters, which then reversed for the last two (2) quarters (**Table 15**). The NIRL1 segment however had significantly larger areas of elevated BSI for all 2017-2019 quarters, while also having the lowest median BSI of all SML and N-NIRL segments. Q2 (April – June) appeared to have the lowest median BSI across the segments for both time periods, but with no clear quarter having the highest.

**Table 15. Comparison of median Bloom Severity Index (BSI) for Southern Mosquito Lagoon and Northern-North Indian River Lagoon between 2017-2019 and 2020-2022 by quarter.**

Quarter	Years	Segment			
		SML1	SML2	NIRL1	NIRL2
Q1 (Jan-Mar)	2017 - 2019	0.004	0.019	<b>0.005</b>	0.008
	2020 - 2022	<b>0.011</b>	<b>0.024</b>	0.000	<b>0.016</b>
Q2 (Apr-Jun)	2017 - 2019	0.004	0.002	<b>0.000</b>	0.005
	2020 - 2022	<b>0.005</b>	<b>0.005</b>	0.000	<b>0.008</b>
Q3 (Jul-Sep)	2017 - 2019	<b>0.030</b>	<b>0.013</b>	<b>0.010</b>	0.027
	2020 - 2022	0.014	0.010	0.000	<b>0.029</b>
Q4 (Oct-Dec)	2017 - 2019	<b>0.021</b>	<b>0.067</b>	<b>0.010</b>	<b>0.017</b>
	2020 - 2022	0.008	0.025	0.000	0.007

*Red cells indicate if there was a significantly ( $p < 0.05$ ) larger area of elevated BSI in either 2017-2019 or 2020-2022.*

The spatial and temporal variability of blooms in the North IRL and Southern ML subbasins during the year 2022 is depicted in **Figure 31** which includes a map for the BSI and time-series graphs of the BDI and BII scores. From the map, it is apparent that most of SML1 and NIRL1 had low bloom severity in 2022 ( $< 0.2$  BSI), while NIRL2 and SML2 experienced higher levels of bloom severity (0.3-0.6 BSI). The line graphs clarify when and how long the bloom activity occurred. In May 2022, both the NIRL1 and NIRL2 segments experienced a period of low intensity, lasting bloom activity.

Starting in October 2022, the bloom activity in NIRL2 remained low but covered more area for a longer period. SML1 bloom duration and intensity remained low the entire year, whereas for SML2 there was more longer lasting bloom activity beginning in September 2022. While both SML1 and SML2 had similarly intense bloom activity between September and November, SML2 experienced longer lasting blooms which contributed to the subbasin's higher BSI score.

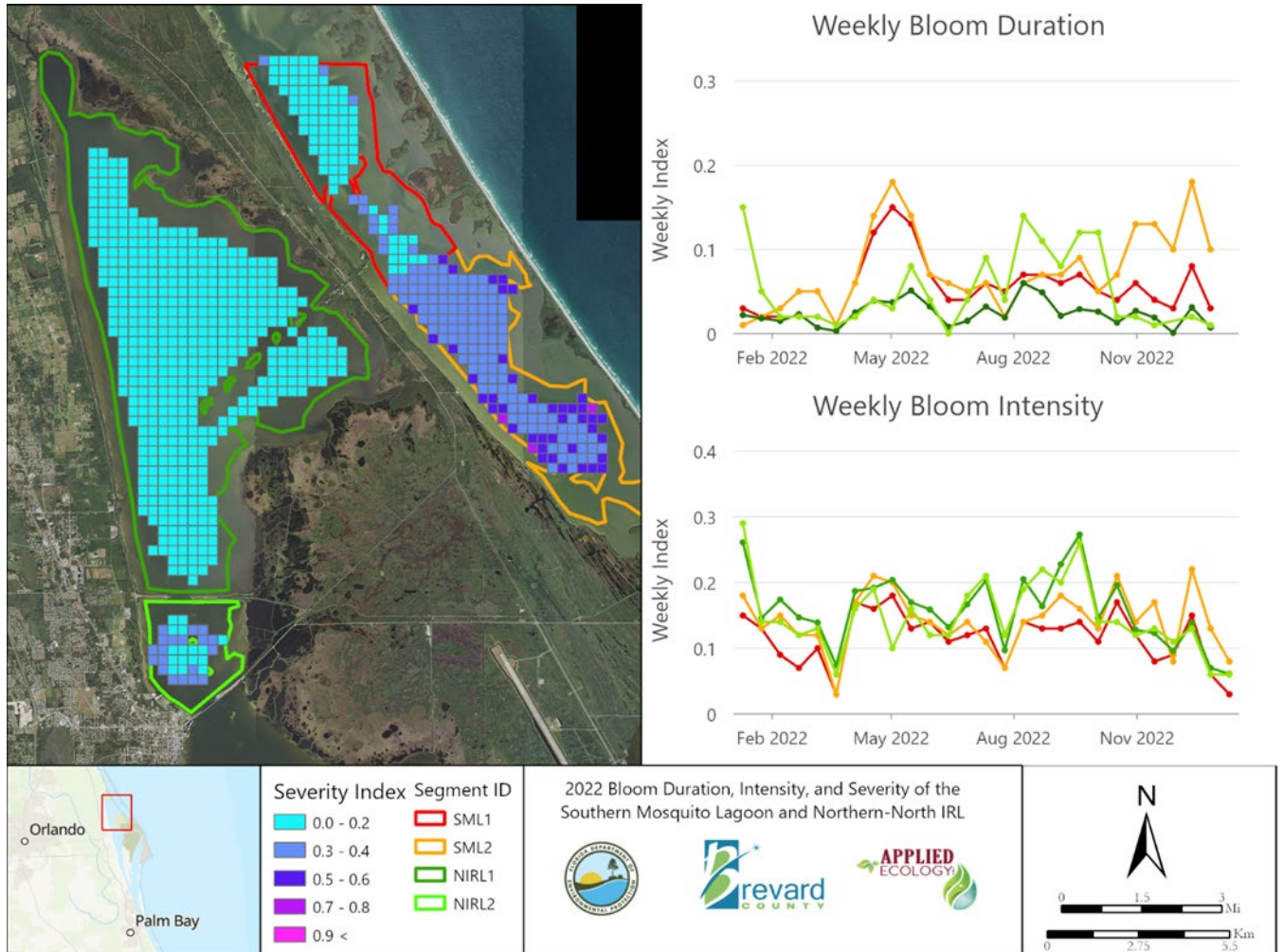


**Figure 31. 2022 Bloom duration, intensity, and severity of the Southern Mosquito Lagoon (SML) and Northern-North IRL (N-NIRL). [Long Description of Figure 31.](#)**

### 3.2.1.2.2 Northern Banana River Lagoon

For the NBRL, Q1 and Q3 had significantly larger areas of elevated BSI in 2017-2019 while for Q2 and Q4 there were significantly larger areas in 2020-2022 (**Table 16**). Of the NBRL segments, BRL4 generally had the higher median BSI across all quarters and both time periods. Q4 appeared to have the lowest median BSI for both 2017-2019 and 2020-2022 with no clear quarter having the highest median BSI.

**Table 16. Comparison of median Bloom Severity Index (BSI) for the Northern Banana River Lagoon between 2017-2019 and 2020-2022 by quarter.**

Quarter	Years	Segment		
		BRL2	BRL3	BRL4
Q1 (Jan-Mar)	2017 - 2019	<b>0.097</b>	<b>0.033</b>	<b>0.035</b>
	2020 - 2022	0.006	0.011	0.021
Q2 (Apr-Jun)	2017 - 2019	0.007	0.006	0.023
	2020 - 2022	<b>0.010</b>	<b>0.010</b>	0.022
Q3 (Jul-Sep)	2017 - 2019	<b>0.032</b>	<b>0.030</b>	<b>0.062</b>
	2020 - 2022	0.007	0.008	0.021
Q4 (Oct-Dec)	2017 - 2019	0.003	0.000	0.003
	2020 - 2022	<b>0.007</b>	<b>0.005</b>	<b>0.009</b>

*Red cells indicate if there was a significantly ( $p < 0.05$ ) larger area of elevated BSI in either 2017-2019 or 2020-2022.*

The map of the NBRL BSI is provided in **Figure 32** along with time-series graphs of the BDI and BII scores. The northern most segment (BRL2) had slightly elevated ( $>0.3$ ) BSI scores in pixels dispersed along the shorelines. The center subbasin (BRL3) had a high ( $>0.7$ ) BSI score area in the northwest corner of the segment against the 528 Causeway. Subbasin BRL4 had a high ( $>0.7$ ) BSI score concentration in the southern-most portion of the segment between Merritt Island and Cocoa Beach. There was little temporal variability in bloom duration and intensity within segments BRL2 and BRL3 over the year 2022. BRL4 had slightly increased intensity and notably higher bloom duration than the other segments with longer blooms occurring in May and September 2022.

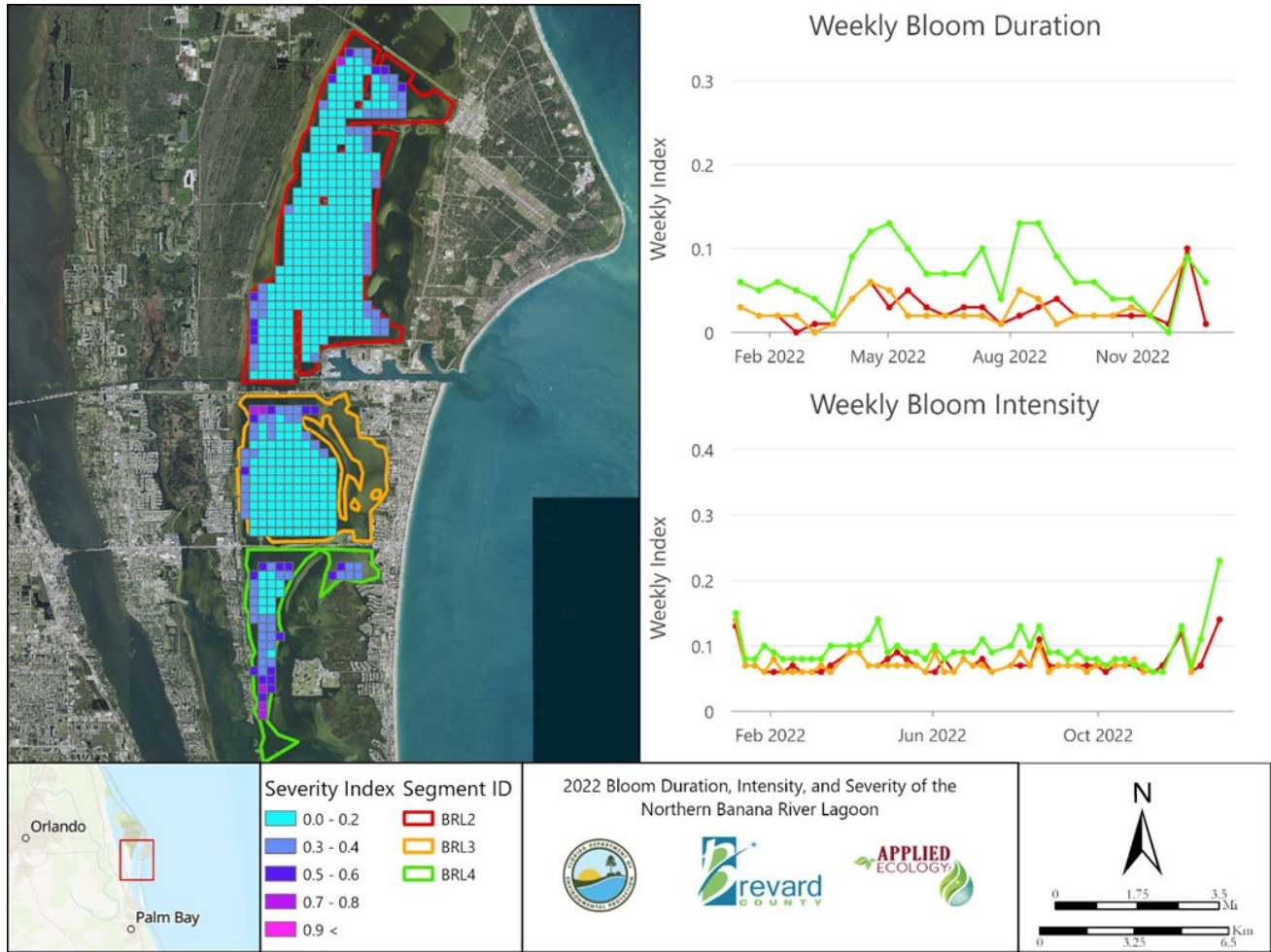


Figure 32. 2022 Bloom duration, intensity, and severity of the Northern Banana River Lagoon (NBRL). [Long Description of Figure 32.](#)

### 3.2.1.2.3 Southern Banana River Lagoon

For the BRL5 and SC segments of the SBRL, the significantly largest areas of elevated BSI occurred during 2017-2019 for all quarters while BRL6 had significantly larger areas of elevated BSI in 2020-2022 for three (3) of the quarters (**Table 17**). BRL5 generally had the lowest median BSI of the SBRL segments across the quarters for both time periods. During 2017-2019 SC had the highest median BSI across the quarters while during 2020-2022 it was BRL6.

**Table 17. Comparison of median Bloom Severity Index (BSI) for the Southern Banana River Lagoon between 2017-2019 and 2020-2022 by quarter.**

Quarter	Years	Segment		
		BRL5	BRL6	SC
Q1 (Jan-Mar)	2017 - 2019	<b>0.082</b>	0.044	<b>0.250</b>
	2020 - 2022	0.012	<b>0.057</b>	0.058
Q2 (Apr-Jun)	2017 - 2019	<b>0.006</b>	0.043	<b>0.052</b>
	2020 - 2022	0.003	0.040	0.033
Q3 (Jul-Sep)	2017 - 2019	<b>0.023</b>	0.022	<b>0.076</b>
	2020 - 2022	0.007	<b>0.038</b>	0.036
Q4 (Oct-Dec)	2017 - 2019	<b>0.002</b>	0.012	<b>0.059</b>
	2020 - 2022	0.001	<b>0.038</b>	0.025

*Red cells indicate if there was a significantly ( $p < 0.05$ ) larger area of elevated BSI in either 2017-2019 or 2020-2022.*

The spatial and temporal variability of the SBRL segments described **Figure 33**, which shows the spatial variability of bloom activity across the region. From the map, it is evident that bloom severity increases along borders of open waterways and in more confined waterways. For example, in BRL5 the large open water area shows low ( $< 0.2$ ) BSI scores with somewhat higher BSI scores dispersed on the periphery of the segment along the shorelines.

Segments SC and BRL6 in comparison are more confined by land and have less open water, reducing wind and wave influence. These two segments also have higher BSI scores ( $> 0.5$ ) covering more area. While SC and BRL6 have no direct hydrologic connection, in 2022 they were more like each other in bloom duration and intensity than either was with segment BRL5 which connects the two segments. All three segments had a peak of duration and intensity in March 2022, followed by a more staggered set of peaks starting in August for BRL5, September for SC, and then October for BRL6.

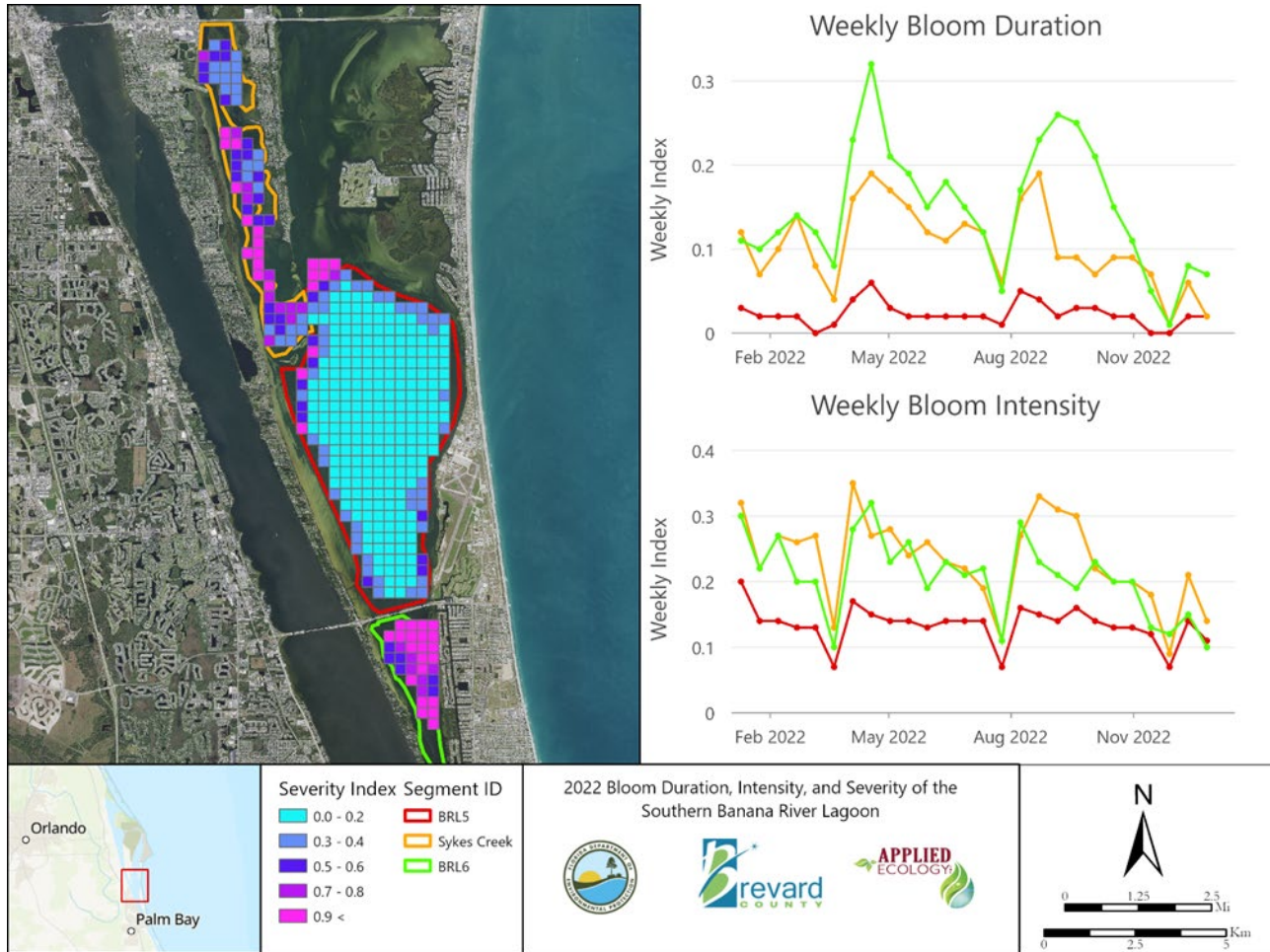


**Figure 33. 2022 Bloom duration, intensity, and severity of the Southern Banana River Lagoon (SBRL). [Long Description of Figure 33.](#)**

#### 3.2.1.2.4 Central-North Indian River Lagoon

The C-NIRL had a mixture of significantly larger areas of elevated BSI across quarters and between 2017-2019 to 2020-2022 (**Table 18**). For Q1 there were significantly larger areas of elevated BSI during 2020-2022 for all C-NIRL segments and then for Q4 it was significantly larger during 2017-2019. Q2 and Q3 had similar median BSI between 2017-2019 and 2020-2022 for each segment, with only NIRL3 having significantly larger areas of elevated BSI in 2020-2022. There did not appear to be a single quarter or segment with the highest or lowest median BSI in the C-NIRL.

**Table 18. Comparison of median Bloom Severity Index (BSI) for the Central-North Indian River Lagoon between 2017-2019 and 2020-2022 by quarter.**

Quarter	Years	Segment		
		NIRL3	NIRL4	NIRL5
Q1 (Jan-Mar)	2017 - 2019	0.021	0.018	0.012
	2020 - 2022	<b>0.031</b>	<b>0.023</b>	<b>0.018</b>
Q2 (Apr-Jun)	2017 - 2019	0.004	0.007	<b>0.019</b>
	2020 - 2022	<b>0.004</b>	0.008	0.011
Q3 (Jul-Sep)	2017 - 2019	0.023	0.019	0.030
	2020 - 2022	<b>0.028</b>	<b>0.021</b>	0.033
Q4 (Oct-Dec)	2017 - 2019	<b>0.049</b>	<b>0.017</b>	<b>0.017</b>
	2020 - 2022	0.002	0.005	0.009

*Red cells indicate if there was a significantly ( $p < 0.05$ ) larger area of elevated BSI in either 2017-2019 or 2020-2022.*

NIRL4 and NIRL5 experienced blooms generally dispersed across the segment with open water BSI scores elevated somewhat ( $>0.3$ ) and more elevated bloom severity scores ( $>0.5$ ) localized along shorelines and causeways (**Figure 34**). The northern-most segment (NIRL3) experienced a large area of bloom severity in its southwest portion along the NASA Causeway.

NIRL4 and NIRL5 had their highest bloom severity located along the northern border of the segments, along the NASA Causeway and SR 528 Causeway. The duration and intensity of all three segments generally varied together over the year, with NIRL5 typically having the highest values. Between May and June 2022, the segments had a peak in duration and intensity with NIRL5 notably higher. Then from July to October, duration and intensity increased with NIRL5 peaking first in September then NIRL3 and NIRL4 in October.

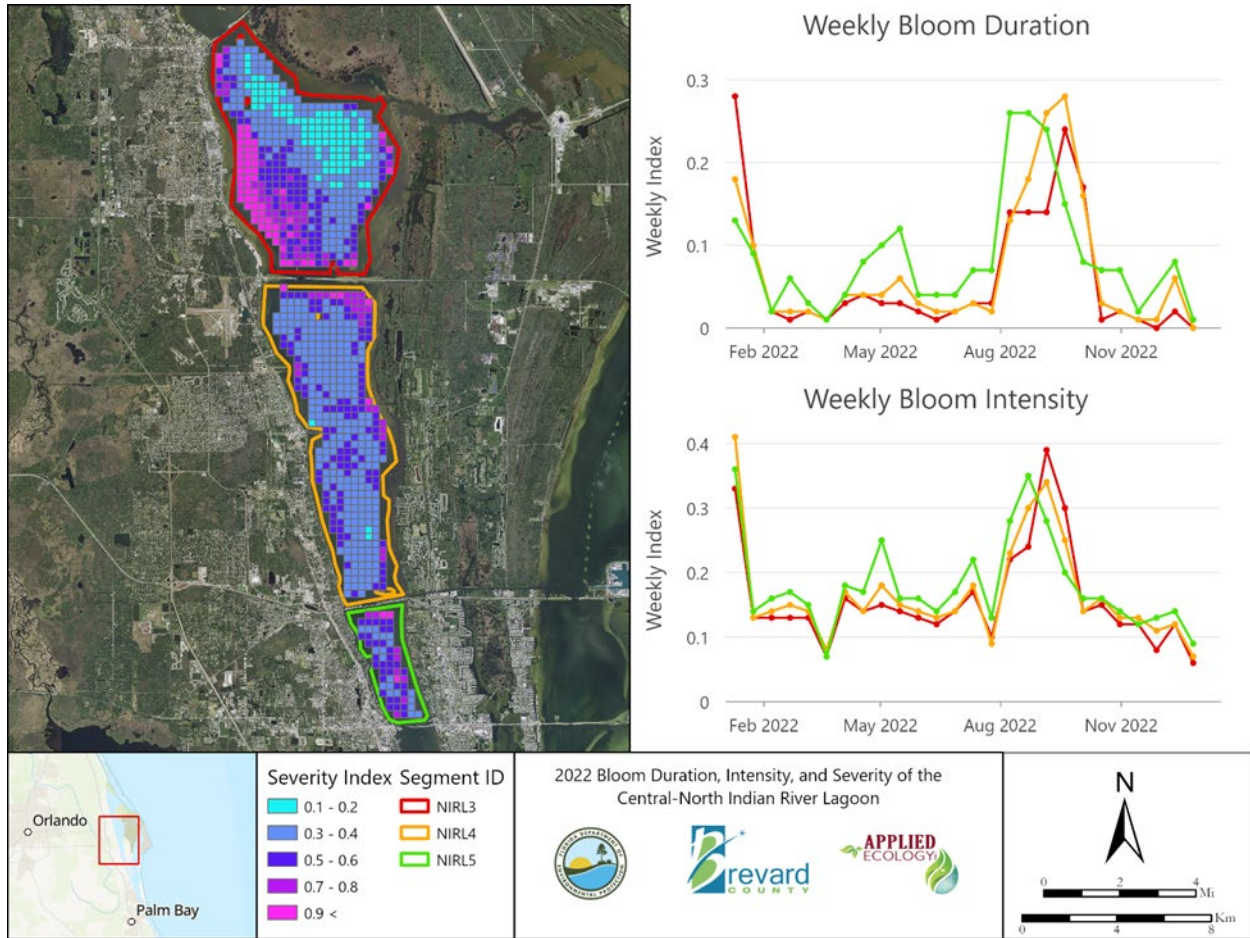


Figure 34. 2022 Bloom duration, intensity, and severity of the Central-North IRL (C-NIRL). [Long Description of Figure 34.](#)

### 3.2.1.2.5 Southern-North Indian River Lagoon

The S-NIRL generally had significantly larger areas of elevated BSI for Q1 and Q4 during 2020-2022 (**Table 19**). During 2017-2019 the NIRL6 segment had significantly larger areas of elevated BSI in Q2 and Q3, while NIRL7 had no significant difference, and then NIRL8 was significantly larger during 2020-2022. NIRL6 had the highest median BSI of the S-NIRL segments across all quarters and both time periods. It did not appear that a single segment or time period had the lowest median BSI.

**Table 19. Comparison of median Bloom Severity Index (BSI) for the Southern-North Indian River Lagoon between 2017-2019 and 2020-2022 by quarter.**

Quarter	Years	Segment		
		NIRL6	NIRL7	NIRL8
Q1 (Jan-Mar)	2017 - 2019	0.012	0.008	0.008
	2020 - 2022	<b>0.019</b>	<b>0.009</b>	<b>0.010</b>
Q2 (Apr-Jun)	2017 - 2019	<b>0.013</b>	0.007	0.005
	2020 - 2022	0.013	0.007	<b>0.007</b>
Q3 (Jul-Sep)	2017 - 2019	<b>0.022</b>	0.008	0.004
	2020 - 2022	0.017	0.008	<b>0.007</b>
Q4 (Oct-Dec)	2017 - 2019	0.008	0.003	0.004
	2020 - 2022	<b>0.009</b>	<b>0.004</b>	0.003

*Red cells indicate if there was a significantly ( $p < 0.05$ ) larger area of elevated BSI in either 2017-2019 or 2020-2022.*

A spatial and temporal representation of bloom activity in the three segments of the S-NIRL in the year 2022 clarifies the differences in bloom severity across the region **Figure 35**). The southern most portion of the S-NIRL between the Eau Gallie and Melbourne Causeways, (NIRL8) had moderate severity scores ( $< 0.4$ ) along the shorelines with two isolated clusters of high severity pixels (0.5-0.6) located in the northeast and central west portions of the segment.

All three segments had similar variations in duration and intensity over time, with the north (NIRL6) to south (NIRL8) trend of high to low values apparent in the time-series graphs. The first intensity and duration peaks were in April 2022 followed by a series of events that reached a high in September 2022 and were followed by two more peaks in October and November.

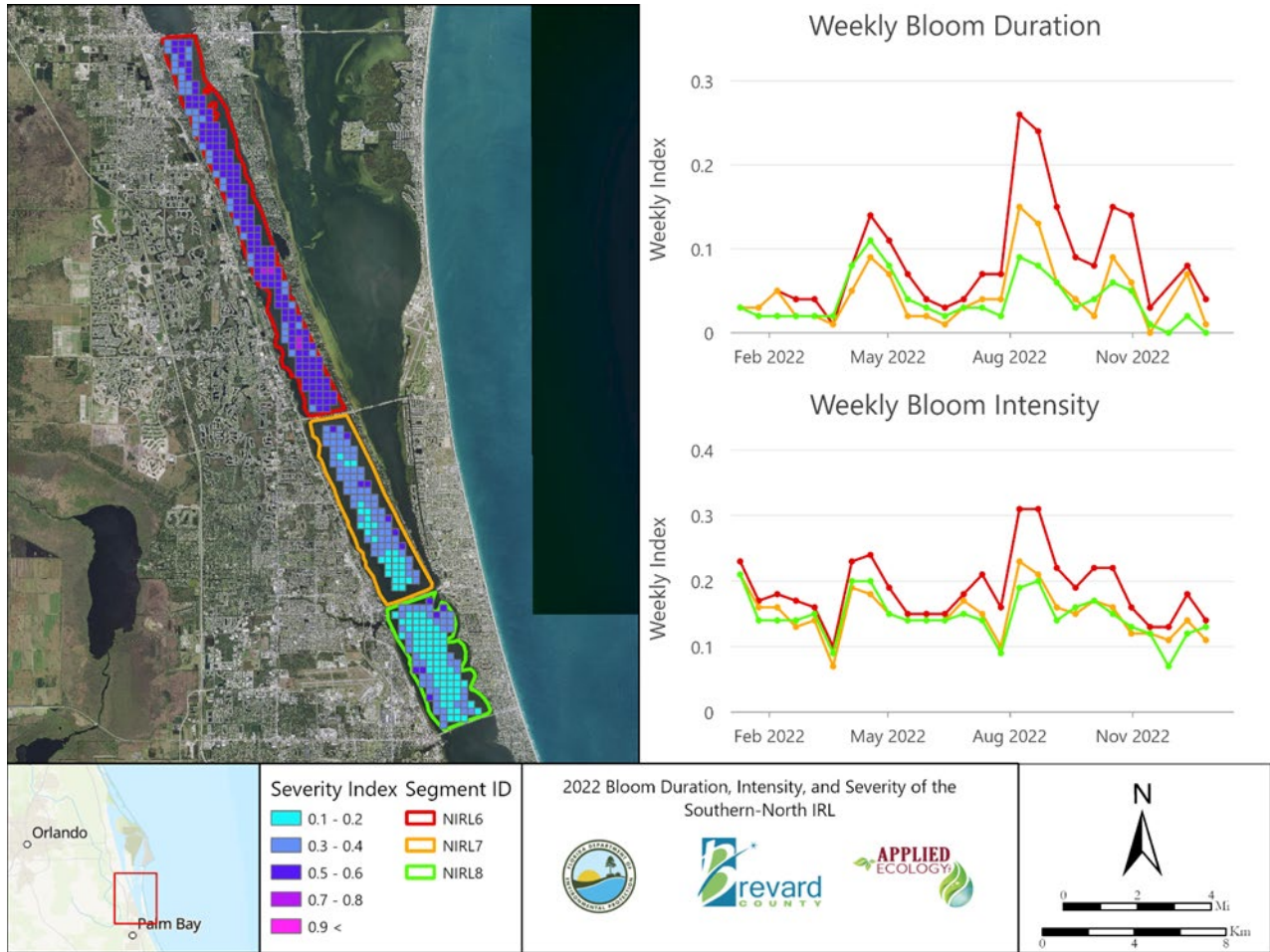


Figure 35. 2022 Bloom duration, intensity, and severity of the Southern-North IRL (S-NIRL). [Long Description of Figure 35.](#)

### 3.2.1.2.6 Northern-Central Indian River Lagoon

For the segments of the N-CIRL, there were significantly larger areas of elevated BSI during 2020-2022 for Q1, Q3, and Q4 (**Table 20**). The CIRL1 segment had the highest median BSI across almost all quarters and time periods. The lowest BSI for CIRL1 and CIRL2 appeared to occur in Q4 for both 2017-2019 and 2020-2022.

**Table 20. Comparison of median bloom duration, intensity, and severity indices for the Northern-Central Indian River Lagoon between 2021 and 2022.**

Quarter	Years	Segment	
		CIRL1	CIRL2
Q1 (Jan-Mar)	2017 - 2019	0.005	0.002
	2020 - 2022	<b>0.008</b>	<b>0.005</b>
Q2 (Apr-Jun)	2017 - 2019	<b>0.005</b>	0.003
	2020 - 2022	0.004	0.003
Q3 (Jul-Sep)	2017 - 2019	0.003	0.002
	2020 - 2022	<b>0.007</b>	<b>0.004</b>
Q4 (Oct-Dec)	2017 - 2019	0.000	0.000
	2020 - 2022	<b>0.004</b>	<b>0.002</b>

*Red cells indicate if there was a significantly ( $p < 0.05$ ) larger area of elevated BSI in either 2017-2019 or 2020-2022.*

Low bloom severity pixels (<0.2) were distributed throughout the open water areas of segment CIRL1 with moderate bloom severity (0.3-0.4) pixels along the periphery of the segment along the shoreline (**Figure 36**). The more southern segment (CIRL2) had two areas of higher bloom severity pixels (>0.5) along the eastern shoreline proximal to Crane Creek and Turkey Creek, two large tributaries to the segment and a third area in the center of the segment.

The time series graphs show that the first peak of bloom duration occurred in both segments in April, August, and November 2022, although bloom intensity remained elevated throughout the year with drops between the intensity peaks. This could be indicative of the movement of blooms in these segments, as high intensity blooms drift through the segment and they result in lower overall bloom duration.

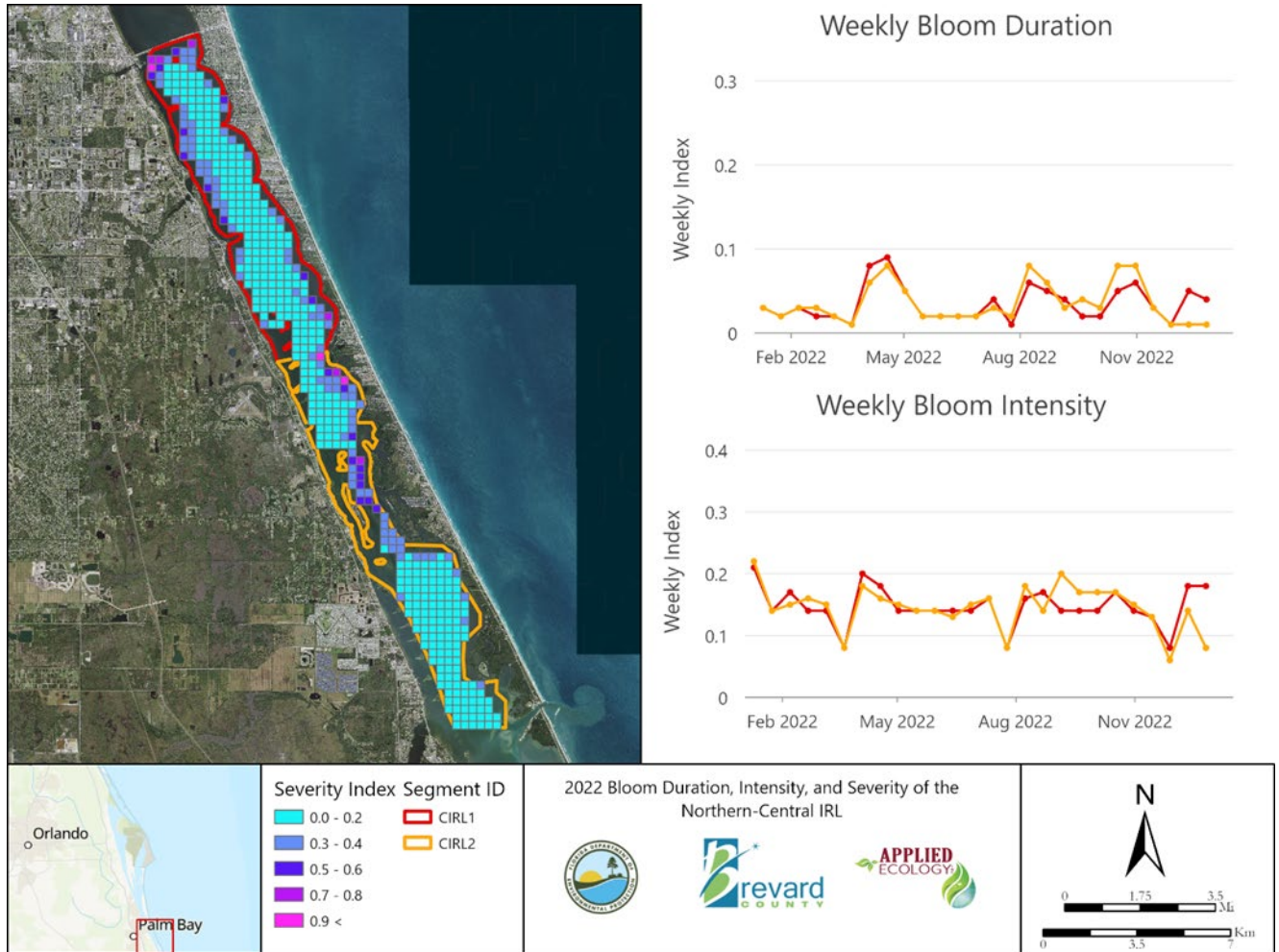


Figure 36. 2022 Bloom duration, intensity, and severity of the Northern-Central IRL (N-CIRL). [Long Description of Figure 36.](#)

### 3.2.1.2.7 Time Series Summary

A comparison of quarterly bloom severity index scores between the first three years in the dataset (2017-2019) and the most recent three years (2020-2022) indicated significant differences in most (89%) of the analyzed lagoon segments. In **Table 21**, the red cells are segments with significantly higher BSI in recent years (2020-2022) compared to earlier years (2017-2019) and the green cells are those segments with significantly lower BSI in recent years. The orange cells had no measured significant difference in BSI score between the two time periods. The spatial and temporal variability is evident, but overall, more areas had higher BSI in recent years. Three segments (NIRL1, SC, and BRL5) exhibiting significantly lower BSI in all four quarters of the recent dataset. In addition to those segments, the entire SML and the northern half of the NIRL had significantly lower BSI in the recent dataset in Q4, whereas most of the

BRL had significantly lower BSI in Q1 and Q3 of the recent years. From NIRL2 to CIRL2, there was significantly higher median BSI in Q1 of the recent dataset (2020-2022).

**Table 21. Summary of significant differences in the median Bloom Severity Index (BSI) comparing three-year periods of 2017-2019 and 2020-2022 by Indian River Lagoon segment.**

Segment	Quarter			
	Q1 (Jan Mar)	Q2 (Apr Jun)	Q3 (Jul Sep)	Q4 (Oct Dec)
SML1	0.01	0.00	-0.02	-0.01
SML2	0.01	0.00	-0.00	-0.04
NIRL1	-0.01	0.00	-0.01	-0.01
NIRL2	0.01	0.00	0.00	-0.01
BRL2	-0.09	0.00	-0.03	0.00
BRL3	-0.02	0.00	-0.02	0.01
BRL4	-0.01	0.00	-0.04	0.01
BRL5	-0.07	-0.00	-0.02	0.00
BRL6	0.01	0.00	0.02	0.03
SC	-0.19	-0.02	-0.04	-0.03
NIRL3	0.01	0.00	0.01	-0.05
NIRL4	0.01	0.00	0.00	-0.01
NIRL5	0.01	-0.01	0.00	-0.01
NIRL6	0.01	-0.00	-0.01	0.00
NIRL7	0.00	0.00	0.00	0.00
NIRL8	0.00	0.00	0.00	0.00
CIRL1	0.00	0.00	0.00	0.00
CIRL2	0.00	0.00	0.00	0.00

Cells highlighted in green had significantly ( $p < 0.5$ ) larger areas of elevated BSI in 2017-2019, cells in red were significantly higher in 2020-2022, and NS cells in orange had no significant differences.

A better understanding of these differences can be explained by examining trends over time in the entire dataset period of record (2016-2022). There were two (2) general BSI trends in the IRL over the entire period - a steady or decreasing BSI in the N-NIRL and BRL and an increasing BSI trend in the C-NIRL, S-NIRL, and N-CIRL (**Table 22**). Almost the entirety of NIRL1 had significantly decreasing BSI trends between 2016 and 2022 and was the only segment to do so. Most of the BRL segments had significantly decreasing trends, except for BRL6 where 90% of the segments had significantly increasing BSI trends. As the BRL6 has a direct surface water connection with the similarly increasing NIRL7 segment, there may be an interaction between the segments.

As you travel south from the C-NIRL to the S-NIRL and the N-CIRL, the amount of the segment area with increasing BSI scores intensifies. NIRL1 had significantly decreasing bloom intensity, NIRL2 and NIRL3 had no significant trends identified, and NIRL4 appears to be a transitional segment with only 10% of the segment having significantly increasing trends. From NIRL5 to CIRL2, most of the segments had an increasing BSI trend from 2016 to 2022. Based on the comparison of the 2017-2019 and 2020-2022 median BSI, it appears that the increasing trends in the C-NIRL, S-NIRL, and N-CIRL were driven by significant increases in BSI observed during Q1 of the 2020-2022 dataset.

**Table 22. Percent of each segment identified to have an increasing, decreasing, or no trend in monthly BSI between 2016 and 2022 as determined by the Seasonal Mann-Kendall trend test per Sentinel-3 pixel.**

Segment	Significantly Decreasing	No Significant Change	Significantly Increasing
SML1	0%	100%	0%
SML2	1%	99%	1%
NIRL1	98%	2%	0%
NIRL2	0%	100%	0%
BRL2	11%	89%	0%
BRL3	18%	82%	0%
BRL4	32%	68%	0%
BRL5	28%	69%	3%
BRL6	0%	10%	90%
SC	37%	63%	0%
NIRL3	0%	100%	0%
NIRL4	1%	90%	10%
NIRL5	0%	48%	52%
NIRL6	0%	0%	100%
NIRL7	0%	19%	81%
NIRL8	0%	7%	93%
CIRL1	0%	13%	88%
CIRL2	4%	25%	71%

Cells colored red identify segments with more than 50% significantly increasing, orange for segments with less than 50% significantly increasing, green for segments with less than 50% significantly decreasing, and blue for more than 50% significantly increasing.

### 3.2.2 BLOOM SEVERITY ASSESSMENT

#### 3.2.2.1 Sentinel 3 Cyanobacteria Estimation Example

To test a method to identify HAB species through satellite imagery, the NDPCI algorithm was applied to two S3 scenes which represent known eukaryotic or cyanobacteria dominated blooms (**Table 23, Figure 37**). The test date of September 9, 2019, was selected as it had a moderate, persistent bloom of an unidentified eukaryotic nanoplankton. Surface water samples were collected in SML and N-NIRL the same day as the S3 scene, with SML having a ChlA concentration of 29.8 µg/L and CB biomass of 15% and N-NIRL having a ChlA concentration of 21.9 µg/L and CB biomass of 27%. As expected, the median NDPCI value in the SML was 0.72 and the median NDPCI value was 0.78 in the N-NIRL, corresponding with the higher CB biomass in this region.

The second test date was August 14, 2020, which was selected as it had comparable ChlA concentrations to September 9, 2019, and was dominated by the CB species *Cyanobium*. The surface samples collected prior to the S3 scene on August 10, 2020, measured ChlA concentration of 10.8 µg/L in the SML and CB biomass of 37% and a ChlA concentration of 33.9 µg/L in the N-NIRL and CB biomass of 53%. The median NDPCI value in the SML was 0.88 and the median NDPCI value in the N-NIRL was 0.94 again corresponding with the higher CB biomass percentage in the N-NIRL.

**Table 23. Cyanobacteria (CB) biomass percentage and Chlorophyll A (ChlA) concentration (µg/L) for the Southern Mosquito Lagoon (SML) and Northern-North IRL in 2019 and 2020.**

Date	Site	CB Biomass (%)	ChlA (µg/L)
9/9/2019	SML	15%	29.8
9/9/2019	N-NIRL	27%	21.9
8/10/2020	SML	37%	10.8
8/10/2020	N-NIRL	53%	33.9

While the CB index calibration requires additional development, the application of the CB algorithms in a qualitative manner to S3 scenes can differentiate between likely eukaryotic or CB blooms. As the two example scenes were selected for minimal cloud cover, glint, and other anomalies, more assessment should be performed to assess the ability of the CB algorithms to successfully differentiate between bloom types in various atmospheric and water conditions, such as water depth, SAV presence, and benthic conditions.

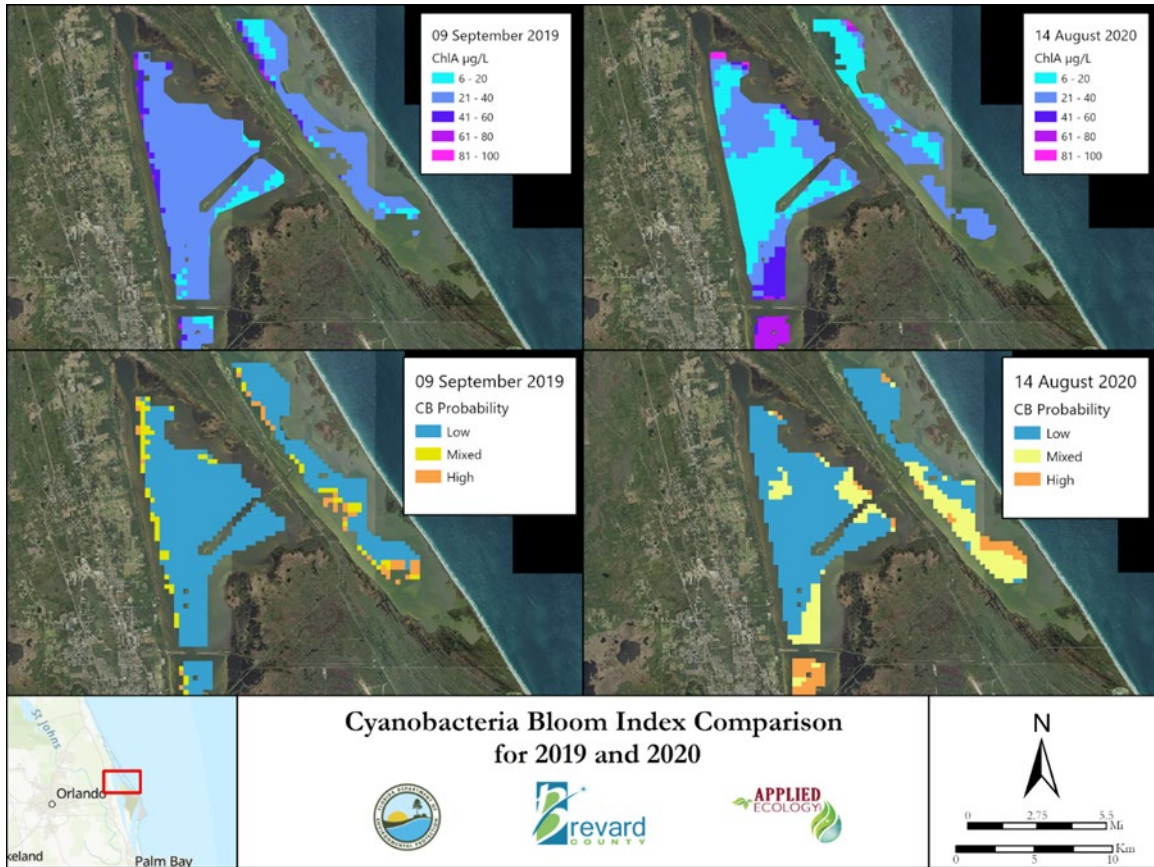


Figure 37. Comparison of the cyanobacteria bloom index for a eukaryotic bloom on September 9, 2019, and a cyanobacteria bloom on August 14, 2020. [Long Description of Figure 37.](#)

### 3.2.2.2 Rainfall and Severity

Hypothesis 2B assumed that during periods of increased rainfall, the influx of nutrients from stormwater runoff through culverts would result in elevated bloom severity (BSI) along the shoreline relative to the open water areas. To examine the relationship between runoff and elevated BSI, AEI selected the segments NIRL5, NIRL6, NIRL7, and NIRL8 for analysis between 2016 and 2022. AEI was unsuccessful at finding a shoreline as a reference for comparison due to the extensive network of stormwater outfalls and large-scale variations in hydrology across the IRL. These segments were selected as they are hydrologically connected, surrounded by a similar mixture of residential and commercial land uses, and have average impervious surface cover ranging from 23% to 29%.

The impact of stormwater runoff on the BSI of the basins was evaluated by comparing it to the percent of the total monthly flow as the baseflow in 10% increments (**Table 24**). The Kruskal-Wallis test identified that months where the total flow was at least 90%

baseflow in a basin, it had the significantly highest median BSI ( $p < 0.001$ ). Comparatively, for all increments below 90% baseflow there was no significant difference in the median BSI. Both median salinity and temperature were significantly highest ( $p < 0.0001$ ) during the periods when baseflow consisted of less than 60% of total monthly flow into the segments. This suggests that for these basins of the IRL the hypothesis 2B may not be accurate, and that elevated BSI may occur more often when there is less monthly rainfall. However, there may be error due to the temperature and salinity for each segment being determined by monthly grab samples. Further assessment of this relationship should be performed using any available continuous data.

**Table 24. Differences in the median BSI, salinity, and temperature by percent of monthly total flow as baseflow for the NIRL5 to NIRL8 segments from 2016 to 2022.**

Analyte	Percent of Monthly Flow from Baseflow				
	100 90%	90 80%	80 70%	70 60%	< 60%
BSI	<b>0.021</b> <sub>a</sub>	0.007 <sub>a,b</sub>	0.006 <sub>b</sub>	0.008 <sub>b</sub>	0.010 <sub>b</sub>
Salinity (PSU)	20.5 <sub>a</sub>	19.3 <sub>a</sub>	20.4 <sub>a</sub>	21.0 <sub>a</sub>	<b>22.9</b> <sub>b</sub>
Temperature (°C)	20.4 <sub>a</sub>	24.1 <sub>b</sub>	26.9 <sub>b,c</sub>	27.6 <sub>c</sub>	<b>29.2</b> <sub>d</sub>

*Different letters indicate row median significant differences at  $p < 0.05$  using Kruskal-Wallis. Pairwise comparisons (SDCF) indicated using subscripts. If there are significant differences, the highest value is in bold.*

### 3.2.2.3 OSTDS and Severity

Hypothesis 2C assumed that HABs occur more frequently in proximity to locations with household Onsite Sewage Treatment & Disposal Systems (OSTDS). This hypothesis was tested by evaluating the density of OSTDS and SWIL estimated TN and TP loading to the NIRL5, NIRL6, NIRL7, and NIRL8 between 2016 and 2022. These basins were selected primarily because their narrow width reduces the impact of wind driven currents that have been observed in the larger basins.

The modeled nutrient loading and OSTDS characteristics of each basin have some variations, however NIRL5 and NIRL6 had the significantly highest median BSI ( $p < 0.0001$ ) between 2016 and 2022 (**Table 25**). NIRL8 had the highest density of estimated OSTDS at 0.33 OSTDS/Acre, followed by NIRL5 at 0.26, NIRL6 at 0.12, and then NIRL7 at 0.11 OSTDS/Acre. NIRL8 had the highest modeled average annual flow at 83,599 ft<sup>3</sup>/Acre, TN at 5.56 lbs/Acre TN, and TP at 0.81 lbs/Acre TP of loading. This was closely followed by NIRL5, then NIRL6, and then NIRL7. There is no clear conclusion that can be drawn from this assessment as the NIRL8 segment with the highest OSTDS and nutrient loading had the lowest median BSI. As NIRL8 is the southernmost of the

segments and may be influenced by the Sebastian Inlet, it also has the largest average annual flow per acre.

**Table 25. Differences in the OSTDS density, average annual flow, TN, and TP loading per acre, and median BSI for the NIRL5 to NIRL8 segments from 2016 to 2022.**

Basin	OSTDS/Acre	Avg. Annual Flow (ft <sup>3</sup> )/Acre	Avg. Annual TN (lbs)/Acre	Avg. Annual TP (lbs)/Acre	Median BSI
NIRL5	0.26	77,981	5.29	0.77	0.012 <sub>a</sub>
NIRL6	0.12	74,169	4.47	0.64	0.009 <sub>a</sub>
NIRL7	0.11	60,785	3.66	0.53	0.005 <sub>b</sub>
NIRL8	0.33	83,599	5.56	0.81	0.004 <sub>b</sub>

*Different letters indicate column median significant differences of BSI at  $p < 0.05$  using Friedman. Pairwise comparisons (Nemenyi's) indicated using subscripts. If there are significant differences, the highest value is in bold.*

Hypothesis 2C was further evaluated by determining if there was a significant difference in BSI between the segments when most of total flow was comprised of subsurface flow (**Table 26**). No significant difference was found in BSI between the basins ( $p < 0.363$ ) when the percent of baseflow was above 90%, however at 80% above baseflow a significant difference in median BSI was identified. The NIRL5 segment had the significantly highest ( $p < 0.009$ ) median BSI at 0.014. As the NIRL8 segment has a higher average annual flow and nutrient loading during  $> 80\%$  subsurface flow conditions, this may also be indicative of the potential influence of flushing caused by the Eau Gallie River within the NIRL8 segment. Based on this analysis, the direct relationship between OSTDS density and the BSI is unclear, however the discharge of the Eau Gallie River into the segment may have suppressing effect.

**Table 26. Differences in the average monthly flow, TN, and TP loading per acre, and median and average BSI for the NIRL5 to NIRL8 segments.**

Basin	Avg. Monthly Flow (ft <sup>3</sup> )/Acre	Avg. Monthly TN (lbs)/Acre	Avg. Monthly TP (lbs)/Acre	Median BSI
NIRL5	4,716	0.28	0.04	<b>0.0140</b> <sub>a</sub>
NIRL6	2,248	0.13	0.02	0.0095 <sub>a,b</sub>
NIRL7	1,858	0.11	0.02	0.0045 <sub>b</sub>
NIRL8	5,332	0.32	0.05	0.0050 <sub>b</sub>

*Different letters indicate row median significant differences at  $p < 0.05$  using Kruskal-Wallis. Pairwise comparisons (SDCF) are indicated using subscripts. If significant differences were found, the highest value is in bold.*

#### **3.2.2.4 SAV Extent Estimation**

An estimation of SAV extents can be performed using the NDCI on days when phytoplankton is low. AEI assessed the change in SAV coverage in the BRL3 segment using the higher resolution S2 estimated ChIA data during the years 2017 and 2022 which represent before and after extreme bloom activity in the BRL (**Figure 38**).

There was a total of 7 scenes available in 2017 and 6 in 2022 selected for no cloud cover and low reported ChIA at the SJRWMD IRLB04 sampling station ( $<10 \mu\text{g/L}$ ) and in the open water of the segment. The average estimated ChIA concentration was calculated for each pixel summarizing 2017 and 2022, which could include various species of SAV such as *Caulerpa*, other macroalgae, and seagrass.

Between 2017 and 2022 the area with an estimated ChIA of  $30 \mu\text{g/L}$  or greater decreased from  $4.37 \text{ km}^2$  (1,079.85 acres) to  $0.92 \text{ km}^2$  (227.43 acres). The eastern half of the segment was estimated to have the largest loss, which also aligns with the SJRWMD 2021 seagrass survey and the 2022 benthic survey. The SAV in the western half of the segment appears to have constricted to the shallower waters close to the shoreline. Notably a new lobe of SAV appears to have formed in the center north of the segment between 2017 and 2022. While the NDCI alone is unable to differentiate between a phytoplankton bloom and SAV ChIA, under ideal circumstances S2 data can identify potential locations of SAV and its change in coverage over time.

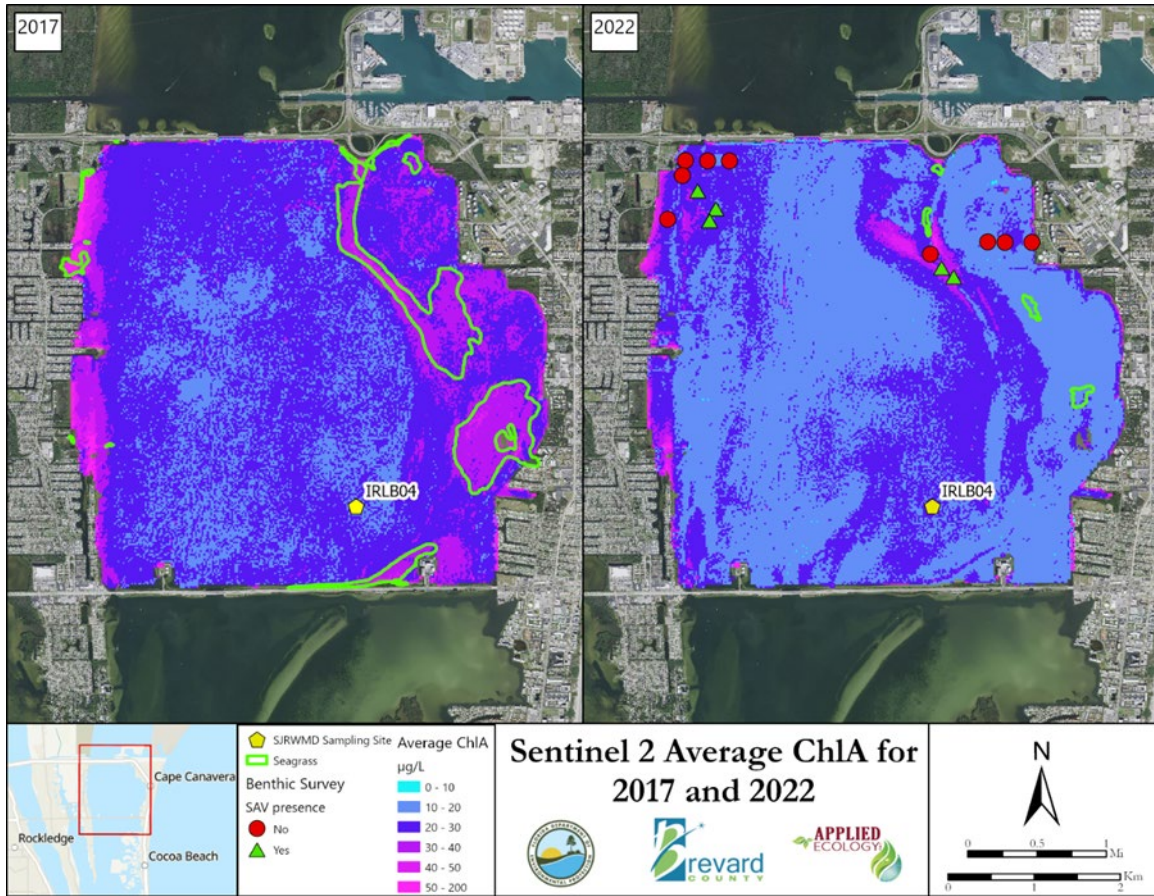


Figure 38. Sentinel 2 cumulative ChlA for 2017 and 2022 for the BRL3 segment. The SJRWMD seagrass extents for 2017 and 2021 are included. [Long Description of Figure 38.](#)

### 3.2.2.5 SAV and Severity

Hypothesis 2D suggested that for a given IRL segment, HABs would occur less frequently in areas with Submerged Aquatic Vegetation (SAV). The larger the SAV area, the less likelihood for severe blooms to occur as the SAV provide ecological services such as preventing sediment resuspension and sequestering nutrients from the water column. AEI selected two subbasins that experienced opposite SAV changes and focused on the years 2017 and 2022, when “Super Bloom” conditions were not present. Between 2017 to 2022, the BRL3 segment was estimated to have lost over 80% of its SAV, a decline from 4.37 km<sup>2</sup> (1,079.85 acres) to 0.92 km<sup>2</sup> (227.43 acres). The second segment, SML2, was selected for comparison as it had a slight (5%) increase in SAV over the same time, an increase from 5.49 km<sup>2</sup> (1,356.80 acres) to 5.89 km<sup>2</sup> (1,456.33 acres).

The BDI, BII, and BSI were compared for BRL3 and SML2 for the years 2017 and 2022. For BRL3, there were 30 scenes available in 2017 and 49 in 2022 and for SML2, there were 33 scenes available in 2017 and 49 in 2022.

From 2017 to 2022, SML2 was observed to have increased high BDI, BII, and BSI scores (**Table 27, Table 28, Table 29**) culminating in an overall greater percentage of high scores for all three indices in 2022. Over the same timeframe, SML2 was estimated to have had a small increase SAV coverage. The opposite occurred in BRL3, where there was an overall decrease in bloom duration, intensity and severity scores and a massive loss of SAV over the same period. This suggests a more complex relationship between SAV coverage and bloom activity than can be simply explained by the presence of SAV. Further exploration is required to determine how SAV coverage interacts with other drivers of bloom activity. Additionally, the apparent resilience of SAV in SML2 to bloom activity should be further explored to identify potential causes.

**Table 27. Binned percent of weeks in 2017 and 2022 of BRL3 and SML2 by their Bloom Duration Index (BDI).**

Segment	Year	0	0.01	0.01	0.02	0.02	0.03	> 0.03
BRL3	2017	27%	43%	7%	23%			
	2022	39%	37%	14%	10%			
SML2	2017	47%	27%	7%	20%			
	2022	18%	29%	18%	35%			

**Table 28. Binned percent of weeks in 2017 and 2022 of BRL3 and SML2 by their Bloom Intensity Index (BII).**

Segment	Year	0.06	0.07	0.07	0.08	0.08	0.09	> 0.09
BRL3	2017	50%	23%	7%	20%			
	2022	57%	22%	6%	14%			
SML2	2017	88%	6%	3%	3%			
	2022	47%	14%	12%	27%			

**Table 29. Binned percent of weeks in 2017 and 2022 of BRL3 and SML2 by their Bloom Severity Index (BSI).**

Segment	Year	0	0.001	0.001	0.002	0.002	0.003	> 0.003
BRL3	2017	10%	43%	23%	23%			
	2022	16%	59%	18%	6%			
SML2	2017	47%	27%	7%	20%			
	2022	12%	33%	16%	39%			

### 3.2.2.6 Muck Removal and Severity

Hypotheses 2E and 2F were that the presence of muck increases bloom activity and that muck removal projects would result in a decrease of proximate bloom activity. To test these hypotheses, the Eau Gallie River was selected as it is a constrained segment with minimal confounding factors. Muck dredging operations were performed between January 2017 to March 2019. All comparisons were performed using a one-tailed Wilcoxon Signed-Rank test.

Prior to the start of dredge operations, there were 24 weeks of S3 estimated BSI of the NIRL8 segment (**Figure 39**). During this period the BSI was significantly above ( $p < 0.0001$ ) the segment average 21 out of the 24 weeks. The most elevated BSI values were observed during the lowest discharge from Eau Gallie, which may suggest less of an influence from the runoff in the watershed and the potential muck flux and baseflow nutrient loading.

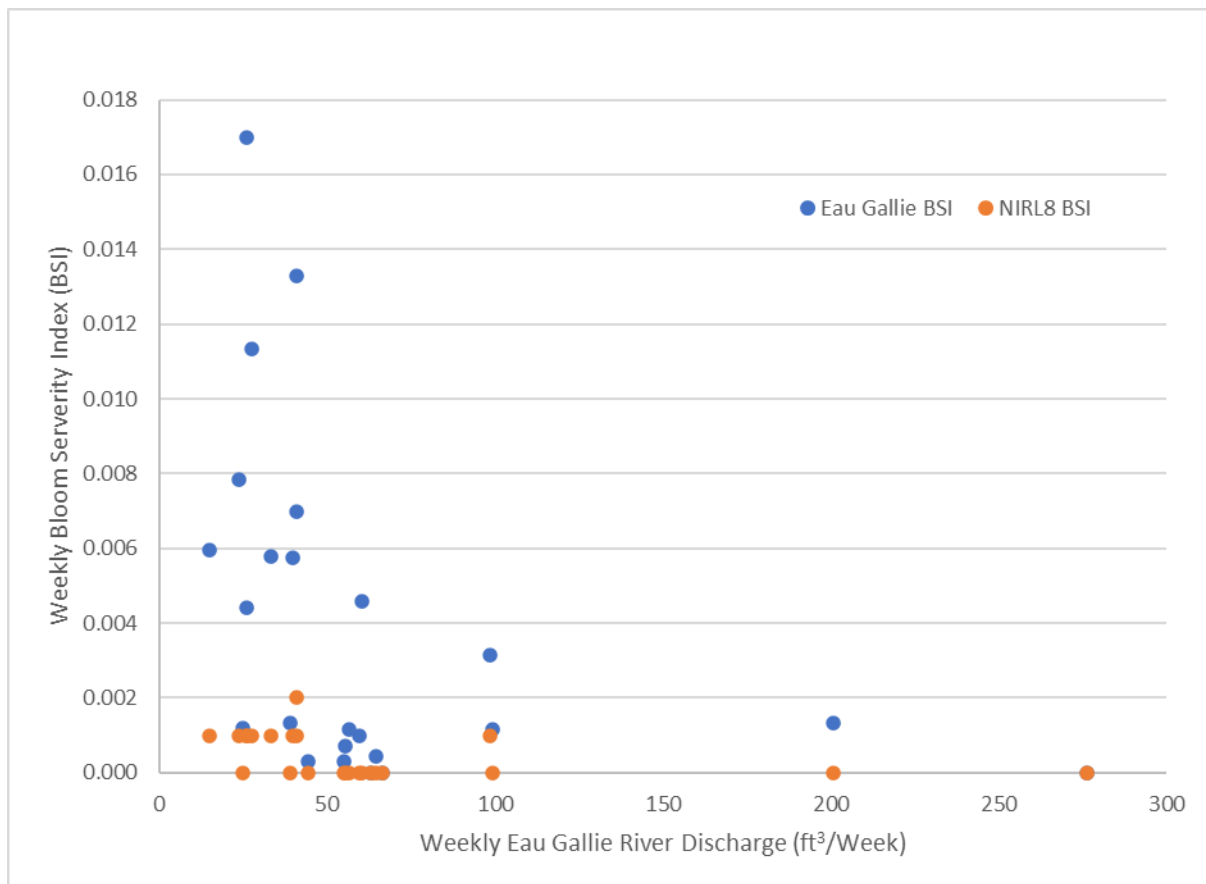


**Figure 39. The weekly Bloom Severity Index (BSI) of the segment of NIRL8 proximate to the mouth of the Eau Gallie River and the entire NIRL8 segment compared to the weekly discharge from the Eau Gallie River between May to December 2016.**  
[Long Description of Figure 39.](#)

During the dredging period there was a super bloom in the BRL starting January 2018, which had spread to the NIRL8 segment by February 2018. Similar, to the pre-dredging period, the area of the NIRL8 segment proximate to the mouth of Eau Gallie had a significantly higher ( $p < 0.0001$ ) BSI than the NIRL8 segment (**Figure 40**). This was doubly so during the bloom period, with the BSI around Eau Gallie being on average 100% higher than the segment.

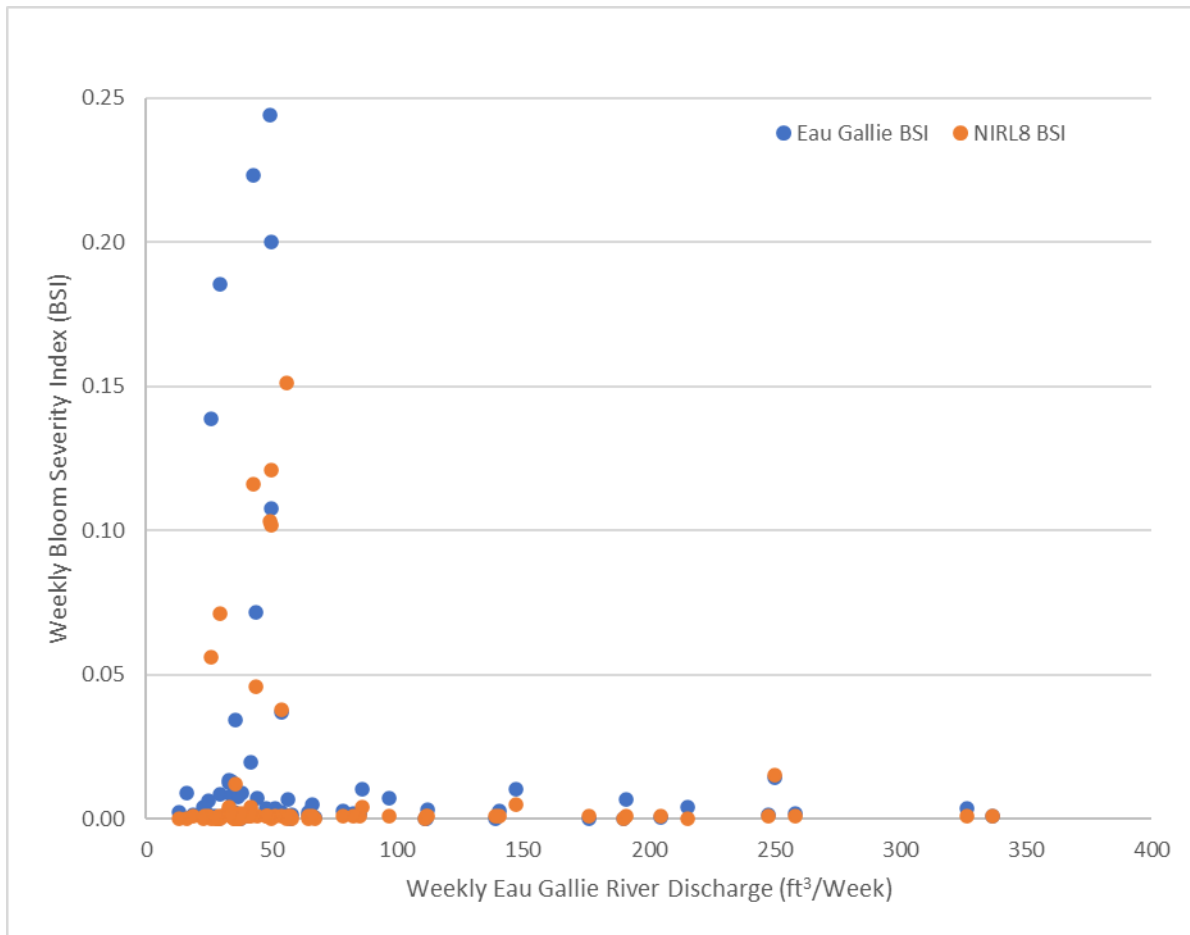


**Figure 40.** The weekly Bloom Severity Index (BSI) of the segment of NIRL8 proximate to the mouth of the Eau Gallie River and the entire NIRL8 segment compared to the weekly discharge from the Eau Gallie River between January 2017 to March 2019. [Long Description of Figure 40.](#)

After the completion of the dredging operation in March 2019, there was another super bloom in the IRL which ran from July to December 2020 primarily in the NIRL. During this period, the BSI for the segment around the mouth of the Eau Gallie was on average 57% lower than the entire segment (**Figure 41**). For the remainder of this period, the Eau Gallie area was significantly below ( $p < 0.0001$ ) the segment BSI.

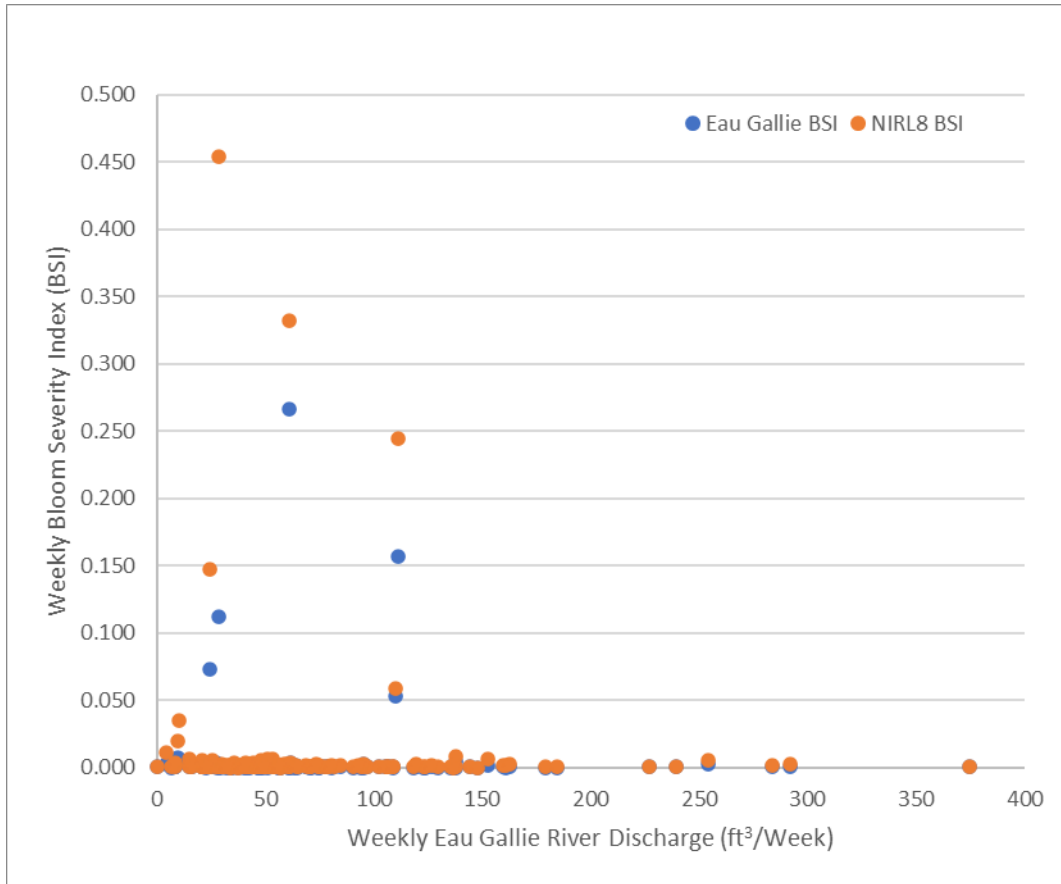


**Figure 41. The weekly Bloom Severity Index (BSI) of the segment of NIRL8 proximate to the mouth of the Eau Gallie River and the entire NIRL8 segment compared to the weekly discharge from the Eau Gallie River between April 2019 to December 2022. [Long Description of Figure 41.](#)**

This assessment of the pre, during, and post muck dredging of the Eau Gallie River appears to identify that the removal of muck from the mouth of the river has reduced the BSI in the immediate area. Hypothesis 6E appears to be accurate for the Eau Gallie muck removal, in that the BSI of blooms decreased in the years following the muck removal. As the BSI of blooms both before and during the muck removal were not significantly different, it appears that the method of muck removal may not have exacerbated bloom activity. Lastly it also appears that hypothesis 6F is accurate for the Eau Gallie River, as the BSI of the area around the river was consistently lower following dredge operations. However, with only 24 weeks of pre-dredge observations, there may be other impacts such as climatic conditions that should be explored.

---

## 4 CONCLUSIONS AND FURTHER RESEARCH

---

### 4.1 CONCLUSIONS

---

#### 4.1.1 REMOTE SENSING ESTIMATED CHLOROPHYLL-A

The first objective of this study was to identify and then evaluate the most efficient Sentinel-2 and Sentinel-3 algorithms for assessing conditions within the IRL. The previously calibrated Normalized Difference Chlorophyll Index (NDCI) was validated using 2022 ground truth data, further supporting Hypothesis 1A that the 708 nm peak can explain the variation in ChlA concentrations. The S2 NDCI algorithm had an  $R^2$  of 0.87 and RMSE of 4.54  $\mu\text{g/L}$  and the S3 NDCI algorithm had an  $R^2$  of 0.93 and RMSE of 4.70  $\mu\text{g/L}$  in 2022. The RMSE values can be interpreted as the algorithms margin of error or ability to estimate ChlA concentrations within 4.54  $\mu\text{g/L}$  for S2 and 4.70  $\mu\text{g/L}$  for S3.

The 708 nm peak was also effective for use with both the FLAME and BaySpec hyperspectral sensors using the NDCI to estimate the water column ChlA concentrations. However, the performance of the hyperspectral sensors was lower compared to S2 and S3. The FLAME NDCI algorithm had an  $R^2$  of 0.66 and RMSE of 4.96  $\mu\text{g/L}$  and the BaySpec NDCI algorithm had an  $R^2$  of 0.53 and RMSE of 3.98  $\mu\text{g/L}$  in 2022. This supported Hypothesis 1B that the 708 nm reflectance peak was consistent between the satellite and terrestrial sensors. However, the NDCI algorithm had difficulty estimating ChlA concentrations below 10  $\mu\text{g/L}$  regardless of sensor type and the majority of the hyperspectral sensor calibration samples were below 10  $\mu\text{g/L}$ . Additionally, the availability of fair weather and ideal light conditions restrict the use of UAS hyperspectral mapping and require careful planning to account for the highly variable weather in locations such as coastal Florida.

The comparison of reflectance between SAV and phytoplankton identified extremely similar reflectance patterns, with substantial overlap at the 708 nm peak. The FLAME and BaySpec hyperspectral reflectance did not appear to confirm any unique features to aid in the differentiation of the two sources of ChlA. S2 and S3 estimated ChlA was also heavily influenced by the presence of SAV and resulted in ChlA overestimations. Using ChlA estimates on days known to not have bloom activity, a mask was created which allowed for the removal of SAV influenced locations from further analysis. Accurate water column ChlA estimation may only be able to be performed in areas with no SAV present. This partially supported Hypothesis 1C in that water column ChlA concentrations are influenced by the presence of SAV.

S2 and S3 estimated ChlA provides a method for the identification of SAV dominated benthic areas within the IRL. The evaluation of SAV coverage estimation for the BRL3 segment from 2017 and 2022 identified a 78% loss in coverage which largely mirrored the reported seagrass loss by the SJRWMD for that segment. Additionally, the identification of likely SAV locations was used in the creation of a mask that was applied to the S2 and S3 water column ChlA estimations to prevent the misidentification of potential blooms.

HAB phytoplankton includes eukaryotic and cyanobacteria (CB) taxa, which both contain ChlA and the 708 nm reflectance peak alone is unable to differentiate between them. The unique CB reflectance peak at 620 nm was confirmed with two CB algorithms to differentiate between the two taxa in the IRL for both the hyperspectral and satellite sensors. The two algorithms had similar performance, with the Normalized Difference Phycocyanin Index (NDPCI) having an  $R^2$  of 0.66 and RMSE of 11.5% and 2 Band Algorithm for Phycocyanin (2BDA-PC) with an  $R^2$  of 0.65 and RMSE of 11.7%. The RMSE values calculated for the S2 and S3 CB algorithms can be interpreted as the algorithms ability to create an estimate of the percent of the phytoplankton within 11.5% and 11.7%, respectively.

Both hyperspectral sensors identified a second unique reflectance peak around 650 nm for a *Picocyanobacteria spp.* dominated sample. While this spectral range is not currently measured by any publicly available satellite sensor, the algorithm can be utilized by other hyperspectral sensors to better differentiate between taxa.

The S2 and S3 NDCI estimated ChlA is a powerful tool for observing HAB activity in the IRL. It can be used to accurately estimate ChlA concentrations and the movement of blooms, then when paired with the NDPCI the presence of CB in a bloom can also be quantified. While the presence of SAV can interfere with these estimations, the NDCI can also be utilized to identify the coverage of SAV within the lagoon. While S2 and S3 provide almost daily imagery of the lagoon, the presence of cloud cover results in data gaps. In these cases, the use of handheld and UAS hyperspectral sensors can be powerful tools for the rapid assessment of HAB activity and benthic conditions of the lagoon.

---

#### **4.1.2 BLOOM DURATION, INTENSITY, AND SEVERITY**

To assess if HAB duration, intensity, and severity was changing within the lagoon a series of indices were created for use with NDCI estimated ChlA concentrations. Bloom severity was defined as the product of the duration of a bloom and its ChlA concentration for a given location. The Bloom Duration Index (BDI) estimated the harm

caused by long lasting blooms while the Bloom Intensity Index (BII) estimated the harm caused by repeated high concentration blooms. The BDI and BSI together create the Bloom Severity Index (BSI) which estimates the harm caused by long lasting, high concentration blooms on a given location.

These indices were applied to determine if HAB duration, intensity, and severity were increasing from 2017-2019 to 2020-2022. There appeared to be a decreasing trend in the BSI for the N-NIRL and BRL. The NIRL1 segment was the only to have significant decreases in BSI across all quarters between 2017-2019 and 2020-2022. The majority of the decreases in BSI observed in the BRL occurred during Q1 (January-March) and Q3 (July-September). However, there also appeared to be an increasing trend in BSI for the C-NIRL, S-NIRL, and N-CIRL. For these areas, the largest increases in BSI between 2017-2019 to 2020-2022 was observed during Q1. The hypothesis appears to have been correct for the segments of the IRL from NIRL5 to NIRL8 and then the N-CIRL.

Additional analysis was performed using the indices to identify the relationship between blooms and their potential drivers. Hypothesis 2B was that blooms occurred more often in areas with larger stormwater inputs. The NIRL-5 through NIRL-8 segments were identified to have significantly higher BSI during months with very low rainfall, while there was no significant difference in BSI during wet months. Hypothesis 2C investigated the impact that Onsite Sewage Treatment and Disposal Systems (OSTDS) or septic systems have on blooms. Using the NIRL-5 through NIRL-8 segments, a significantly higher BSI was identified in the northernmost NIRL-5 segment both overall and during low rainfall periods. NIRL-8 had a higher density of OSTDS and modeled nutrient inputs from its drainage area, suggesting that factors other than OSTDS may be causing the elevated BSI in NIRL-5.

Hypothesis 2D suggested that blooms would occur less frequently in areas with SAV present. SML2 was identified as one of the few segments to not experience a loss of SAV from 2017 to 2022, whereas BRL3 experienced a 78% decline in SAV coverage. The comparison of the bloom indices in 2017 and then in 2022 did not support Hypothesis 2D. SML2, which did not lose SAV, was observed to have increased occurrences of higher BDI, BII, and BSI values, while there was a decline observed in BRL3. The relationship between blooms and SAV will require additional assessment using a more comprehensive analysis.

Hypotheses 2E and 2F were that the presence of muck increases bloom activity and that muck removal projects would result in a decrease of bloom activity. To assess these hypotheses, the BSI of the area near the mouth of the Eau Gallie River was compared to

the overall BSI of the NIRL-8 segment it flows into. Both prior to and during the dredging project, the BSI around the mouth of the Eau Gallie River was significantly higher than the NIRL-8 segment. This suggests that for the Eau Gallie River, the presence of muck may have been leading to elevated BSI. Following the completion of the muck dredging in March 2019, this segment had significantly lower BSI than the NIRL-8 segment.

## 4.2 FURTHER RESEARCH

---

### 4.2.1 PHYTOPLANKTON REMOTE SENSING

In 2022 there were few long-lasting blooms compared to previous years, which reduced opportunities for targeted hyperspectral analysis. The continued collection of hyperspectral data alongside the SJRWMD monthly sampling effort would be a cost-effective means to increase the probability of capturing bloom measurements. Additionally, the S2 bloom estimates identified substantial spatial variation in IRL phytoplankton. A higher spatial density of water and hyperspectral samples should be collected to increase the probability of capturing a higher concentration sample and to provide a more accurate assessment of the ChlA in a given Sentinel pixel.

Since the NDCI was confirmed as an effective ChlA estimation algorithm along with the CB indices, customizable multispectral sensors can be utilized to overcome the interference associated with weather conditions while saving equipment costs. There are handheld and UAS mounted systems currently commercially available that have fewer spectral bands which perform better in low light conditions and then the bands can be set to the specific reflectance peaks of ChlA and phycocyanin identified in this study.

### 4.2.2 HAB PATTERN ANALYSIS

The formation and lifecycle of HABs has been documented in literature and this study to be impacted by a range of climatic, geochemical, and hydrological factors. Further analysis of changes in BDI, BII, and BSI within the IRL should be performed using a larger range of drivers. Wind strength, direction, and duration were observed to strongly correlate with bloom movements observed by S2 and S3 from day to day. The determination of the relationship between wind and bloom movement could be used to inform the assessment of severity by delineating between static and transient blooms.

Wind was also a confounding factor during analysis of bloom patterns at the small scale. Further assessment of muck sediment influences would likely benefit from the inclusion of wind driven currents, as muck driven blooms could appear downwind of the muck pocket. Additionally, some of the high BSI locations were proximate to the causeways

crossing the IRL which could be the result of blooms accumulated in these areas due to the restricted flow and wind direction.

The influence of other climatic factors such as precipitation and temperature should be further explored as some of the bloom patterns observed in this study appeared to be contrary to expected bloom patterns from literature. The most notable of these patterns is the apparent increase in BSI during the cooler months (October-March). This pattern can be further explored through the inclusion of NEXRAD precipitation estimates and the S3 Sea and Land Surface Temperature Radiometer (SLSTR).

Lastly, as the BSI weighting was assigned based on a conceptual understanding of potential harm caused by extreme ChIA concentrations it should be compared against known bloom related events. The Florida Fish and Wildlife Conservation Commission (FWC) maintains a spatial record of reported marine mass mortality events such as fish kills, which could be compared against the BSI. The BSI could also be compared against the S2 estimated ChIA extents to identify any potential patterns between changes in SAV extents and BSI.

## 5 REFERENCES

---

- Applied Ecology Inc (AEI). (2022a). Indian River Lagoon HAB Remote Sensing Historical Time Series Analysis Technical Memorandum. Prepared for Brevard County
- Applied Ecology Inc (AEI). (2022b). 2022 SWIL Model Simulation Update. Prepared for Florida Institute of Technology
- Ammenberg, P., Flink, P., Lindell, T., Pierson, D., & Strombeck, N. (2002). Bio-optical modelling combined with remote sensing to assess water quality. *International Journal of Remote Sensing*, 23(8), 1621-1638.
- Beck, R., Xu, M., Zhan, S., Liu, H., Johansen, R. A., Tong, S., & Huang, Y. (2017). Comparison of satellite reflectance algorithms for estimating phycochlorophyll values and cyanobacterial total biovolume in a temperate reservoir using coincident hyperspectral aircraft imagery and dense coincident surface observations. *Remote Sensing*, 9(6), 538.
- Caballero, I., Navarro, G., Fernández, R., Mamán, L., & Escalante, O. M. (2020). New capabilities of Sentinel-2A/B satellites combined with in situ data for monitoring small harmful algal blooms in complex coastal waters. *Scientific Reports*, 10(1).
- Dey, J. & Vijay, R. (2021). A critical and intensive review on assessment of water quality parameters through geospatial techniques. *Environmental Science and Pollution Research*, 28(31), 41612-41626.
- Duan, H., Ma, R., & Hu, C. (2012). Evaluation of remote sensing algorithms for cyanobacterial pigment retrievals during spring bloom formation in several lakes of East China. *Remote Sensing of Environment*, 126, 126-135.
- El-Alem, A., Chokmani, K., Venkatesan, A., Rachid, L., Agili, H., & Dedieu, J. P. (2021). How Accurate Is an Unmanned Aerial Vehicle Data-Based Model Applied on Satellite Imagery for Chlorophyll-a Estimation in Freshwater Bodies?. *Remote Sensing*, 13(6), 1134.
- Eugenio, F., Marcello, J., & Martin, J. (2015). High-resolution maps of bathymetry and benthic habitats in shallow-water environments using multispectral remote sensing imagery. *IEEE Transactions on Geoscience and Remote Sensing*, 53(7), 3539-3549.
- Gitelson, A. A., Kaufman, Y. J., & Merzlyak, M. N. (1996). Use of a green channel in remote sensing of global vegetation from EOS-MODIS. *Remote sensing of Environment*, 58(3), 289-298.

- Gower, J., King, S., & Goncalves, P. (2008). Global monitoring of plankton blooms using MERIS MCI. *International Journal of Remote Sensing*, 29(21), 6209-6216.
- Hartoni, H., Siregar, V. P., Wouthuyzen, S., & Agus, S. B. (2022). Object based classification of benthic habitat using Sentinel 2 imagery by applying with support vector machine and random forest algorithms in shallow waters of Kepulauan Seribu, Indonesia. *Biodiversitas Journal of Biological Diversity*, 23(1).
- Hu, C. & Feng, L. (2016). Modified MODIS fluorescence line height data product to improve image interpretation for red tide monitoring in the eastern Gulf of Mexico. *Journal of Applied Remote Sensing*, 11(1), 012003.
- Hu, C., Muller-Karger, F. E., Taylor, C. J., Carder, K. L., Kelble, C., Johns, E., & Heil, C. A. (2005). Red tide detection and tracing using MODIS fluorescence data: A regional example in SW Florida coastal waters. *Remote Sensing of Environment*, 97(3), 311-321.
- Huisman, J., Codd, G. A., Paerl, H. W., Ibelings, B. W., Verspagen, J. M., & Visser, P. M. (2018). Cyanobacterial blooms. *Nature Reviews Microbiology*, 16(8), 471-483.
- Judice, T. J., Widder, E. A., Falls, W. H., Avouris, D. M., Cristiano, D. J., & Ortiz, J. D. (2020). Field-Validated Detection of *Aureoumbra lagunensis* Brown Tide Blooms in the Indian River Lagoon, Florida, Using Sentinel-3A OLCI and Ground-Based Hyperspectral Spectroradiometers. *GeoHealth*, 4(6), e2019GH000238.
- Kallio, K., Attila, J., Härmä, P., Koponen, S., Pulliainen, J., Hyytiäinen, U. M., & Pyhälähti, T. (2008). Landsat ETM+ images in the estimation of seasonal lake water quality in boreal river basins. *Environmental Management*, 42(3), 511-522.
- Kalogirou, V., Ramos Perez, J., & Arino, O. (2013). A first analysis on the Culture-MERIS products. *Remote sensing letters*, 4(3), 211-218.
- Kamerosky, A., Cho, H. J., & Morris, L. (2015). Monitoring of the 2011 super algal bloom in Indian River Lagoon, FL, USA, using MERIS. *Remote Sensing*, 7(2), 1441-1460.
- Kamerosky, A., Listopad, C., Barker, V. (2023). Remote sensing of harmful algal blooms in the Indian River Lagoon and connected waterways in Brevard County. *Florida scientist*, 386-399.
- Kang, Y., Koch, F., & Gobler, C. J. (2015). The interactive roles of nutrient loading and zooplankton grazing in facilitating the expansion of harmful algal blooms caused by the pelagophyte, *Aureoumbra lagunensis*, to the Indian River Lagoon, FL, USA. *Harmful Algae*, 49, 162-173.

- Khan, R. M., Salehi, B., Mahdianpari, M., Mohammadimanesh, F., Mountrakis, G., & Quackenbush, L. J. (2021). A Meta-Analysis on Harmful Algal Bloom (HAB) Detection and Monitoring: A Remote Sensing Perspective. *Remote Sensing*, 13(21), 4347.
- Koponen, S., Attila, J., Pulliainen, J., Kallio, K., Pyhälähti, T., Lindfors, A., ... & Hallikainen, M. (2007). A case study of airborne and satellite remote sensing of a spring bloom event in the Gulf of Finland. *Continental Shelf Research*, 27(2), 228-244.
- Kravitz, J., Matthews, M., Bernard, S., & Griffith, D. (2020). Application of Sentinel 3 OLCI for chl-a retrieval over small inland water targets: Successes and challenges. *Remote Sensing of Environment*, 237, 111562.
- Kudela, R. M., Palacios, S. L., Austerberry, D. C., Accorsi, E. K., Guild, L. S., & Torres-Perez, J. (2015). Application of hyperspectral remote sensing to cyanobacterial blooms in inland waters. *Remote Sensing of Environment*, 167, 196-205.
- Kutser, T., Paavel, B., Verpoorter, C., Ligi, M., Soomets, T., Toming, K., & Casal, G. (2016). Remote sensing of black lakes and using 810 nm reflectance peak for retrieving water quality parameters of optically complex waters. *Remote Sensing*, 8(6), 497.
- Kwan, C. & Budavari, B. (2020). Enhancing small moving target detection performance in low-quality and long-range infrared videos using optical flow techniques. *Remote Sensing*, 12(24), 4024.
- Kwon, Y. S., Pyo, J., Kwon, Y. H., Duan, H., Cho, K. H., & Park, Y. (2020). Drone-based hyperspectral remote sensing of cyanobacteria using vertical cumulative pigment concentration in a deep reservoir. *Remote Sensing of Environment*, 236, 111517.
- Lazuardi, W. & Wicaksono, P. (2021). Assessment of Coral Reef Life-Form Classification Scheme using Multiresolution Images on Parang Island, Indonesia. *Geosfera Indonesia*, 6(3), 377-397.
- Lopez, C. B., Tilney, C. L., Muhlbach, E., Bouchard, J. N., Villac, M. C., Henschen, K. L., ... & Hubbard, K. A. (2021). High-Resolution Spatiotemporal Dynamics of Harmful Algae in the Indian River Lagoon (Florida)—A Case Study of *Aureoumbra lagunensis*, *Pyrodinium bahamense*, and *Pseudo-nitzschia*. *Frontiers in Marine Science*, 1737.
- Matthews, M. W. & Bernard, S. (2015). Eutrophication and cyanobacteria in South Africa's standing water bodies: A view from space. *South African journal of science*, 111(5), 1-8.

Maxwell, K. & Johnson, G. N. (2000). Chlorophyll fluorescence—a practical guide. *Journal of experimental botany*, 51(345), 659-668.

Mishra, S. & Mishra, D. R. (2012). Normalized difference chlorophyll index: A novel model for remote estimation of chlorophyll-a concentration in turbid productive waters. *Remote Sensing of Environment*, 117, 394-406.

Mishra, S., Stumpf, R. P., Schaeffer, B., Werdell, P. J., Loftin, K. A., & Meredith, A. (2021). Evaluation of a satellite-based cyanobacteria bloom detection algorithm using field-measured microcystin data. *Science of The Total Environment*, 774, 145462.

Morel, A. & Prieur, L. (1977). Analysis of variations in ocean color 1. *Limnology and Oceanography*, 22(4), 709-722

Ogashawara, I., Mishra, D. R., Mishra, S., Curtarelli, M. P., & Stech, J. L. (2013). A performance review of reflectance based algorithms for predicting phycocyanin concentrations in inland waters. *Remote Sensing*, 5(10), 4774-4798.

Ogashawara, I. (2019). The use of Sentinel-3 Imagery to monitor cyanobacterial blooms. *Environments*, 6(6), 60.

Ouillon, S., Douillet, P., Petrenko, A., Neveux, J., Dupouy, C., Froidefond, J. M., ... & Muñoz-Caravaca, A. (2008). Optical algorithms at satellite wavelengths for total suspended matter in tropical coastal waters. *Sensors*, 8(7), 4165-4185.

Pahlevan, N., Smith, B., Alikas, K., Anstee, J., Barbosa, C., Binding, C., ... & Ruiz-Verdù, A. (2022). Simultaneous retrieval of selected optical water quality indicators from Landsat-8, Sentinel-2, and Sentinel-3. *Remote Sensing of Environment*, 270, 112860.

Pahlevan, N., Smith, B., Schalles, J., Binding, C., Cao, Z., Ma, R., ... & Stumpf, R. (2020). Seamless retrievals of chlorophyll-a from Sentinel-2 (MSI) and Sentinel-3 (OLCI) in inland and coastal waters: A machine-learning approach. *Remote Sensing of Environment*, 240, 111604.

Pahlevan, N., Smith, B., Schalles, J., Binding, C., Cao, Z., Ma, R., Alikas, K., Kangro, K., Gurlin, D., Hà, N., Matsushita, B., Moses, W., Greb, S., Lehmann, M. K., Ondrusek, M., Oppelt, N., & Stumpf, R. (2020). Seamless retrievals of chlorophyll-a from Sentinel-2 (MSI) and Sentinel-3 (OLCI) in inland and coastal waters: A machine-learning approach. *Remote Sensing of Environment*, 240.

Phlips, E. J., Badylak, S., Nelson, N. G., Hall, L. M., Jacoby, C. A., Lasi, M. A., ... & Miller, J. D. (2021). Cyclical Patterns and a Regime Shift in the Character of Phytoplankton Blooms in

a Restricted Sub-Tropical Lagoon, Indian River Lagoon, Florida, United States. *Frontiers in Marine Science*, 1351.

Reyier, E. A., Shenker, J. M., & Christian, D. (2008). Role of an estuarine fisheries reserve in the production and export of ichthyoplankton. *Marine Ecology Progress Series*, 359, 249-260.

Rodríguez-Benito, C. V., Navarro, G., & Caballero, I. (2020). Using Copernicus Sentinel-2 and Sentinel-3 data to monitor harmful algal blooms in Southern Chile during the COVID-19 lockdown. *Marine Pollution Bulletin*, 161, 111722.

Roulet, N. & Moore, T. R. (2006). Browning the waters. *Nature*, 444(7117), 283-284.

Ruddick, K.G.; De Cauwer, V.; Park, Y.J.; Moore, G. Seaborne measurements of near infrared water-leaving reflectance: The similarity spectrum for turbid waters. *Limnol. Oceanogr.* 2006, 51, 1167–1179.

Sent, G., Biguino, B., Favareto, L., Cruz, J., Sá, C., Dogliotti, A. I., ... & Brito, A. C. (2021). Deriving water quality parameters using Sentinel-2 imagery: A case study in the Sado estuary, Portugal. *Remote Sensing*, 13(5), 1043.

Shi, K., Zhang, Y., Qin, B., & Zhou, B. (2019). Remote sensing of cyanobacterial blooms in inland waters: present knowledge and future challenges. *Science Bulletin*, 64(20), 1540-1556.

Slonecker, T., Bufford, B., Graham, J., Carpenter, K., Opstal, D., Simon, N., & Hall, N. (2021). Hyperspectral Reflectance Characteristics of Cyanobacteria. *Advances in Remote Sensing*, 10(3), 66-77.

Smith, N. P. (1993). Tidal and nontidal flushing of Florida's Indian River Lagoon. *Estuaries*, 16(4), 739-746.

Sòria-Perpinyà, X., Vicente, E., Urrego, P., Pereira-Sandoval, M., Tenjo, C., Ruíz-Verdú, A., ... & Moreno, J. (2021). Validation of Water Quality Monitoring Algorithms for Sentinel-2 and Sentinel-3 in Mediterranean Inland Waters with In Situ Reflectance Data. *Water*, 13(5), 686.

Steward, J. S. & Green, W. C. (2007). Setting load limits for nutrients and suspended solids based upon seagrass depth-limit targets. *Estuaries and Coasts*, 30(4), 657-670.

Steward, J. S., Virnstein, R. W., Morris, L. J., & Lowe, E. F. (2005). Setting seagrass depth, coverage, and light targets for the Indian River Lagoon system, Florida. *Estuaries*, 28(6), 923-935.

Tedetti, M., Cuet, P., Guigue, C., & Goutx, M. (2011). Characterization of dissolved organic matter in a coral reef ecosystem subjected to anthropogenic pressures (La Réunion Island, Indian Ocean) using multi-dimensional fluorescence spectroscopy. *Science of the Total Environment*, 409(11), 2198-2210.

Tyler, A. N., Hunter, P. D., Carvalho, L., Codd, G. A., Elliott, J. A., Ferguson, C. A., ... & Scott, E. M. (2009). Strategies for monitoring and managing mass populations of toxic cyanobacteria in recreational waters: a multi-interdisciplinary approach. *Environmental Health*, 8(1), 1-8.

US Census. (2021). "U.S. Census Bureau Quickfacts: Florida." QuickFacts United States.

Wang, G., Lee, Z., Mishra, D. R., & Ma, R. (2016). Retrieving absorption coefficients of multiple phytoplankton pigments from hyperspectral remote sensing reflectance measured over cyanobacteria bloom waters. *Limnology and Oceanography: Methods*, 14(7), 432-447.

Wynne, T. T., Meredith, A., Briggs, T., Litaker, W., & Stumpf, R. P. (2018). Harmful algal bloom forecasting branch ocean color satellite imagery processing guidelines.

## 6 FIGURE DESCRIPTIONS

### Figure 1

Figure 1 shows the study area boundary with the basins of the Indian River Lagoon (IRL) within Brevard County identified. There is a small map showing the state of Florida inset in the bottom left corner and it shows the study area, Brevard County, outlined in red. The Indian River Lagoon Basins included are the north and south Mosquito Lagoon, Northern IRL, Banana River, and the Central IRL. The Mosquito Lagoon is located on the northern edge of the county, along the east side, between the Atlantic and the Merritt Island National Wildlife Reserve. The Northern IRL runs from the northern edge of the county north to Melbourne. It is between Merritt Island and the mainland. The Banana River runs through the middle of the county, between beachside and mainland. The Central IRL runs from Melbourne to the northern edge of the county and is between beachside and mainland. There are 18 watershed basins within the IRL, each one is outlined with a different color within the map and tagged. In the northern half of the IRL, from Rockledge north, there are the following basins: NIRL1, NIRL2, NIRL3, NIRL4, SML1, SML2, BR1, BR2, and BR3. The central IRL basins, located between Rockledge on the north and Melbourne on the south, contain the following: NIRL6, NIRL7, NIRL8, R4, BR5, and BR6. The southern IRL, from Melbourne south to Roseland, include the following basins: CIRL1 and CIRL2.

[Return to Figure 1](#)

### Figure 2

Figure 2 contains a study area boundary with the St Johns River Water Management District's (SJRWMD) monthly estuary surface water sampling sites. There is a small map showing the state of Florida inset in the bottom left corner and it shows the study area, Brevard County, outlined in red. In the northern Indian River Lagoon (IRL), from Rockledge north to Canaveral National Seashore, the following sites are outlined: BFRR, I02, I06, IRCMTITUS01, I07, I10, I13, SCPW, ML02, I09E, B02, and B04. In the central IRL, Rockledge south to Melbourne, the following sites are outlined: I15, NFH01S, I16, I18, I21, B05, B06, and B09. In the southern portion of the IRL, Melbourne south to Roseland, the following sites are outlined: I24, I27, I23, I26, and I28.

[Return to Figure 2](#)

## Figure 3

---

Figure 3 is showing the Applied Ecology, Inc. Unmanned Aircraft System (UAS) survey locations within the Indian River Lagoon (IRL) in Brevard County. There is a small map showing the state of Florida inset in the bottom left corner and it shows the study area, Brevard County, outlined in red. The survey locations are depicted as different color circles to indicate the 6 different survey areas. There are three survey locations in the Northern Indian River Lagoon (N-NIRL), three in the Central Banana River Lagoon (C-BRL), five in the Southern Banana River Lagoon (S-BRL), four in the Southern Indian River Lagoon (S-NIRL), eight in the North-Central Indian River Lagoon (N-CIRL), and one survey location in the Central Indian River Lagoon (C-NIRL).

[\*\*Return to Figure 3\*\*](#)

## Figure 4

---

Figure 4 consists of Sentinel 2 and Sentinel 3 data inventory from 2015 to 2023 by year and season. Number of images, ranging from 0 to 90, is depicted along the Y-axis while dates 2015 to 2023 separated into Dry and Wet, with Sentinel 2 and Sentinel 3 shown as different colored bars during each season, is depicted along the X-axis. During the entire study period, Sentinel 3 had the most images with as many as 80 images taken during the dry season of 2022. Sentinel 2 images were low for the majority of the study period with the exception of 2022 where over 30 images were taken during the dry season and just under 30 images were taken during the wet season.

[\*\*Return to Figure 4\*\*](#)

## Figure 5

---

Figure 5 shows the Sentinel 2 (S2) Scattering Line Height (SLH) Calibration Validation Dataset comparison between the estimated and measured ChlA concentrations. Measured ChlA in ug/L from 0.00 to 80.00 is noted along the Y-axis while the S2 Estimated ChlA measured in ug/L from 0.00 to 70.00 is noted along the X-axis. The S2 calibration validation dataset included measured ChlA concentrations in the IRL that ranged from 1.70 to 67.90  $\mu\text{g/L}$  and had a median value 10.20  $\mu\text{g/L}$ . The dataset included 113 sampling locations with 7 points in the Mosquito Lagoon, 59 in the NIRL, 28 in the Banana River Lagoon, and 19 in the CIRL. The NDCI algorithm validation dataset had an  $R^2$  of 0.87, RMSE of 4.54  $\mu\text{g/L}$ , Bias of -1.20  $\mu\text{g/L}$ , and a Nash criterion of 0.98. There did not appear to be any notable outliers in the validation dataset.

[\*\*Return to Figure 5\*\*](#)

## Figure 6

---

Figure 6 shows the Sentinel 3 (S3) Scattering Line Height (SLH) Calibration Validation Dataset comparison between the estimated and measured ChlA concentrations. Measured ChlA in ug/L from 0.00 to 80.00 is noted along the Y-axis while the S2 Estimated ChlA measured in ug/L from 0.00 to 80.00 is noted along the X-axis. The S3 calibration validation dataset was also found to be representative of the measured ChlA in the IRL with the highest ChlA value at 67.9  $\mu\text{g/L}$ , lowest at 1.10  $\mu\text{g/L}$ , and a median value of 7.10  $\mu\text{g/L}$ . This calibration dataset contained a total of 180 sampling locations with 15 in the Mosquito Lagoon (ML), 83 in the NIRL, 49 in the Banana River Lagoon (BRL), and 27 in the CIRL. The S3 NDCI algorithm had a  $R^2$  of 0.93, RMSE of 4.70  $\mu\text{g/L}$ , a Bias of 2.20  $\mu\text{g/L}$ , and a Nash criterion of 0.95. The NDCI algorithm did not have any clear outliers ChlA. However, for 37 points where the measured ChlA was below 10  $\mu\text{g/L}$ , the NDCI estimated ChlA was negative.

[\*\*Return to Figure 6\*\*](#)

## Figure 7

---

Figure 7 is a scatter plot comparison of the ChlA estimation error of S2 and S3 for synchronous sampling days. The S3 Estimated ChlA Error, measured in ug/L, is shown on the Y-axis while the S2 Estimated ChlA Error measured in ug/L is shown on the X-axis. Where both the S2 and S3 overpass were within 24 hours of the SJRWMD surface water grab. The error of ChlA estimation for S2 and S3 for a given sample site on a given day

was plotted to determine if there was a systematic pattern of over or underestimation by either sensor.

A total of 34 samples in 2022 were used in the analysis, including 4 in SML, 21 in NIRL, 3 in BRL, and 6 in the CIRL. The highest measured ChlA in this dataset was 67.9 µg/L, lowest was 10.45 µg/L, and the median was 15.7 µg/L. For 28 of the 34 (82%), the estimated ChlA from both S2 and S3 sites were within 5 µg/L of the measured ChlA. There was at least one clear outlier for both S2 and S3, which is likely the result of spatial variation between the sample collection location and sensor's pixel. This low level of ChlA error between the S2 and S3 sensors supports the interchangeability of their ChlA estimates in the IRL.

**[Return to Figure 7](#)**

**Figure 8**

Figure 8 is a comparison of FLAME spectral signals from two Saint Johns River Water Management District's (SJRWMD) sampling locations sampled the same day and the same location on different days. There are three different colored lines depicting the date and location. Along the Y-axis is the percentage of Remote Sensing Reflectance, ranging from 0% to 6%. Along the X-axis is the Spectrum measured in nm and ranging from 400 to 900 nm. There is a solid green, vertical line, at the 705nm mark on the graph that is highlighting the ChlA reflectance at 705 nm. As expected, there was a strong peak reflectance around the 705 nm spectrum from the sample collected on July 7, 2022, at the SJRWMD sampling site I18. For comparison, the reflectance collected on the same day at another location (I10) with minimal ChlA lacked this 705 nm peak as did a sample collected at the I18 site two months prior. This supports the conclusion that the NDCI can be applied to the FLAME data to create an estimate of ChlA.

**[Return to Figure 8](#)**

**Figure 9**

Figure 9 contains the OceanInsight FLAME Normalized Difference Chlorophyll Index (NDCI) Calibration Dataset. Depicted in a Scattering Line Height (SLH) graph, measured ChlA in ug/L is listed along the Y-axis while the FLAME NDCI measuring from -0.06 to 0.08 is along the X-axis. The FLAME NDCI algorithm regressed against the measured ChlA had a R<sup>2</sup> of 0.66, RMSE of 4.96 µg/L, Bias of 0.00 µg/L, and a Nash criterion of 0.90. There did not appear to be any clear outlier points or trends within the dataset. Due to

the lower range of ChIA concentrations in the calibration dataset, estimations of ChIA around the range of 60-80 µg/L have a higher chance of error.

While there was a low RMSE, little to no bias in the estimation of ChIA, and a high Nash criterion, because the FLAME had a lower  $R^2$  than the S2 and S3 NDCI estimations compared to actual measurement, further refinement of the FLAME method is recommended to improve its accuracy and validity. Potential sources of error could be from local variations in the ChIA concentration around the sampling site, as the spectral reading was taken from the bow of the boat and the SJRWMD grab sample from the stern. Additionally, as the SJRWMD water sampling was performed primarily in the mornings there was often insufficient ambient light to collect a hyperspectral measurement.

### [\*\*Return to Figure 9\*\*](#)

## Figure 10

---

Figure 10 is a comparison of BaySpec spectral signals from the same location (B04) on different days. There are two lines in the graph that represent the two days the signals were taken. Along the Y-axis is the Relative Reflectance measured in percent and ranging from 0% to 10%. Along the X-axis is the Spectrum measured in nm and ranging from 475 nm to 895 nm. There is a green vertical line highlighting the ChIA reflectance at 705 nm. There were thirty-one (31) hyperspectral readings successfully collected with the UAV mounted, BaySpec spectrometer in conjunction with SJRWMD water quality sampling events, including 14 in the NIRL, 5 in the BRL, and 12 in the CIRL. The highest ChIA concentration was 29.58 µg/L, the lowest was 1.99 µg/L, and the median was 6.11 µg/L. As with the FLAME measurements, there was a strong peak reflectance around the 705 nm spectrum collected on November 1, 2022, at SJRWMD sampling site B04 where a bloom was occurring. For comparison, the reflectance collected almost 6 months prior during low ChIA conditions lacks the 705 nm peak. This supports the conclusion that the NDCI can be applied to the BaySpec data to create an estimate of ChIA.

### [\*\*Return to Figure 10\*\*](#)

## Figure 11

---

Figure 11 contains the BaySpec OCI-F Normalized Difference Chlorophyll Index (NDCI) Calibration Dataset. Depicted in a Scattering Line Height (SLH) graph, measured ChIA in ug/L is listed along the Y-axis while the BaySpec NDCI measuring from -0.20 to 0.10 is along the X-axis. There did not appear to be any clear outlier points or trends within the

dataset. Due to the lower range of ChlA concentrations in the calibration dataset, estimations of ChlA around the range of 60-80 µg/L are likely to have greater error.

While there was also a low RMSE, little to no bias in the estimation of ChlA, and a high Nash criterion in the comparison of BaySpec estimates and actual concentrations, the lower  $R^2$  suggests that further refinement of the use of the BaySpec for ChlA estimation is required to ensure valid and reproducible results. Potential sources of error could be due to local variations in the ChlA concentration around the sampling sites, differences between the time of the flyover and sample collection. Due to logistical constraints, every effort was made to ensure no more than 1 hour between sample collection and the UAV flyover. Additionally, as the SJRWMD water sampling was performed primarily in the mornings there was often insufficient ambient light to collect a hyperspectral measurement.

**[Return to Figure 11](#)**

## Figure 12

Figure 12 shows a comparison of the ChlA estimation errors between synchronous Sentinel, FLAME, and Saint Johns River Water Management District (SJRWMD) measurements. The Sentinel ChlA Error measured in ug/L, is shown on the Y-axis while the BaySpec ChlA Error measured in ug/L is shown on the X-axis.

The compatibility of the NDCI estimated ChlA concentrations between the hyperspectral and Sentinel was evaluated by comparing their respective estimation errors to a SJRWMD surface water sample. In 2022 there were a total of fourteen (14) events where a FLAME measurement was collected within 24 hours of either a S2 or S3 overpass and a SJRWMD sample. For BaySpec there were a total of thirteen (13) events that were within 24 hours of either a S2 or S3 overpass and a SJRWMD surface water sample. There were no events when both FLAME and BaySpec measurements were within 24 hours of Sentinel overpasses and a SJRWMD surface water sample.

There were four (4) events when the FLAME and S2 measurements and ten (10) events when the FLAME and S3 measurements aligned with SJRWMD surface water samples. The SJRWMD observed ChlA for these events ranged from 2.51 to 15.47  $\mu\text{g/L}$ . Thirteen (13) of the fourteen (14) events were collected within the NIRL, with one (1) in the BRL. Three (3) of the FLAME and S2 measurements and three (3) of the FLAME and S3 measurements were within 5  $\mu\text{g/L}$  of the SJRWMD measured ChlA concentration. There was a notable outlier with an S3 measurement having a -10.6 ug/L error.

[\*\*Return to Figure 12\*\*](#)

## Figure 13

Figure 13 is a comparison of the ChlA estimation errors between synchronous Sentinel, BaySpec, and Saint Johns River Water Management District (SJRWMD) measurements. The Sentinel ChlA Error measured in ug/L, is shown on the Y-axis while the BaySpec ChlA Error measured in ug/L is shown on the X-axis. There were three (3) events when the BaySpec and S2 measurements aligned and ten (10) events when the BaySpec and S3 measurements aligned with SJRWMD surface water samples. Six (6) measurements were collected within the NIRL, one (1) in the SML, and five (5) in the BRL. The SJRWMD measured ChlA for these events ranged from 6.22 to 17.02  $\mu\text{g/L}$ .

None of the BaySpec and S2 measurements were within the 5  $\mu\text{g/L}$  marginal error of the SJRWMD ChlA. However, five (5) of the BaySpec and S3 measurements were within an error of 5 ug/L of the SJRWMD ChlA. There does not appear to be a clear pattern

between error of ChlA estimation. Overall, there is general agreement between the FLAME and Sentinel satellites and between the BaySpec and Sentinel satellites regarding ChlA spectral features. It appeared that the FLAME measurements had better agreement, but due to both the small sample size and low ChlA concentrations, more measurements should be collected of higher ChlA concentrations to improve this analysis.

[\*\*Return to Figure 13\*\*](#)

## Figure 14

---

Figure 14 is a comparison of *Caulerpa Prolifera* FLAME reflectance to open sand with and without bloom conditions, as well as muck sediment. This is a line graph that contains four lines, different colors, representing *Caulerpa* – No Bloom, Sand – No Bloom, Sand – Bloom, and Muck – No Bloom. Along the Y-axis is the Remote Sensing Reflectance measured in percentage ranging from 0% to 10%. Along the X-axis is the Spectrum measured in nm and ranging from 400 to 880 nm.

Of the 22 benthic sampling events, *Caulerpa Prolifera* was the only Submerged Aquatic Vegetation (SAV) found in abundance. There was a total of 9 FLAME readings collected over dense *Caulerpa* beds when the water had low turbidity (<5 NTU). As *Caulerpa* contains ChlA, it has a similar reflectance and absorption as phytoplankton (650 - 705 nm). This overlap could lead to overestimations of water column ChlA concentration by Sentinel remote sensing. As the *Caulerpa* is distinct from open sand and muck benthic types, it can be identified by the NDCI during low phytoplankton conditions. There were 3 FLAME readings over IRL muck, all from the mouth of Turkey Creek.

[\*\*Return to Figure 14\*\*](#)

## Figure 15

---

Figure 15 shows a comparison of the dense *Caulerpa Prolifera* FLAME reflectance to water depth. This line graph contains three lines, different colors, representing the location and water depth; S-BRL (2.3 ft), N-CIRL (5.3 ft), and S-NIRL (11.1 ft). At shallower depths, there appears to be a small reflectance peak around 640 nm. Additionally, the 705 peak appears to shift towards 650 with increasing depths. Based on the FLAME readings, there does not appear to be a significant difference between the reflectance of phytoplankton and *Caulerpa* ChlA.

[\*\*Return to Figure 15\*\*](#)

## Figure 16

---

Figure 16 is an example of the Indian River Lagoon (IRL) benthic sediments. There are three pictures; A, B, and C. Picture A depicts clean sand with low organics; photo B depicts a mixture of sand, shell hash, and organics while photo C depicts the highly organic IRL muck. Of these three sediment types, the clean sand had the strongest reflectance with well-defined peaks across the spectrum.

[\*\*Return to Figure 16\*\*](#)

## Figure 17

---

Figure 17 is a comparison of the Indian River Lagoon (IRL) sediment FLAME reflectance for clean sand, mucky sand, and IRL muck. There are three lines depicted by different colors and referencing Clean Sand, Mucky Sand, and IRL Muck. Along the Y-axis is the Remote Sensing Reflectance measured in percentage and ranging from 0% to 7%. Along the X-axis is the Spectrum, measured in nm, and ranging from 400 to 880 nm. The difference in mucky sand and IRL muck reflectance were minor, with the mucky sand having more pronounced reflectance peaks between 600 and 705 nm. The lack of a strong difference between these two benthic types suggests that classification at higher spectral and spatial resolutions may not be viable.

[\*\*Return to Figure 17\*\*](#)

## Figure 18

---

Figure 18 is a comparison of *Caulerpa Prolifera* BaySpect reflectance to open sand with and without bloom conditions, as well as muck sediment. This is a line graph that contains four lines, different colors, representing *Caulerpa* – No Bloom, Sand – No Bloom, Sand – Bloom, and Muck – No Bloom. Along the Y-axis is the Relative Reflectance measured in percentage ranging from 0.0% to 0.16%. Along the X-axis is the Spectrum measured in nm and ranging from 400 to 900 nm.

From the 22 benthic sampling events, a total of 50 field confirmed *Caulerpa* beds were extracted from the BaySpec imagery with low turbidity (<5 NTU). Similar to the FLAME measurements, the *Caulerpa* 705 nm reflectance peak overlaps with the phytoplankton peak and no significant difference was found between the reflectance of phytoplankton and *Caulerpa* ChlA.

[\*\*Return to Figure 18\*\*](#)

## Figure 19

Figure 19 shows Sykes Creek BaySpec imagery collected on October 12, 2022. There are two images, A and B, situated on top of each other. Image A is the true color image while image B is showing the estimated ChlA concentration. This figure is an example flight of the BaySpec over Sykes Creek.

This example highlights the impact of the *Caulerpa* beds on the estimation of water column ChlA. The western portion of the flight path includes the shallowest point that *Caulerpa* was observed (2.3 ft), and here the NDCI estimated ChlA was 30 µg/L. Following the path from west to east, the depth increases to 5.4 ft and the *Caulerpa* influence on the NDCI decreases. This mirrors the findings of the FLAME observation of *Caulerpa* beds at increasing depths. Additionally, the change in depth demonstrates the impact of water depth where there are sandy bottoms, showing higher estimated ChlA in shallow water than the deeper water to the east. While the presence of *Caulerpa* complicates the estimation of water column ChlA, under low phytoplankton conditions the NDCI could be used to map the SAV coverage in the IRL.

[\*\*Return to Figure 19\*\*](#)

## Figure 20

Figure 20 shows two boxplots of the cyanobacteria (CB) biomass for 2019 and 2020 by lagoon segment. The scales of the two years are not equal, 2020 is an order of magnitude larger than 2019. The Y-axis is showing the Biomass measured in µm<sup>3</sup>/ml ranging from 0 to 12,000,000 while the X-axis contains the lagoon segment, SML, N-NIRL, BRL, C-NIRL, and N-CIRL. The abundance of CB has varied across time and space within the IRL. A prolonged CB bloom in 2020 was focused in the BRL whereas in 2019 and 2020 CB blooms were more frequent in the SML and NIRL. The North CIRL was the only segment to have consistently low CB dominated blooms. The blooms of 2020 included the longest period that *cyanobium* was observed in the lagoon with 26 consecutive events from August 2020 to March 2021.

[\*\*Return to Figure 20\*\*](#)

## Figure 21

Figure 21 shows two boxplots of the cyanobacteria (CB) biomass for 2021 and 2022 by lagoon segment. The Y-axis is showing the Biomass measured in µm<sup>3</sup>/ml ranging from 0 to 12,000,000 while the X-axis contains the lagoon segment, SML, N-NIRL, BRL, C-NIRL,

and N-CIRL. The abundance of CB has varied across time and space within the IRL. A prolonged CB bloom in 2020 was focused in the BRL whereas in 2019 and 2020 CB blooms were more frequent in the SML and NIRL. The North CIRL was the only segment to have consistently low CB dominated blooms. The blooms of 2020 included the longest period that *cyanobium* was observed in the lagoon with 26 consecutive events from August 2020 to March 2021.

[\*\*Return to Figure 21\*\*](#)

## Figure 22

---

Figure 22 is a comparison of the FLAME hyperspectral readings of eukaryotic and cyanobacteria phytoplankton blooms in the Indian River Lagoon (IRL). The four spectra related to Phycocyanin and Chlorophyll A are each highlighted by vertical bars, from left to right, at the following Spectrums: 620, 665, 705, and 755 nm.

Two of the samples were dominated by eukaryotic phytoplankton, *Pyrodinium bahamense* on 9/26/2022 in the NIRL3 segment and *Akashiwo sanguinea* on 1/6/2023 in the NIRL8 segment. One sample was dominated by the CB *Picocyanobacteria spp.* in the BRL4 on 12/7/2022, The three CB algorithms were applied to the averaged spectral data to generate representative index values. As there were insufficient samples to perform statistical analysis, a qualitative assessment was performed.

[\*\*Return to Figure 22\*\*](#)

## Figure 23

---

Figure 23 is a comparison of the BaySpec hyperspectral readings of eukaryotic and cyanobacteria phytoplankton blooms in the Indian River Lagoon (IRL). The four spectra related to Phycocyanin and Chlorophyll A are each highlighted by vertical bars, from left to right, at the following Spectrums: 620, 665, 705, and 755 nm. There was a total of 4 sampling events using the UAV mounted BaySpec spectrometer that coincided with measurable phytoplankton ( $> 10 \mu\text{g/L}$ ), an algal enumeration sample, and consistent benthic conditions. The dominant phytoplankton in these samples was the eukaryotic *Pyrodinium bahamense* on 9/26/2022 in the NIRL3 segment, the CB *Picocyanobacteria spp.* in BRL4 on 12/7/2022, eukaryotic *Akashiwo sanguinea* on 1/6/2023 in the NIRL8, and eukaryotic *Ceratium furca* in BRL6 on 3/7/2023. The three CB algorithms were applied to the averaged spectral data to generate representative index values. As there were insufficient samples to perform statistical analysis, a qualitative assessment was performed.

In comparison to the FLAME indices, the 2BDA-PC and NDPCI had similar behavior with the CB dominated sample having the largest index value of all the samples. Also, the BaySpec 3BDA-PC index appeared to differentiate between CB dominated samples than the FLAME. Due to the lack of additional samples, a strong conclusion cannot be reached regarding the best performing algorithm.

[\*\*Return to Figure 23\*\*](#)

## Figure 24

---

Figure 24 is a comparison of the measured ChlA concentrations to the percent of the sample's biomass as cyanobacteria. This is a scatter plot graph that shows ChlA measured in  $\mu\text{g/L}$ , from 0 to 80, along the Y-axis and the Percent of Biomass as CB ranging from 0% to 100% along the X-axis.

The assessment of the CB estimation algorithms was performed on S3 data due to the higher spectral resolution of its bands as well as specific bands targeted to CB spectral features. The dataset contained a total of 86 points including 17 points in Mosquito Lagoon, 24 in NIRL, 32 in Banana River, and 13 in CIRL with ChlA concentrations that ranged from 1.7 to 69.9  $\mu\text{g/L}$  and a median value of 12.1  $\mu\text{g/L}$ . The percentage of the phytoplankton biomass as CB ranged from 80.1% at the highest, 0.1% at the lowest, and a median of 10.4%, demonstrating that this subset represents the full range of measurements in the measured dataset. There does not appear to be a relationship between the ChlA concentration and the percent CB biomass.

[\*\*Return to Figure 24\*\*](#)

## Figure 25

---

Figure 25 is showing Sentinel 3 spectral comparison of low and high cyanobacteria (CB) biomass blooms. There are four spectra, each highlighted by vertical bars, from left to right, at the following Spectrums: 620, 665, 708.75, and 753.75 nm. The Y-axis shows the Top of the Atmosphere Reflectance in percentage ranging from 0% to 40%. Along the X-axis is the Spectrum, measured in nm, ranging from 400 nm to 1020 nm.

A comparison of a single high CB biomass bloom (ML02) and a low CB biomass bloom (NFH01S) was performed to evaluate the CB estimation algorithms in various conditions. ML02 had a ChlA concentration of 69.9  $\mu\text{g/L}$  and a CB biomass percentage of 80.1%, which was dominated by a mixture of Cyanobium and Synechococcus as determined by the UF Philips lab. NFH01S had a similarly high ChlA of 63.9  $\mu\text{g/L}$  but a CB biomass

percentage of 1.3%, which was dominated by the eukaryote *Cerataulina pelagica*. All three of the algorithms had larger index values for the CB dominated sample having higher values. The 3BDA-PC algorithm was the inverse of what was expected, as a CB dominated sample would have more PC absorption which should result in a lower 620 nm reflectance relative to the ChlA 705 nm reflectance. The 3BDA-PC algorithm was not evaluated for the full calibration dataset.

**[Return to Figure 25](#)**

**Figure 26**

Figure 26 is a comparison of the Sentinel 3 (S3) 2BDA-PC index to the measured cyanobacteria (CB) biomass at Saint Johns River Water Management (SJRWMD) sampling sites with ChlA more than 10 µg/L. The Y-axis contains the Measured Percent CB Biomass ranging from 0% to 100%. Along the X-axis is the PC Index ranging from 0.7 to 1.0.

For the calibration dataset, both the 2BDA-PC and NDPCI algorithms had a low but significant ( $p < 0.0001$ )  $R^2$  of 0.23 and 0.22, respectively. However, after the application of a ChlA filter, removing concentrations below 10 µg/L, a stronger correlation was identified. This filter reduced the calibration dataset from 86 to 17 points, which resulted in an increased median ChlA of 25.22 µg/L and a moderately strong  $R^2$  of 0.66 and 0.65 ( $p < 0.0001$ ) and no obvious outliers. The RMSE, Bias, and Nash criterion between the two algorithms was practically the same. With 2BDA-PC and NDPCI RMSE's of 11.5% and 11.7% then Bias of -2% and -1%, respectively. Both algorithms had a Nash criterion of 0.99. For this calibration dataset, either of the equations could be used with S3 and have similar estimates of CB concentrations.

**[Return to Figure 26](#)**

**Figure 27**

Figure 27 is a comparison of the Sentinel 3 (S3) NDPCI index to the measured cyanobacteria (CB) biomass at Saint Johns River Water Management (SJRWMD) sampling sites. The Y-axis contains the Measured Percent CB Biomass ranging from 0% to 100%. Along the X-axis is the PC Index ranging from -0.2 through 0.0.

For the calibration dataset, both the 2BDA-PC and NDPCI algorithms had a low but significant ( $p < 0.0001$ )  $R^2$  of 0.23 and 0.22, respectively. However, after the application of a ChlA filter, removing concentrations below 10 µg/L, a stronger correlation was

identified. This filter reduced the calibration dataset from 86 to 17 points, which resulted in an increased median ChIA of 25.22 µg/L and a moderately strong  $R^2$  of 0.66 and 0.65 ( $p < 0.0001$ ) and no obvious outliers. The RMSE, Bias, and Nash criterion between the two algorithms was practically the same. With 2BDA-PC and NDPCI RMSE's of 11.5% and 11.7% then Bias of -2% and -1%, respectively. Both algorithms had a Nash criterion of 0.99. For this calibration dataset, either of the equations could be used with S3 and have similar estimates of CB concentrations.

[\*\*Return to Figure 27\*\*](#)

## Figure 28

---

Figure 28 is a spatial comparison of the 2022 Annual Bloom Intensity (BII), duration (BDI), and severity indices (BSI) for the Banana River Lagoon segment 3. Over the course of the year, there was more intense and longer lasting bloom activity in the north portion of the segment along the SR 528 causeway. However, there also appeared to be long lasting, low intensity blooms occurring on the west of the segment and then short lived, high intensity blooms in the eastern half. With the BII and BDI combined to calculate the BSI, the most severe bloom activity appears to be in the northwest corner of the segment, followed by the northeast corner, and then the entire west border. The identification of these locations can then lead to a more focused analysis of the bloom patterns in this segment.

[\*\*Return to Figure 28\*\*](#)

## Figure 29

---

Figure 29 is a comparison of the annual Bloom Severity Index (BSI) between 2021 and 2022 for the NIRL3 segment. This figure is showing the spatial distribution of bloom severity (BSI) in the years 2021 and 2022 and three SJRWMD monthly surface water monitoring sites located in the NIRL-3 segment. The two SJRWMD sampling sites missed the elevated bloom levels along the southwest edge of the segment in 2022.

[\*\*Return to Figure 29\*\*](#)

## Figure 30

---

Figure 30 is a comparison of the Bloom Severity Index (BSI) and the Saint Johns River Water Management District (SJRWMD) monthly surface water ChIA in NIRL3 segment between 2021 and 2022. In the top graph, titled Bloom Severity Index for NIRL3, the Y-axis contains the Monthly Sum Severity Index ranging from 0.00 to 0.08 and the X-axis

contains the months January through December. The bottom graph, titled SJRWMD ChIA in NIRL3, is depicting the ChIA measured in ug/L, ranging from 0.00 to 40.00 along the Y-axis while the dates January through December are depicted on X-axis. The years 2021 and 2022 are being shown as bars color coated for each year.

The two SJRWMD sampling sites missed the elevated bloom levels along the southwest edge of the segment in 2022. This is likely the reason there are such large differences in the estimated monthly BSI scores and the SJRWMD ChIA measurements for the basin. Additionally, in 2021 there was an annual sum of 0.22 BSI compared to 0.12 for 2022. The 2021 bloom activity was dispersed across the segment, whereas in 2022 there was a hot spot of bloom activity comprising less than a quarter of the segment. This highlights the challenge of calculating segment wide statistics due to the highly spatial nature of blooms in the IRL.

[\*\*Return to Figure 30\*\*](#)

## Figure 31

---

Figure 31 depicts the 2022 Bloom duration, intensity, and severity of the Southern Mosquito Lagoon (SML) and the Northern-North Indian River Lagoon (N-NIRL). This figure includes a map for the BSI and time-series graphs of the BDI and BII scores. Based on the median quarterly BSI from 2016 to 2021, from April to June (Q2) 2022 there appeared to be significantly more areas with elevated BSI in all segments. Then from July to September (Q3) 2022, only NIRL2 had significantly more areas of elevated BSI. From January to March (Q1) and then October to December (Q4) 2022, all the segments were below the median 2016-2021 BSI.

From the map, it is apparent that most of SML1 and NIRL1 had low bloom severity in 2022 (<0.2 BSI), while NIRL2 and SML2 experienced higher levels of bloom severity (0.3-0.6 BSI). The line graphs clarify when and how long the bloom activity occurred. In May 2022, both the NIRL1 and NIRL2 segments experienced a period of low intensity, lasting bloom activity. Starting in October 2022, the bloom activity in NIRL2 remained low but covered more area for a longer period. SML1 bloom duration and intensity remained low the entire year, whereas for SML2 there was more longer lasting bloom activity beginning in September 2022. While both SML1 and SML2 had similarly intense bloom activity between September and November, SML2 experienced longer lasting blooms which contributed to the subbasin's higher BSI score.

[\*\*Return to Figure 31\*\*](#)

---

## Figure 32

---

Figure 32 depicts the 2022 Bloom duration, intensity, and severity of the Northern Banana River Lagoon (NBRL). This figure includes a map for the BSI and time-series graphs of the BDI and BII scores. BRL2 and BRL3 had significantly larger areas of elevated BSI in only during Q4 2022. BRL4 had no significant differences during 2022.

The northern most segment (BRL2) had slightly elevated ( $>0.3$ ) BSI scores in pixels dispersed along the shorelines. The center subbasin (BRL3) had a high ( $>0.7$ ) BSI score area in the northwest corner of the segment against the 528 Causeway. Subbasin BRL4 had a high ( $>0.7$ ) BSI score concentration in the southern-most portion of the segment between Merritt Island and Cocoa Beach. There was little temporal variability in bloom duration and intensity within segments BRL2 and BRL3 over the year 2022. BRL4 had slightly increased intensity and notably higher bloom duration than the other segments with longer blooms occurring in May and September 2022.

[\*\*Return to Figure 32\*\*](#)

---

## Figure 33

---

Figure 33 shows the Bloom duration, intensity, and severity of the Southern Banana River Lagoon (SBRL). The BRL6 segment had significantly more areas of elevated BSI for the entirety of 2022. BRL5 had significantly more areas only in Q2 and Q4 2022, with SC below the median 2016-2021 BSI.

From the map, it is evident that bloom severity increases along borders of open waterways and in more confined waterways. For example, in BRL5 the large open water area shows low ( $<0.2$ ) BSI scores with somewhat higher BSI scores dispersed on the periphery of the segment along the shorelines. Segments SC and BRL6 in comparison are more confined by land and have less open water, reducing wind and wave influence. These two segments also have higher BSI scores ( $>0.5$ ) covering more area. While SC and BRL6 have no direct hydrologic connection, in 2022 they were more similar to each other in bloom duration and intensity than either was with segment BRL5 which connects the two segments. All three segments had a peak of duration and intensity in March 2022, followed by a more staggered set of peaks starting in August for BRL5, September for SC, and then October for BRL6.

[\*\*Return to Figure 33\*\*](#)

## Figure 34

---

Figure 34 shows the 2022 Bloom duration, intensity, and severity of the Central-North IRL (C-NIRL). In 2022, all the C-NIRL segments had significantly larger areas of elevated BSI in Q2 and Q3 2022 compared with 2016 to 2021. Only NIRL5 had significantly larger areas of elevated BSI in Q1 2022 while none of the segments were significantly higher in Q4. NIRL4 and NIRL5 experienced blooms generally dispersed across the segment with open water BSI scores elevated somewhat ( $>0.3$ ) and more elevated bloom severity scores ( $>0.5$ ) localized along shorelines and causeways. The northern-most segment (NIRL3) experienced a large area of bloom severity in its southwest portion along the NASA Causeway. NIRL4 and NIRL5 had their highest bloom severity located along the northern border of the segments, along the NASA Causeway and SR 528 Causeway. The duration and intensity of all three segments generally varied together over the year, with NIRL5 typically having the highest values. Between May and June 2022, the segments had a peak in duration and intensity with NIRL5 notably higher. Then from July to October, duration and intensity increased with NIRL5 peaking first in September then NIRL3 and NIRL4 in October.

[\*\*Return to Figure 34\*\*](#)

## Figure 35

---

Figure 35 depicts the 2022 Bloom duration, intensity, and severity of the Southern-North Indian River Lagoon (S-NIRL). A spatial and temporal representation of bloom activity in the three segments of the S-NIRL in the year 2022 clarifies the differences in bloom severity across the region. All of the S-NIRL segments had significantly larger areas of elevated BSI for all quarters in 2022 when compared with 2016 to 2021. Segment NIRL6 had moderate bloom severity index scores ( $>0.5$ ) throughout the segment whereas the other two segments had lower BSI scores ( $<0.4$ ). Segment NIRL7 shows several higher severity pixels grouped in its northern half, with some along the eastern shorelines, possibly algae distributed south from segment NIRL6 by wind and wave activity.

The southern most portion of the S-NIRL between the Eau Gallie and Melbourne Causeways, (NIRL8) had moderate severity scores ( $<0.4$ ) along the shorelines with two isolated clusters of high severity pixels (0.5-0.6) located in the northeast and central west portions of the segment. All three segments had similar variations in duration and intensity over time, with the north (NIRL6) to south (NIRL8) trend of high to low values apparent in the time-series graphs. The first intensity and duration peaks were in April

2022 followed by a series of events that reached a high in September 2022 and were followed by two more peaks in October and November.

[\*\*Return to Figure 35\*\*](#)

## Figure 36

---

Figure 36 shows the 2022 Bloom duration, intensity, and severity of the Northern-Central Indian River Lagoon (N-CIRL). Despite having generally low BSI in 2022 in comparison to the other segments, the two (2) segments of the N-CIRL had significantly larger areas of elevated BSI in 2022 when compared with 2016 to 2021. Low bloom severity pixels (<0.2) were distributed throughout the open water areas of segment CIRL1 with moderate bloom severity (0.3-0.4) pixels along the periphery of the segment along the shoreline. The more southern segment (CIRL2) had two areas of higher bloom severity pixels (>0.5) along the eastern shoreline proximal to Crane Creek and Turkey Creek, two large tributaries to the segment and a third area in the center of the segment. The time series graphs show that the first peak of bloom duration occurred in both segments in April, August, and November 2022, although bloom intensity remained elevated throughout the year with drops between the intensity peaks. This could be indicative of the movement of blooms in these segments, as high intensity blooms drift through the segment and they result in lower overall bloom duration.

[\*\*Return to Figure 36\*\*](#)

## Figure 37

---

Figure 37 is a comparison of the cyanobacteria bloom index for a eukaryotic bloom on September 9, 2019, and a cyanobacteria bloom on August 14, 2020. To test a method to identify HAB species through satellite imagery, the NDPCI algorithm was applied to two S3 scenes which represent known eukaryotic or cyanobacteria dominated blooms. The test date of September 9, 2019, was selected as it had a moderate, persistent bloom of an unidentified eukaryotic nanoplankton. Surface water samples were collected in SML and N-NIRL the same day as the S3 scene, with SML having a ChlA concentration of 29.8 µg/L and CB biomass of 15% and N-NIRL having a ChlA concentration of 21.9 µg/L and CB biomass of 27%. As expected, the median NDPCI value in the SML was 0.72 and the median NDPCI value was 0.78 in the N-NIRL, corresponding with the higher CB biomass in this region.

The second test date was August 14, 2020, which was selected as it had comparable ChlA concentrations to September 9, 2019, and was dominated by the CB species

*Cyanobium*. The surface samples collected prior to the S3 scene on August 10, 2020, measured ChlA concentration of 10.8 µg/L in the SML and CB biomass of 37% and a ChlA concentration of 33.9 µg/L in the N-NIRL and CB biomass of 53%. The median NDPCI value in the SML was 0.88 and the median NDPCI value in the N-NIRL was 0.94 again corresponding with the higher CB biomass percentage in the N-NIRL.

[\*\*Return to Figure 37\*\*](#)

## Figure 38

---

Figure 38 depicts Sentinel 2 cumulative ChlA for 2017 and 2022 for the Banana River Lagoon 3 segment. The Saint Johns River Water Management District (SJRWMD) seagrass extents for 2017 and 2021 are also included in this figure. Applied Ecology Inc. assessed the change in SAV coverage in the BRL3 segment using the higher resolution S2 estimated ChlA data during the years 2017 and 2022 which represent before and after extreme bloom activity in the BRL.

There was a total of 7 scenes available in 2017 and 6 in 2022 selected for no cloud cover and low reported ChlA at the SJRWMD IRLB04 sampling station (<10 µg/L) and in the open water of the segment. The average estimated ChlA concentration was calculated for each pixel summarizing 2017 and 2022, which could include various species of SAV such as *Caulerpa*, other macroalgae, and seagrass.

Between 2017 and 2022 the area with an estimated ChlA of 30 µg/L or greater decreased from 4.37 km<sup>2</sup> (1,079.85 acres) to 0.92 km<sup>2</sup> (227.43 acres). The eastern half of the segment was estimated to have the largest loss, which also aligns with the SJRWMD 2021 seagrass survey and the 2022 benthic survey. The SAV in the western half of the segment appears to have constricted to the shallower waters close to the shoreline. Notably a new lobe of SAV appears to have formed in the center north of the segment between 2017 and 2022. While the NDCI alone is unable to differentiate between a phytoplankton bloom and SAV ChlA, under ideal circumstances S2 data can identify potential locations of SAV and its change in coverage over time.

[\*\*Return to Figure 38\*\*](#)

## Figure 39

---

Figure 39 is a scatter plot that shows the weekly Bloom Severity Index (BSI) of the segment of the North Indian River Lagoon 8 (NIRL8) proximate to the mouth of the Eau Gallie River and the entire NIRL8 segment compared to the weekly discharge from the

Eau Gallie River between May and December 2016. Hypotheses 2E and 2F were that the presence of muck increases bloom activity and that muck removal projects would result in a decrease of proximate bloom activity. To test these hypotheses, the Eau Gallie River was selected as it is a constrained segment with minimal confounding factors. Muck dredging operations were performed between January 2017 to March 2019. All comparisons were performed using a one-tailed Wilcoxon Signed-Rank test.

Prior to the start of dredge operations, there were 24 weeks of S3 estimated BSI of the NIRL8 segment. During this period the BSI was significantly above ( $p < 0.0001$ ) the segment average 21 out of the 24 weeks. The most elevated BSI values were observed during the lowest discharge from Eau Gallie, which may suggest less of an influence from the runoff in the watershed and the potential muck flux and baseflow nutrient loading.

[\*\*Return to Figure 39\*\*](#)

## Figure 40

---

Figure 40 is a scatter plot that shows the weekly Bloom Severity Index (BSI) of the segment of the North Indian River Lagoon 8 (NIRL8) proximate to the mouth of the Eau Gallie River and the entire NIRL8 segment compared to the weekly discharge from the Eau Gallie River between January 2017 and March 2019. During the dredging period there was a super bloom in the BRL starting January 2018, which had spread to the NIRL8 segment by February 2018. Similar, to the pre-dredging period, the area of the NIRL8 segment proximate to the mouth of Eau Gallie had a significantly higher ( $p < 0.0001$ ) BSI than the NIRL8 segment. This was doubly so during the bloom period, with the BSI around Eau Gallie being on average 100% higher than the segment.

[\*\*Return to Figure 40\*\*](#)

## Figure 41

---

Figure 41 is a scatter plot that shows the weekly Bloom Severity Index (BSI) of the segment of the North Indian River Lagoon 8 (NIRL8) proximate to the mouth of the Eau Gallie River and the entire NIRL8 segment compared to the weekly discharge from the Eau Gallie River between April 2019 and December 2022. After the completion of the dredging operation in March 2019, there was another super bloom in the IRL which ran from July to December 2020 primarily in the NIRL. During this period, the BSI for the segment around the mouth of the Eau Gallie was on average 57% lower than the entire segment. For the remainder of this period, the Eau Gallie area was significantly below ( $p < 0.0001$ ) the segment BSI.

**[Return to Figure 41](#)**